REGULATION AND FUNCTION OF LIPID DROPLETS IN MELANOMA

By

Eleanor Johns

A Dissertation

Presented to the Faculty of the Louis V. Gerstner, Jr.

Graduate School of Biomedical Sciences

Memorial Sloan Kettering Cancer Center

In Partial Fulfillment of the Requirements for the Degree of

Doctor of Philosophy

New York, NY

September, 2024

Richard M. White, MD/PhD Dissertation Mentor	Date
Michael Overholtzer, PhD Dissertation Mentor	Date

Copyright by Eleanor Johns, 2024

DEDICATION

To my parents, Rob and Jennifer. Your support in all my endeavors means the world to me.

ABSTRACT

Lipid droplets are storage organelles found in most cell types, from adipocytes to cancer cells. However, the factors regulating lipid droplet formation and function in these different cellular contexts remains incompletely understood. We have previously characterized the transfer of fatty acids from adipocytes to melanoma cells, which leads to a high level of lipid storage in tumor-associated lipid droplets. Importantly, we have also shown that lipid droplets are enriched in certain melanoma cell states, and that inhibition of lipid droplet formation through knockout of DGAT1a slows tumor progression *in vivo*. To better study the role of lipid droplets in melanoma and the tumor microenvironment, we created a transgenic lipid droplet reporter in zebrafish. By fusing the lipid droplet resident protein PLIN2 to tdTOMATO, we were able to visualize lipid droplets both *in vivo* (i.e. adipocytes) and *in vitro* (i.e. ZMEL1 melanoma cells). Both dietary and pharmacologic manipulations lead to dynamic changes in lipid droplet fluorescence, enabling us to screen for novel regulators of lipid droplets in melanoma.

Lipid droplets are composed of a protein envelope which surrounds a lipid rich core. We hypothesized that components of this protein envelope could regulate lipid droplet function in melanoma. We performed proteomic analysis of lipid droplets isolated from melanoma cells. As expected, many of the proteins are shared with lipid droplet proteomes from other cell types. However, we also found that many proteins were differentially enriched in distinct melanoma cell states; from melanocytic to undifferentiated. DHRS3, which converts all-trans-retinal to all-trans-retinol, is upregulated in the $MITF^{LO}$/undifferentiated/neural crest-like melanoma cell state and

reduced in the $MITF^{HI}$/melanocytic state. Increased DHRS3 expression is sufficient to drive $MITF^{HI}$/melanocytic cells to a more undifferentiated/invasive state. These changes are due to retinoic acid mediated regulation of melanocytic genes. Our data demonstrate that melanoma cell state can be regulated by expression of lipid droplet proteins which affect downstream retinoid signaling.

BIOGRAPHICAL SKETCH

Eleanor Johns was born March 2nd, 1996 in Chicago, Illinois to parents Robert and Jennifer Johns. Eleanor was raised in Philadelphia, Pennsylvania alongside her older sister Emily Johns and younger brother Samuel Johns. She attended Central High School in Philadelphia. After graduation in 2014, Eleanor attended the University of Pennsylvania in Philadelphia, Pennsylvania where she majored in Biology with a Cell and Molecular Biology concentration. It was here that Eleanor discovered her interest in biomedical research in the labs of Dr. Bradley Johnson and Dr. Xiaolu Yang. Following graduation from college in 2018, Eleanor moved to New York City to attend the Gerstner Sloan Kettering Graduate School of Biomedical Sciences for her PhD work. In 2019 Eleanor joined the laboratory of Dr. Richard White for her dissertation research on cutaneous melanoma.

ACKNOWLEDGEMENTS

I would like to thank my mentor Dr. Richard White for his continued support both in New York City and while at the University of Oxford. It has been a fantastic opportunity to be in your laboratory. Thank you for pushing me to develop as an independent researcher and for your continuous enthusiasm towards my projects. I am grateful for your mentorship at all stages of my Ph.D. and for your support of my professional development.

I am also incredibly grateful to all past and present members of the White lab, many who have become my dear friends. All of you have played a pivotal role in my development as a scientist and I will always be grateful for your mentorship, support and advice. In particular, I'd like to thank my fellow graduate students; Dr. Dianne Lumaquin, Dr. Yilun Ma, and Dr. Sarah Perlee. Our many happy hours have been a great source of support and comradery and definitely helped get me through some of those tough Ph.D. moments.

I would also like to thank Dr. Michael Overholtzer. I am incredibly appreciative of you offering me a second home in your lab. From my early days as an undergraduate student in SURP until now, your enthusiasm for science is infectious and it has been a lot of fun to be a part of your lab. Your continued support and advice has been instrumental to my success.

Thank you to all the members of the Overholtzer Lab for welcoming me in the last year of my PhD to the lab. It has been so much fun getting to know all of you. Moving labs at

the end of grad school was daunting, and you all of you have made that transition incredibly enjoyable.

I'd also like to thank the members of my thesis committee, all of my collaborators, and anyone not named here. In addition, I'm so grateful to the administration of GSK for creating an incredible graduate school and for fostering such a tight knit and supportive community.

Thanks to my classmates and the broader GSK graduate school. In particular, I'd like to thank Dr. Alex Settle, Dr. Katelyn Mullen, and Dr. Bradley Benjamin. Since those early days in class it has been so much fun being friends with all of you. I'm so grateful for our trips, brewery sessions etc. and it's been awesome to be a part of some huge life events (weddings, babies...). Your friendship and commiseration is an amazing source of support (even if sometimes it makes us miss our highway exit) and I know we will be friends for many years.

Outside of graduate school I am incredibly grateful to have so many close friends in NYC who have been steadfast supporters of me throughout my PhD. I don't know where I'd be without all of you.

Finally, and most importantly I'd like to thank my family; Sam, Emily and my parents Rob and Jennifer. To Emily who I've grown up with side-by-side, thank you for being an amazing friend and sister. And to my parents, I certainly would not be where I am without your unconditional love, support, and advice. Thank you for all you've done to support me and to push me to succeed in whatever I choose to do.

TABLE OF CONTENTS

LIST OF FIGURES

LIST OF TABLES

LIST OF ABBREVIATIONS

Ac-CoA	Acetyl-CoA
ACLY	ATP Citrate Lyase
ACSS2	Acyl-CoA Synthetase Short Chain 2
ATGL	Adipose triglyceride lipase
ATP	Adenosine Triphosphate
BMI	Body Mass Index
BSA	Bovine Serum Albumin
CCLE	Cancer Cell Line Encyclopedia
CCTα	CTP:phosphocholine cytidylyltransferase
CDKN2A	Cyclin-dependent kinase inhibitor 2A
cDNA	Copy Deoxyribonucleic Acid
CI	Confidence Interval
CSC	Cancer Stem Cell
DGAT	Diacylglycerol O-Acyltransferase
DHRS3	Dehydrogenase/reductase 3
DNA	Deoxyribonucleic Acid
DPF	Days Post Fertilization
EMT	Epithelial to Mesenchymal Transition
ER	Endoplasmic Reticulum
FA	Fatty Acid
FABP	Fatty Acid Binding Protein
FASN	Fatty Acid Synthase
FATP	Fatty Acid Transport Protein
FFA	Free Fatty Acid
GFP	Green Fluorescent Protein
GSEA	Gene Set Enrichment Analysis
GPAT4	Glycerol-3-phosphate acyltransferase 4
HIF	Hypoxia inducible factor
HSL	Hormone-sensitive lipase
H_2O_2	Hydrogen Peroxide
iBAQ	Intensity Based Absolute Quantification
LC-MS/MS	Liquid Chromatography with Tandem Mass Spectrometry
LDAC	Lipid Droplet Assembly Complexes
LDAF1	Lipid Droplet Assembly Factor 1
LD	Lipid Droplet
MAPK	Mitogen Activated Protein Kinase
MFI	Mean Fluorescence Intensity
MGL	Monoacylglycerol lipase
MITF	Micropthalmia-associated transcription factor
mRNA	Messenger Ribonucleic Acid
MUFA	Monounsaturated Fatty Acid
NAFLD	Nonalcoholic fatty liver disease
NC	Neural Crest

NCSC	Neural Crest Stem Cell
NF-1	Neurofibromatosis type 1
OA	Oleic Acid
PLIN2	Perilipin 2
PUFA	Polyunsaturated Fatty Acid
qRT-PCR	Quantitative Real Time Polymerase Chain Reaction
RAR	Retinoic Acid Receptor
RDH10	Retinol Dehydrogenase 10
RXR	Retinoid X Receptor
SB	Swim Bladder
SCD	Stearoyl-CoA Desaturase
SFA	Saturated Fatty Acid
SREBP	Sterol Regulatory Element Binding Protein
TAG	Triacylglycerol
TCGA	The Cancer Genome Atlas
TME	Tumor Microenvironment
TXN	Thioredoxin
TYR	Tyrosinase
VEGF	Vascular Endothelial Growth Factor
9-cis-RA	9-cis-retinoic acid
ZMEL	Zebrafish Melanoma Cell Line
ZMEL-LD	Zebrafish Melanoma Cell Line with Lipid Droplet Reporter

CHAPTER 1: INTRODUCTION

1.1 Introduction to Melanoma

Melanoma is the deadliest form of skin cancer. In the United States, it is estimated that over 100,000 new cases of melanoma will be diagnosed in 2024.[1] While recent therapeutic advances, in particular immune checkpoint therapy, have drastically improved melanoma survival rates,[2] metastatic disease remains a challenge. This is due, in part, to the significant genetic and transcriptional heterogeneity that is present in melanoma lesions. A result of this heterogeneity is phenotypic plasticity of melanoma cells within individual tumors, where a range of factors can contribute to cell phenotype switching, a major factor in metastatic disease and drug resistance.[3] While significant work has been done to transcriptionally profile these different cell states, the cell intrinsic and extrinsic factors that underlie switching between states remains a critical question.

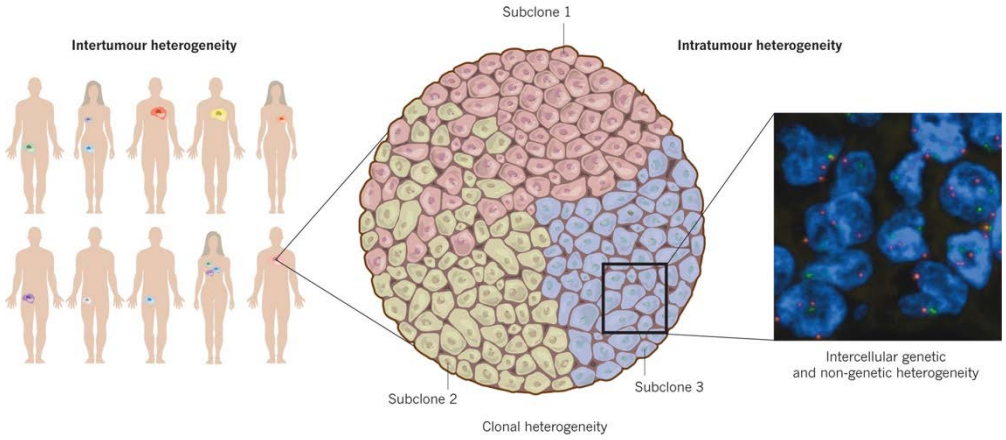

Figure 1. An overview of heterogeneity in cancer.

Intertumour heterogeneity refers to genetic and non-genetic variation that exists between patients with the same tumor type. Intratumour variation refers to the presence of genetic and non-genetic variation within a single tumor. This generates sub-clonal populations of

cells which can be responsible for differences in tumor growth, metastasis, and response to therapy. This figure was reprinted[4] with permission from Springer Nature.

1.2 Tumor Heterogeneity in Melanoma

Genetic Heterogeneity

Cancer is fundamentally a disease caused by genetic mutations. Decades of work have identified the genetic mutations, alterations, and rearrangements that cause oncogenic transformation of normal cells across tumor types.[5-7] Alterations which are sufficient to induce transformation are termed driver mutations, while additional mutations that do not confer a selective growth advantage are known as passenger mutations.[5] However, further work has highlighted that the selective advantage of mutations is highly dependent on cellular environment, emphasizing the role of inter and intra-tumor genetic heterogeneity in tumor evolution (Figure 1).[8] Increased heterogeneity contributes to the presence of sub-clonal populations in the tumor which can provide selective advantage under different conditions including metastasis and response to therapy.[9] Therefore, the clonality of a tumor, and the proportionality of sub-clonal populations of cells, is critical to understanding tumor evolution (Figure 2).

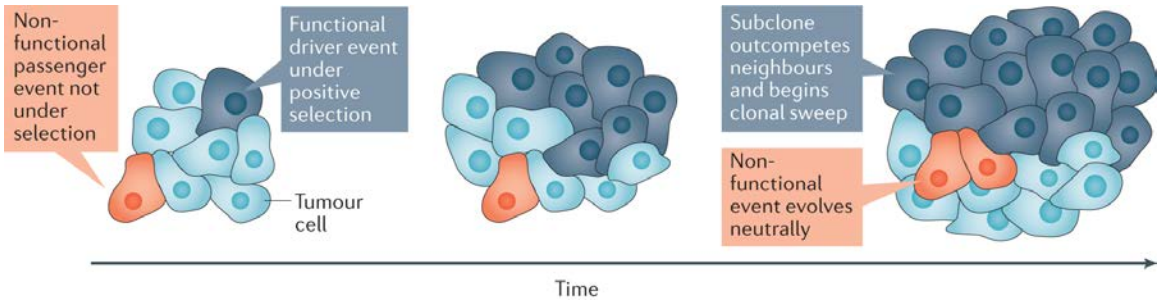

Figure 2. A simplified model of tumor evolution.

Variation within a tumor, through genetic and non-genetic mechanisms contributes to significant phenotypic diversity. Under selective pressure, such as during metastasis or in

response to therapy, sub-clonal populations of cells can outcompete other clones to reshape the tumor. Reprinted from[10] with permission from Springer Nature.

For many years it has been known that melanoma exhibits significant genetic heterogeneity. This can be at least partially explained by the high frequency of mutations in melanoma which are associated with exposure to ultraviolet radiation.[11] Other factors that contribute to significant intra and inter-tumor heterogeneity in melanoma and across cancer types more generally includes genomic instability.[4] Genomic instability can not only be caused by defects in DNA repair and replication machinery, but also by cellular stress induced by the tumor microenvironment.[8] Genomic instability is fundamentally linked to cancer evolution across tumor types.[8,12] In melanoma, significant work has been done to understand how genetic diversity contributes to tumor progression, phenotypic heterogeneity, and response to therapy.

Melanoma Mutational Burden & Response to Therapy

While melanoma is characterized by a high mutational burden there are several genetic alterations which are shared by most tumors. The most affected pathway is the Mitogen-activated protein kinase (MAPK) pathway, which is known to be mutated in about 80% of melanomas[13] (Figure 3). Constitutive activation of this pathway is sufficient to cause malignant transformation of melanocytes to melanoma[14] through dysregulation of growth signaling, apoptosis, and differentiation.[15] Within this pathway, BRAF, NRAS, and NF1 are the most frequently mutated.[16-20] Other common mutations that can cooperate with MAPK pathway activation include inactivating mutations in PTEN and CDKN2A, among others.[14,15,21,22] The high prevalence of driver mutations affecting MAPK signaling in melanoma makes components of this pathway ideal candidates for targeted therapy.

Numerous therapeutics have been developed; in particular, agents which target BRAF and MEK.[23-27] However, success of these inhibitors is limited by the ability of melanoma cells to evolve and develop resistance under selective pressure. This is thought to be due, in large part, to the significant intra-tumoral heterogeneity that exists in melanoma, enabling sub-clonal populations which have regained MAPK pathway activation or undergone alternative oncogenic transformation to expand and cause disease relapse (Figure 2 & 3).[8,9,15,28]

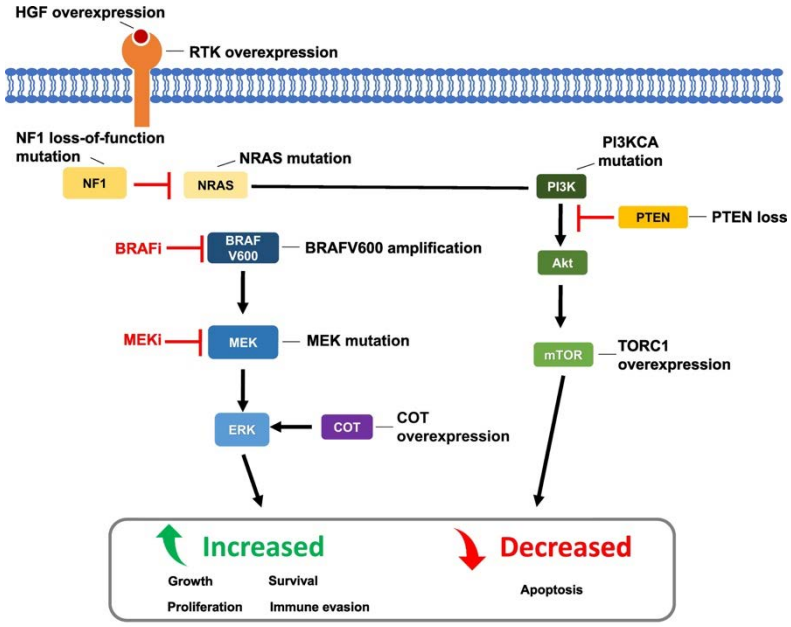

Figure 3. Common mutations & resistance mechanisms in cutaneous melanoma.

The MAPK pathway is frequently activated in melanoma, either through mutations in NRAS or BRAF. The most common targeted therapies are BRAF and MEK inhibitors, which are often used in combination. Resistance frequently occurs through reactivation of the pathway or through alternative mechanisms, some of which are shown here. Reprinted with permission from[29] under the Creative Commons Attribution 4.0 International License https://creativecommons.org/licenses/by-nc-nd/4.0/.

Combination Therapy & Immunotherapy

The prevalence of resistance to single agent targeted inhibitors of BRAF is well established.[15,30] For instance, treatment with BRAF inhibitors dabrafenib or vemurafenib

moderately increases progression free survival by approximately 6 months.[24,31,32] Resistance leading to relapse is largely due to the reactivation of the MAPK pathway through MEK,[30,33] leading to the introduction of combination therapies that enable simultaneous inhibition of BRAF and MEK.[27,31,34] This approach has further improved overall survival, however, unresectable or metastatic disease still presents a challenge. Another significant advancement in melanoma treatment was the development of immunotherapy, particularly immune checkpoint inhibitors. These therapies target the molecules PD-1/PD-L1 and CTLA-4, which serve as negative regulators of T-cell activation. In normal physiology, T-cell recognition of CTLA-4 or PD-L1 serves to temper T-cell response and is important in self vs. non-self-recognition. Importantly, by aberrantly expressing these proteins, tumor cells can escape surveillance by the immune system.[35,36] This knowledge led to the revolutionary idea to block these receptor-ligand interactions between tumor cells and T-cells, thereby allowing T-cells to recognize and target cancer cells for immune destruction.[35,36] Immune checkpoint therapy has been applied to numerous tumor types with clear efficacy.[37-40] In particular, this treatment option has revolutionized melanoma therapy with anti PD-1/PD-L1 and CTLA-4 therapeutics leading to significant survival improvements even in metastatic disease.[41-47] Although continued advancement has led to sharp increases in survival rates, even for advanced disease (from 15 to 35% between 2010 and 2019),[41] research into other mechanisms to target advanced and metastatic disease are still being explored.

Transcriptional Heterogeneity in Melanoma

Genetic variation is not sufficient to explain the significant intratumor heterogeneity that has long been observed in tumor cells.[48] In recent years, focus has shifted to emphasize the role of the epigenetic and transcriptional pathways which contribute to tumor evolution and disease progression. In particular, the popularity of the cancer stem cell (CSC) hypothesis highlighted the importance of transcriptional heterogeneity in tumor development.[49] This concept posits that there is a rare population of tumorigenic cells within a given tumor (CSCs) and that these cells undergo a hierarchical differentiation to give rise to the phenotypic diversity present within the tumor[49] (Figure 4). Modulation of transcriptional activity of specific genes or pathways, rather than mutations, could explain the underlying differences in intra-tumor differentiation state. However, while the cancer stem cell paradigm holds for certain cancer types, such as leukemia, it falls short in others, including melanoma[50]

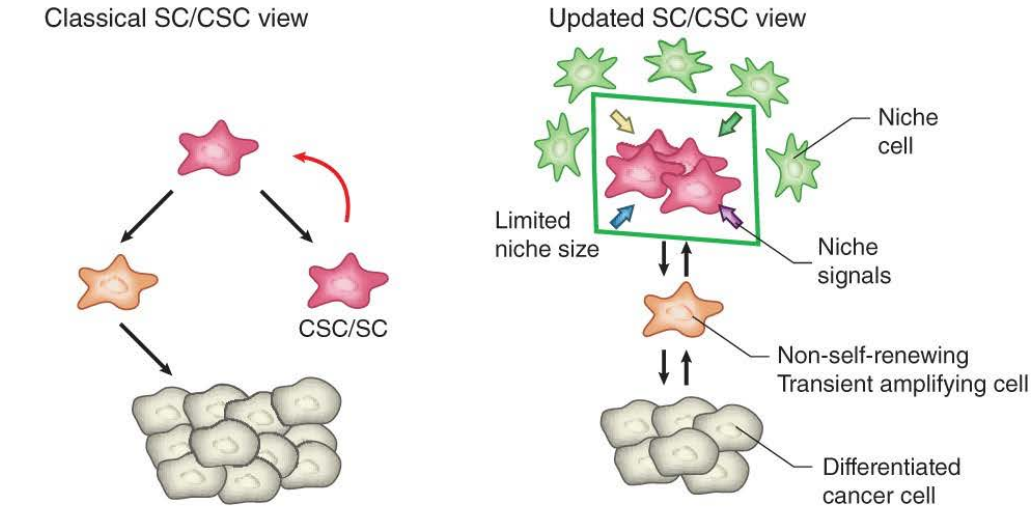

Figure 4. The cancer stem cell model.

On the left is the initial cancer stem cell hypothesis. This theory asserts that cancer stem cells can undergo a hierarchical differentiation trajectory that gives rise to the tumor cells while also self-renewing. On the right is the evolution of the cancer stem cell model. Here, cancer stem cells can be more abundant than previously thought and impacted by the surrounding microenvironment. In addition, differentiation is reversible, with more

differentiated cancer cells able to transit back to stem cells due to cell plasticity. This figure is adapted from[51] with permission from Springer Nature.

Transcriptional Heterogeneity & Phenotype Switching

In melanoma the presence of true cancer stem cells was debated for a number of years. Currently it is thought that melanoma cells undergo phenotype switching, whereby cells can transit reversibly between discrete cell states, some of which can be tumor-initiating (Figure 4).[52] These cell states have been extensively characterized by transcriptomic profiling, which demonstrates that cells within individual tumors present clear transcriptional heterogeneity. These transcriptional signatures are associated with distinct cellular phenotypes such as proliferation, migration, and invasion.[53,54] These findings are not limited to melanoma. In particular, with the advent of single cell RNA-seq (scRNA-seq), there has been a meaningful advancement in our understanding of the expression signatures that underlie diversity in cell states in many different cancer types. A recent study combined scRNA-seq data from 77 different studies across 24 tumor types to identify a number of "meta-programs" that define cell states within a tumor or across tumor types.[55]

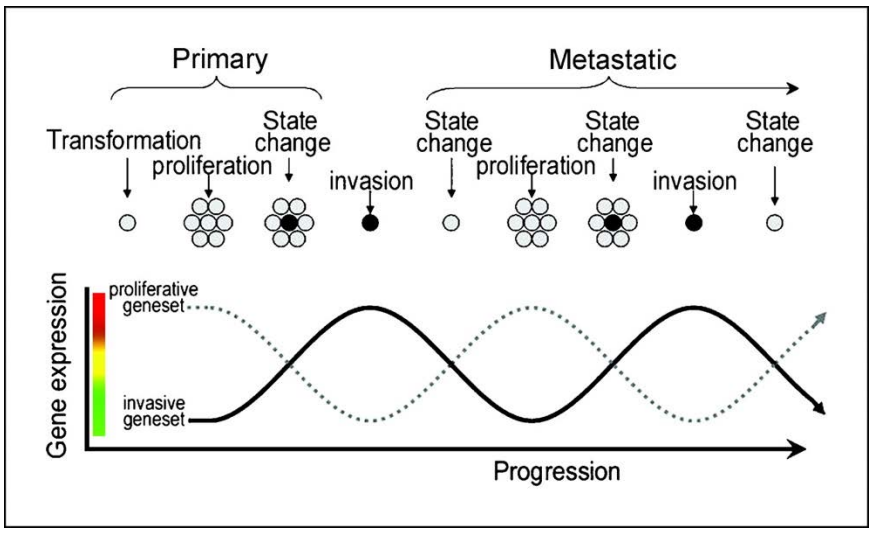

Figure 5. Phenotype switching in melanoma.

Melanoma cell lines can be grouped by transcriptomic signatures to define two distinct cell states during tumor development; proliferative and invasive. These states are highly plastic and reversible. This model proposes that through tumor development, from the primary tumor to metastasis, cells are switching between these two cell states by changing gene expression signatures. Reprinted from[54] with permission from the American Association for Cancer Research.

Melanoma Transcriptional Cell State

Although phenotype switching is not limited to melanoma, there has been significant advancement in our understanding of the different cell states that underlie melanoma intra-tumoral heterogeneity. This work began with the critical discovery that distinct transcriptional signatures can account for differences in metastatic potential. In a panel of 86 melanoma cell lines weakly metastatic/proliferative cells had a unique transcriptional profile compared to metastatic/invasive cells (Figure 5).[53] Numerous other studies have built off this data, using a combination of cell lines, human patient samples, and mouse in vivo modeling, to expand our understanding of the definition of these cell states, as well as the intermediate states that exist between the two.[3,53,54,56-59]

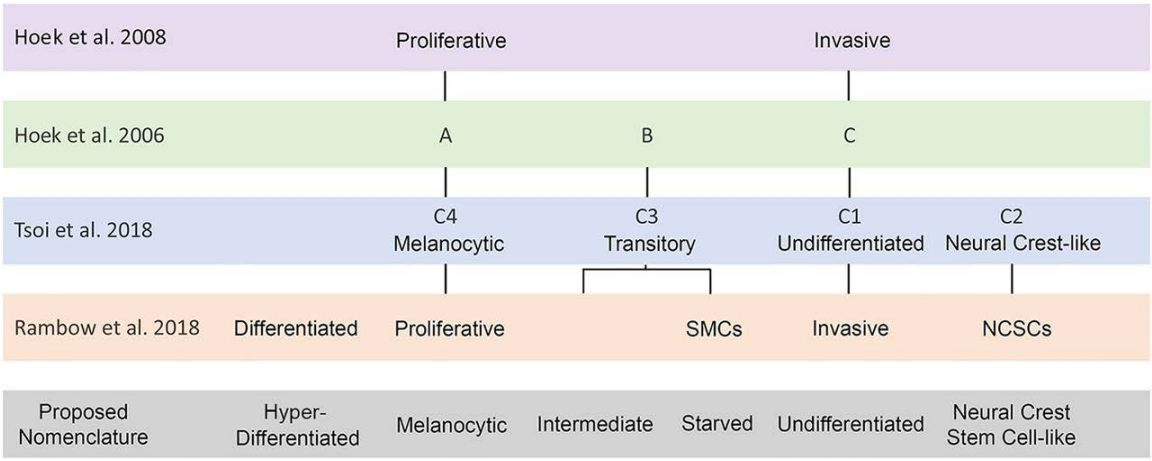

Figure 6. Evolution of melanoma transcriptional cell state definitions.

Since the initial description of melanoma transcriptional states by Hoek et al., several groups have added to the refinement of these states. It is now clear that intermediate

states can exist between proliferative and invasive cells. In addition, more invasive cells that are more neural crest-like, as well as hyper-differentiated and senescent cell states have also been identified. Reprinted from[56] under the Creative Commons Attribution 4.0 International License https://creativecommons.org/licenses/by-nc/4.0/.

While there are varying definitions of these cell states, it is generally accepted that melanoma cells exist on a phenotypic spectrum, from "undifferentiated" to "melanocytic" (Figure 6). This phenotypic spectrum also coincides with variation in MITF expression levels, which is described by the MITF rheostat model (Figure 7).[60]

MITF is a transcription factor in the MiT subfamily[61] and was first discovered for its role in normal melanocyte differentiation. Mutations in MITF in mice and humans cause albinism,[62-65] along with other phenotypes. This striking phenotype is due to the lack of melanocyte differentiation from their neural crest derivatives, leading to the absence of proper skin pigmentation.[63,65-67] These phenotypes highlight one major role of MITF which is also relevant in melanoma; the regulation of pigmentation and differentiation genes.[68] However, further study of MITF has demonstrated its ability to regulate numerous processes, including cell survival, metabolism, autophagy and lysosome biogenesis, as well as proliferation and invasion.[67] In melanoma, the MITF rheostat model posits that epigenetic mechanisms regulate MITF activity, and that high levels of MITF promote proliferation and differentiation, while low levels trigger cell cycle arrest and acquisition of invasive characteristics.[60] Although this model has been significantly expanded upon, particularly with increased understanding of the variety of downstream effects of MITF activity,[67] it is widely accepted that undifferentiated/invasive cells are $MITF^{LO}$ and melanocytic/proliferative cells are $MITF^{HI}$ (Figure 7).[56] In addition to MITF, numerous other transcription factors and epigenetic regulators have been identified which synergize with MITF and each other to regulate melanoma phenotypic state.[3,57,59]

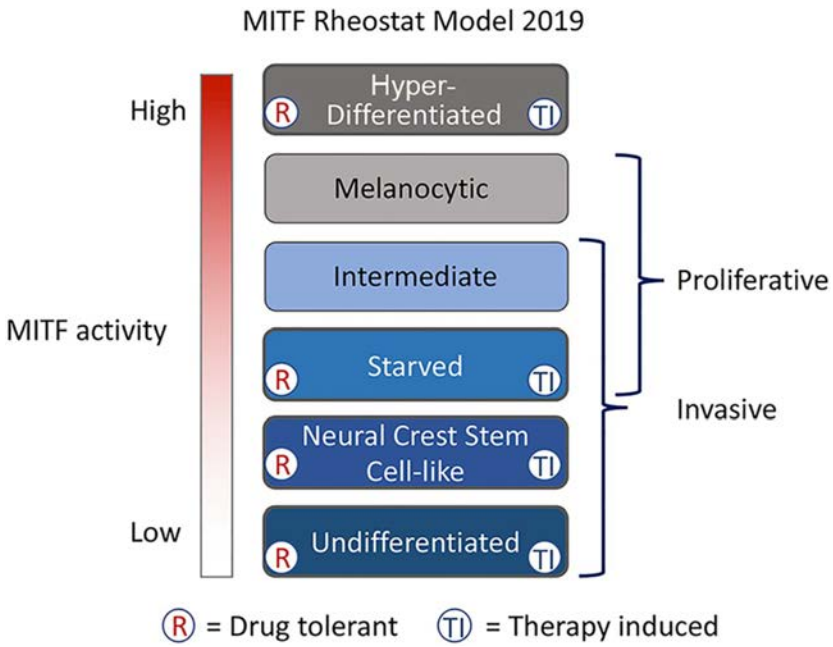

Figure 7. MITF Rheostat Model.

Melanoma cells can be grouped into different transcriptional cell states, ranging from undifferentiated to differentiated. These states are highly plastic and can be induced by therapy. The activity of the melanocyte transcription factor MITF can serve as a rheostat of these cell states, with high MITF correlating with the melanocytic, proliferative state and low MITF correlating with more undifferentiated, invasive cells. Reprinted from[56] under the Creative Commons Attribution 4.0 International License https://creativecommons.org/licenses/by-nc/4.0/.

Melanoma Phenotype Switching

Concomitant with the identification of these cell states it was discovered that melanoma cells can undergo phenotype switching to move between cell states.[54] One major driver of phenotype switching is thought to be changes in the tumor microenvironment (TME), whereby changes in the stromal cell population, access to nutrients, and treatment with therapeutics can trigger cells to reversibly transit between cell states.[56] While some of these cues have been identified[3,69-73] this remains an open area of investigation.

1.3 Lipid Metabolism

One mechanism by which the tumor microenvironment can influence cell state is through altered cellular metabolism, either in cells in the TME or in the cancer itself. During tumor development cancer cells encounter numerous metabolic challenges which can trigger adaptive rewiring not only of intracellular metabolism but also changes in transcriptional and epigenetic regulation and phenotypic state (Figure 8).[12,74,75] The metabolic challenges induced by the tumor microenvironment account for many aspects of cancer cell metabolism. For example, cells at the tumor core can have limited access to vasculature, resulting in hypoxia and nutrient restriction.[74,75] These restrictions stimulate numerous adaptive mechanisms within the tumor. Hypoxic conditions stabilize hypoxia inducible factor (HIFs) which are transcription factors that mediate metabolic rewiring and tumor adaptation to nutrient restriction.[76,77] One of the most well studied downstream targets of HIF is Vascular Endothelial Growth Factor (VEGF) which stimulates angiogenesis under hypoxic conditions. Increased angiogenesis can restore tumor access to oxygen and other nutrients essential to tumor growth.[78-80] In addition to nutrient restriction caused by limited access to vasculature, there are other metabolic challenges a cancer cell will face within the primary tumor, during invasion, and with metastatic spread to new sites. Interaction with diverse cell types in the tumor microenvironment further shapes the metabolic and phenotypic rewiring of cancer cells through mechanisms

such as inflammatory signaling, secretion of metabolites, and release of other signaling molecules.[75,81]

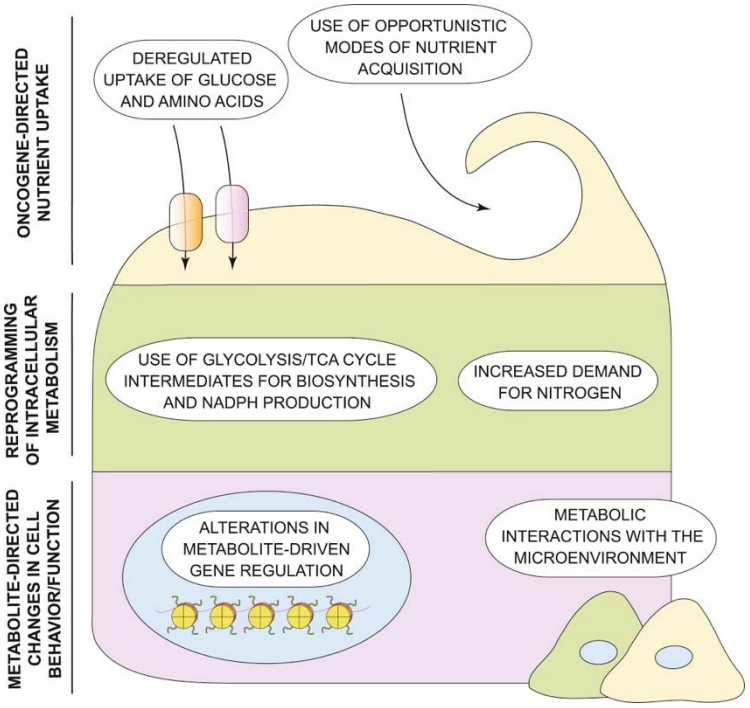

Figure 8. Hallmarks of cancer cell metabolism.

During tumor development cancer cells can significantly rewire their metabolism to adapt to the fluctuating nutrient demands associated with tumor growth, cell proliferation, and metastasis. These changes begin with differences in nutrient supply and uptake, followed by intracellular metabolic changes, which can lead to altered gene expression and therefore cell state. Reprinted from[74] with permission from Elsevier.

Lipid Metabolism in Cancer

Altered lipid metabolism, in both cell intrinsic and extrinsic pathways, has been shown to play a critical role in tumor evolution and progression across multiple cancer types. Acquisition of fatty acids, either through endogenous fatty acid synthesis, or through increased uptake from the tumor microenvironment can be significantly advantageous to the tumor (Figure 9). Regardless of their source, the cancer cell can utilize these metabolites for a variety of downstream pathways. Common examples include the production of Acetyl-CoA and NADPH through β-oxidation. Acetyl-CoA produced

through β-oxidation can then be used by the cancer cell as an alternative energy source to produce ATP as well as for epigenetic modification of chromatin.[82] As discussed above, epigenetic changes in the tumor cell can have significant consequences for tumor progression, for example as a driver of phenotype switching in melanoma.[56,83] In addition to Acetyl-CoA production, increased synthesis of fatty acids or uptake from the tumor microenvironment provides the cell with an increased and diverse lipid pool, which can be used to support increased cell division, membrane structure, and as bioactive signaling molecules.[82]

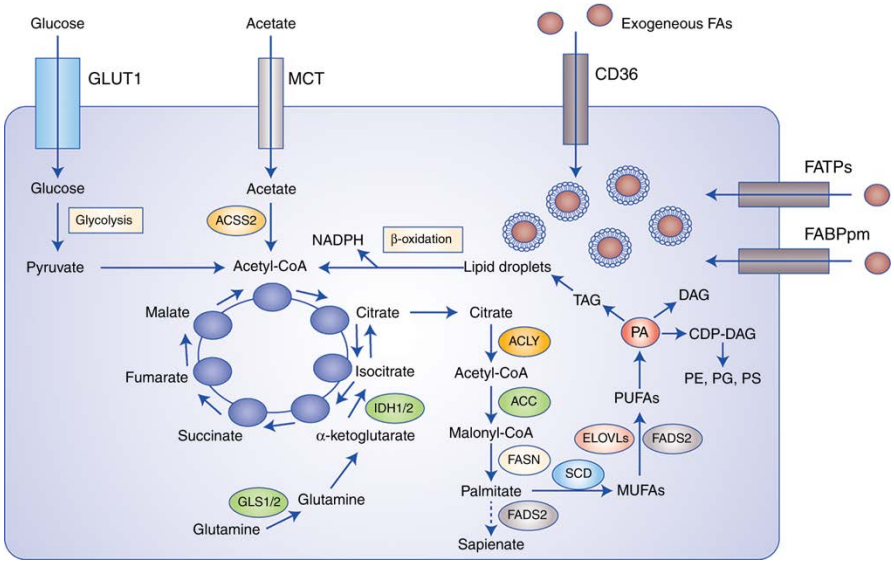

Figure 9. Lipid metabolism in cancer cells.

Cancer cells can acquire increased FA by two means: 1. By upregulating fatty acid transporters (CD36, FATPs, FABPs) to increase uptake from extrinsic sources. 2. By increasing rates of endogenous FA synthesis; through upregulation of FA synthesis enzymes and/or increased shuttling of other nutrients such as glucose and acetate towards FA production. Inside the cancer cell FA's can be used for ATP production through β-oxidation, epigenetic modifications through increased Acetyl-CoA production, storage in lipid droplets, or production of more complex lipids. Reprinted from[82] under the Creative Commons Attribution 4.0 International License http://creativecommons.org/licenses/by/4.0/

Fatty Acid & Lipid Uptake

Fatty acid and lipid uptake from the tumor microenvironment has been shown to affect tumor progression across multiple tumor types.[75] In order to acquire these metabolites from the TME, many tumors will upregulate fatty acid transporters (Figure 9). For instance, in oral carcinoma higher levels of the fatty acid transporter CD36 is advantageous during initiation of metastasis.[84] In addition, during ovarian tumor progression, upregulation of the Fatty Acid Binding Protein FABP4 supports metastatic growth presumably through increasing fatty acid uptake to support increased β-oxidation within the tumor.[85] Similar observations have been seen in additional tumor types such as breast and prostate cancer,[82,86,87] as well as melanoma. During melanoma tumor progression higher levels of the Fatty Acid Transport Protein 1 FATP1 facilitate increased uptake of fatty acids from adipocytes in the tumor microenvironment. Increased FA levels in the tumor were demonstrated to support cell proliferation and invasion during metastasis.[88] Similarly, in the aged TME, melanoma cells will increase the expression of Fatty Acid Transport Protein 2 (FATP2) to increase FA uptake from aged fibroblasts.[89] Independent of the FATP family, other studies have found additional pathways for fatty acid and lipid uptake from the tumor microenvironment to support melanoma progression.[90,91] Similar to what has been shown in other tumor types, a major downstream effect of increased FA uptake is increased production of Acetyl-CoA through β-Oxidation, driving metabolic and epigenetic changes in the tumor cell.[83,88,92,93]

Endogenous Fatty Acid and Lipid Metabolism

Increased FA and lipid uptake is only one aspect of FA metabolism that can be altered in cancer.[94] Alternative to uptake, the other way that cancer cells can increase fatty acid levels is by increasing endogenous fatty acid synthesis (Figure 9). One of the most common ways to do this is through upregulation of individual enzymes required for fatty acid synthesis such as Fatty Acid Synthase (FASN),[95,96] ACLY,[97,98] and ACSS2.[94,99] In melanoma, upregulation of fatty acid synthesis has been linked to the increased transcriptional activity of sterol regulatory element-binding protein 1 (SREBP1).[100] SREBP1 belongs to the SREBP family which is the major regulator of numerous fatty acid and lipid metabolism genes, including the enzymes which are required for fatty acid synthesis. These transcription factors are also frequently altered in cancer.[82] In addition to increased FA synthesis, downstream processing of FAs into more complex lipid species can play key roles in cancer progression. In melanoma, stearoyl-CoA desaturase (SCD) controls the levels of saturated (SFAs) vs. monounsaturated FAs (MUFAs) in the cell. This balance is linked to the activity of MITF and in turn melanoma cell state. Undifferentiated, $MITF^{LO}$ cells have lower levels of SCD, which leads to increase SFA levels. Higher SFA levels can in turn affect differentiation state, inflammatory signaling, and membrane homeostasis.[71] Thus, regardless of fatty acid source, downstream effects of increased fatty acid levels can have meaningful impacts on melanoma cell state and tumor progression.

1.4 Lipid droplets

Lipid Droplet Structure and Formation

One downstream fate for fatty acids in both normal cells and cancer is storage in specialized storage organelles called lipid droplets. The primary components of a lipid droplet are a lipid rich core surrounded by a phospholipid monolayer which contains peripheral and integral membrane proteins (Figure 10).[101,102] The majority components of the neutral lipid core are triacylglycerols and sterol esters,[102,103] however, additional components can include retinyl esters, wax esters, ether lipids, and others,[104-106] with relative abundance varying depending on cell type.[107] Lipid droplets sequester and regulate release of these lipid species to perform a variety of functions within the cell.

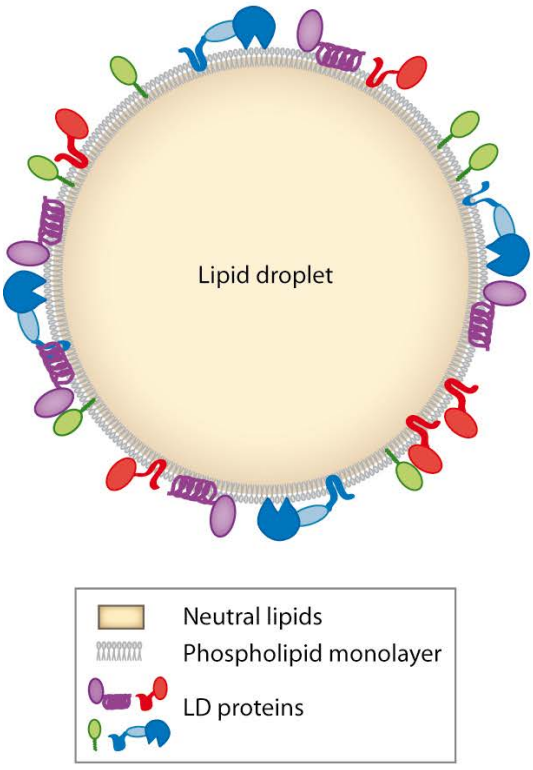

Figure 10. Lipid droplet structure.

Lipid droplet structure is defined by a phospholipid monolayer surrounding the lipid core. The proportion of neutral lipid species within the core can vary depending on cell type, as well as the number, localization, and size. Reprinted from[107] with permission from Annual Reviews, Inc.

Lipid droplet formation begins with neutral lipid synthesis, for instance of TAGs, between the leaflets of the endoplasmic reticulum (ER) (Figure 11). The rate limiting enzymes required for the esterification of fatty acids into TAGs are Diacylglycerol O-acyltransferase 1 and 2 (DGAT1 and DGAT2).[108-110] As the concentration of neutral lipids between the monolayers increases above 3 mol%[111] phase separation occurs and a lipid lens will form.[112] After lipid lens formation, several proteins are recruited to the emerging lipid droplet to facilitate lipid droplet budding and maturation. Collectively, these are referred to as lipid droplet assembly complexes (LDACs) which contain the protein seipin and its interacting protein LDAF1.[112,113] Seipin was identified for its role in facilitating lipid droplet maturation from nascent lipid droplets.[114] Further work has revealed that seipin forms an oligomeric cage-like structure,[115] which together with LDAF1 promotes LD formation at specific sites and a lower TAG concentration.[114] Lipid droplet formation and budding from the ER facilitated by LDACs is required to make mature lipid droplets. These droplets will then go on to perform a variety of functions within the cell including regulated release of fatty acids, interaction with other organelles, and buffering of lipotoxicity, among others.

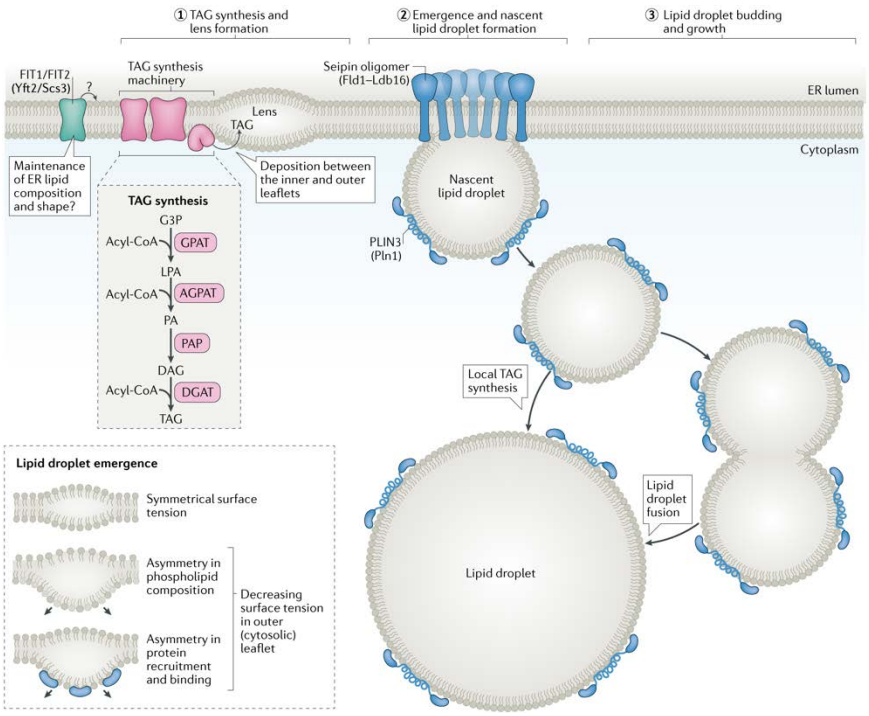

Figure 11. Overview of lipid droplet formation.

Triacylglycerols are synthesized at the ER membrane and accumulate between the two bilayers. As TAG levels increase, seipin oligomerizes and facilitates lipid droplet formation and budding from the ER. After budding, mature lipid droplets can undergo cycles of shrinkage (lipolysis), growth (local TAG synthesis), as well as fusion with other lipid droplets. Reprinted from[101] with permission from Springer Nature.

The Lipid Droplet Proteome

Beyond the lipid components of the lipid droplet, protein localization at the droplet is critical to its function. Lipid droplet proteins are thought to be grouped into two classes, Class I and Class II proteins. Class I proteins are localized to the ER and diffuse laterally through the membrane to the lipid droplet during lipid droplet formation.[116,117] Typically, these proteins have a hydrophilic hairpin structure that is inserted into the membrane. On the other hand, Class II proteins are found in the cytosol and localize to the lipid droplet through an amphipathic helix.[116,117] Additionally, proteins can also be associated with lipid droplets through the presence of a lipid modification or by binding to proteins already present on the lipid droplet (Figure 12).[118]

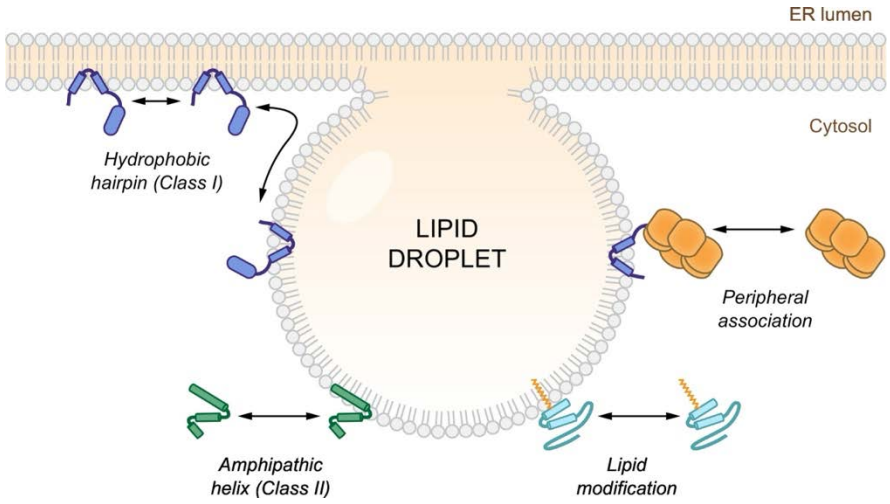

Figure 12. Lipid droplet proteins.

Beyond the lipid components of the droplet, LDs contain many proteins embedded in the phospholipid monolayer. These are generally grouped into Class I and Class II proteins. Proteins can also associate with the lipid droplet through lipid anchors, or by forming complexes with existing lipid droplet proteins. Reprinted from[118] with permission from Elsevier.

Regardless of their mechanism of association, lipid droplet proteins are required for lipid droplet function. During the life cycle of the droplet, it can undergo significant shrinkage and expansion. During expansion, association of proteins like GPAT4 and DGAT2, for TAG synthesis,[119] and CCTα are critical. CCTα binding to lipid droplets is required to catalyze the phosphatidylcholine necessary for expansion of the phospholipid monolayer, which maintains proper LD structure.[120] In addition, lipid droplet shrinkage can be due to lipolytic breakdown by lipolysis machinery. Localization of the enzymes MGL, HSL, and ATGL to the lipid droplet is required for lipolysis and free fatty acid (FFA) release from the droplet.[121]

Outside of alterations in lipid droplet size, differential localization of proteins to the lipid droplet can facilitate interaction with various organelles including, but not limited to, mitochondria, lysosomes, and peroxisomes.[101] For example, it is thought that lipid droplets can be tethered to the mitochondria to facilitate efficient exchange of FFAs to the

mitochondria during lipolysis, although the proteins which mediate these interactions have not been fully elucidated.[122,123] Finally, studies have shown an unexpected role for the lipid droplet in sequestering proteins inside the cell, including the transcription factor MLX and histone proteins.[124,125]

Approaches to Lipid Droplet Proteomics

Given the diverse and dynamic localization of proteins to the lipid droplet discussed above, there have been many attempts to characterize the lipid droplet proteome in a number of contexts. Early studies of the lipid droplet proteome have relied mainly on traditional approaches of density gradient ultracentrifugation.[126-128] While these studies have yielded significant insight into how the lipid droplet proteome is remodeled,[128-132] they are complicated by the close association of lipid droplets to other organelles, most significantly the ER. Contamination of LD proteome datasets with ER proteins has led to the development of additional approaches to further enrich for true lipid droplet proteins. One method to do this is by applying Protein Correlation Profiling to traditional lipid droplet isolation techniques.[133] This approach utilizes known markers of each organelle or cellular compartment to map the location of proteins in each fraction.[134] Application of this method to lipid droplet proteomics has generated high confidence lipid droplet proteomes and enabled the study of dynamic re-localization of proteins to the lipid droplet under different contexts.[122,133] Another approach to reduce contamination from other membranes utilizes proximity labeling methods. By combining APEX2 proximity labeling of lipid droplet proteins with density gradient methods, it is possible to generate highly enriched lipid droplet proteomes that are relatively devoid of contaminants (Figure

13).[135,136] This approach eliminates the complex analytical steps required for Protein Correlation Profiling. These recent advances in lipid droplet proteomics have been collated into a lipid droplet protein database; The Lipid Droplet Knowledge Portal.[137] The database combines several high confidence lipid droplet proteomics datasets with functional studies of lipid droplet proteins to serve as a repository of knowledge on lipid droplet regulation. These approaches and resources serve as valuable tools to further the study of lipid droplet regulation in a variety of contexts which can be relevant in both normal physiology and disease.

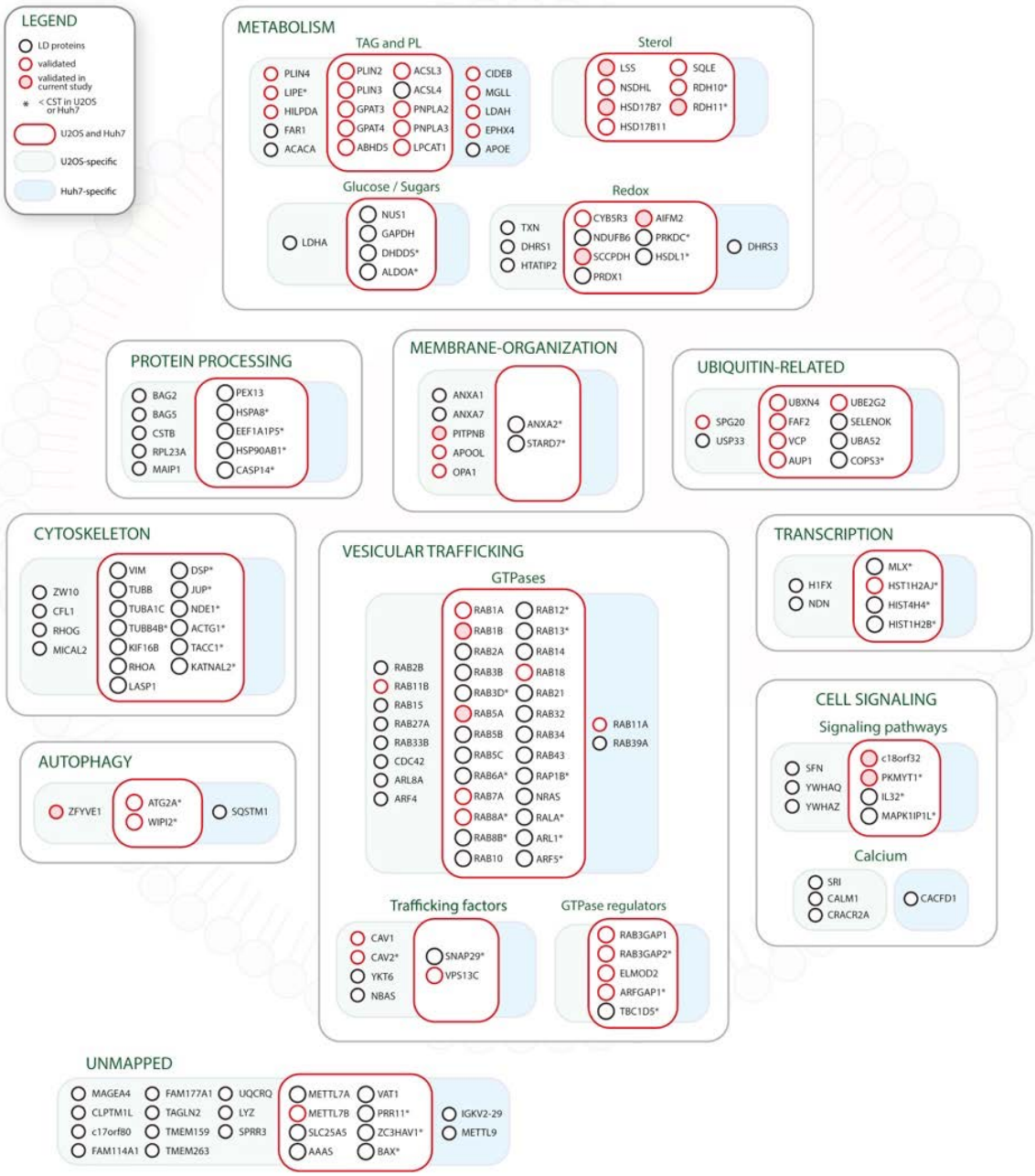

Figure 13. Consensus LD proteome by APEX2 proximity labeling.
Lipid droplet proteins from Huh7 and U2OS cell lines were characterized by mass spectrometry. Shown is the overlap between the two proteomes which yields a high confidence consensus LD proteome. Additionally, this highlights that while many LD proteins are shared, there are several which are unique to each cell line. Reprinted from[135] with permission from Elsevier.

Lipid Droplets in Cancer

As touched on above, lipid droplets can have diverse functions within the cell, many of which are mediated by lipid droplet proteins. These functions can include buffering of lipotoxicity, protection against ER stress and oxidative stress, interaction with other organelles, and sequestration of specific or damaged proteins.[132,138-143] Importantly, many of these functions have begun to be appreciated in the context of cancer.[144] The functions of the lipid droplet in buffering cellular stress are co-opted by the cancer cell to promote cell survival and proliferation (Figure 14). During oxidative stress, lipid droplets can sequester polyunsaturated fatty acids (PUFAs) to prevent lipid peroxidation which can lead to ferroptotic cell death.[145,146] In addition, regulated release of lipids from the droplet prevents ER stress and supports the increased cell proliferation which is characteristic of cancer cells.[147] Furthermore, storage of excess fatty acids inside LDs not only prevents lipotoxicity but can also serve as an energetic reservoir when cancer cells are under nutrient stress.[148,149] While the role of lipid droplets in cancer is still an active area of investigation these points are meant to highlight the diverse supportive functions that LDs can have in this disease context.

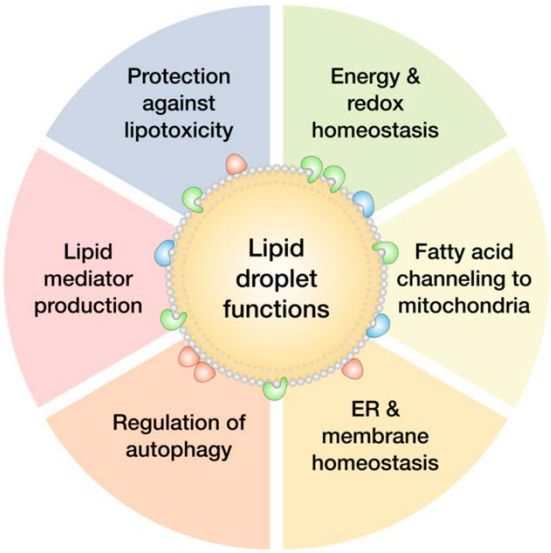

Figure 14. The role of lipid droplets in cancer.

Lipid droplets are increasingly appreciated for their diverse roles in cancer. Lipid droplets can buffer various forms of cellular stress which are frequently implicated in cancer. Reprinted from [150] under the Creative Commons CC BY 4.0 License.

Lipid Droplets and Melanoma

The role of lipid droplets in contributing to tumor progression has begun to be appreciated in melanoma. During melanoma growth, increased uptake of fatty acids from adipocytes in the TME leads to storage of excess lipids in lipid droplets.[88] Importantly, the ability to form lipid droplets is critical for melanoma progression.[93,151] Overexpression of Diacylglycerol O-acyltransferase 1 (DGAT1) can cooperate with both BRAF and NRAS to increase the rate of tumorigenesis.[151] DGAT1 is required for triacylglycerol (TAG) synthesis and has been shown to be critical for lipid droplet formation.[108-110] Conversely, knock-out of DGAT1 slows tumor progression in a $BRAF^{V600E}$ model of melanoma.[93] This data suggests that lipid droplet formation is required to support melanoma tumor growth. Furthermore, melanocytic melanoma cells rely on lipid droplets to support a more oxidative cell state.[93] Although this work

highlights the importance of lipid droplets in melanoma, further work is needed to better understand how lipid droplet regulation synergizes with other aspects of the tumor microenvironment, cancer cell metabolism, and cell fate.

Imaging of Lipid Droplets in Melanoma

Like all organelles, robust imaging methods are needed to study all aspects of lipid droplet biology. In the context of in vivo melanoma modeling, the tools to study lipid droplet accumulation in tumor cells and the TME are relatively limited. Mouse models of melanoma and other lipid droplet associated diseases exist, however, imaging of lipid droplets in these contexts generally relies on sectioning of fixed tissues,[152] or whole mount approaches which are limited by tissue thickness.[152,153] Given the dynamic nature of lipid droplets, and their ability to change and accumulate over time, live imaging approaches are essential to further our understanding of their role in melanoma. Lipid droplet reporters, created by fusing a lipid droplet protein to a fluorophore, have been successfully employed in cell lines and invertebrate organisms.[154-157] However, these systems have their limitations, particularly in the context of melanoma, given that Drosophila and C. Elegans do not have melanocytes.

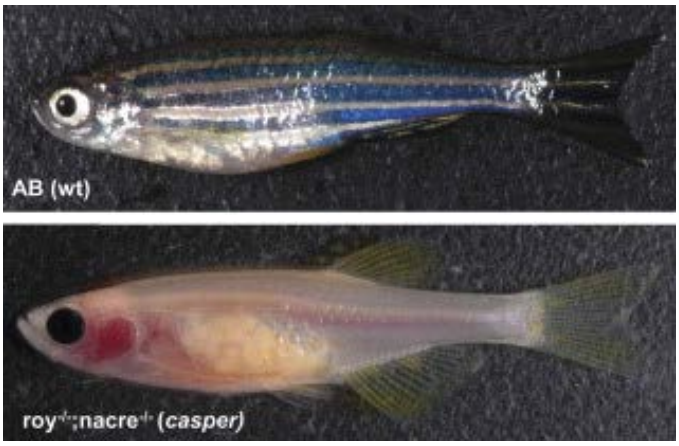

Figure 15. Casper zebrafish as a tool for imaging.

The top image is a WT fish which possesses the typical pigment pattern made up of xanthophores, iridophores, and melanophores. The bottom image is the casper zebrafish, which are devoid of all three pigment cell lineages through the mutations mitfa$^{-/-}$, and mpv17$^{-/-}$. Adapted from[158] with permission from Elsevier.

Zebrafish are an established model organism to study melanocytes and melanoma.[159,160] Key benefits of the zebrafish include high fecundity, ease of genetic manipulation, and the ability to conduct high throughput, high resolution imaging. In addition, the development of the transparent *casper* zebrafish[158] further magnified their utility in studying melanoma. *Casper* zebrafish are *mitfa*$^{-/-}$, *mpv17*$^{-/-}$, resulting in a complete lack of skin pigmentation (Figure 15).[158] This makes the line well suited for in vivo modeling of melanoma with high resolution imaging of developing tumor cells.[158,161] More recent technology, which focally induces melanoma tumor growth in an immunologically competent zebrafish[162,163] has further increased the ability to study in vivo tumor development at single cell resolution. Combining these technologies with lipid droplet imaging approaches presents a unique opportunity to study lipid droplet dynamics in the tumor and the tumor microenvironment.

Recent discoveries highlight the role of lipid metabolism and lipid droplets in melanoma. In addition, advances in the study of lipid droplets, through proteomics and imaging approaches, present an opportunity to advance our understanding of how lipid droplets are regulated in this lineage, and how this may impact melanoma development and progression.

CHAPTER 2: AN IN VIVO REPORTER FOR TRACKING LIPID DROPLET DYNAMICS IN TRANSPARENT ZEBRAFISH

This chapter is based on the following published manuscript:

Reproduced here under the Creative Commons CC-BY 4.0 License

Lumaquin D*, Johns E*, Montal E, Weiss JM, Ola D, Abuhashem A, White RM. An in vivo reporter for tracking lipid droplet dynamics in transparent zebrafish. *Elife*. 2021 Jun 11;10:e64744. doi: 10.7554/eLife.64744. PMID: 34114952; PMCID: PMC8195600.

2.1 Abstract

Lipid droplets are lipid storage organelles found in nearly all cell types from adipocytes to cancer cells. Although increasingly implicated in disease, current methods to study lipid droplets in vertebrate models rely on static imaging or the use of fluorescent dyes, limiting investigation of their rapid in vivo dynamics. To address this, we created a lipid droplet transgenic reporter in whole animals and cell culture by fusing tdTOMATO to Perilipin-2 (PLIN2), a lipid droplet structural protein. Expression of this transgene in transparent *casper* zebrafish enabled in vivo imaging of adipose depots responsive to nutrient deprivation and high-fat diet. Simultaneously, we performed a large-scale in vitro chemical screen of 1280 compounds and identified several novel regulators of lipolysis in adipocytes. Using our *Tg(-3.5ubb:plin2-tdTomato)* zebrafish line, we validated several of these novel regulators and revealed an unexpected role for nitric oxide in modulating adipocyte

lipid droplets. Similarly, we expressed the PLIN2-tdTOMATO transgene in melanoma cells and found that the nitric oxide pathway also regulated lipid droplets in cancer. This model offers a tractable imaging platform to study lipid droplets across cell types and disease contexts using chemical, dietary, or genetic perturbations.

2.2 Main Text

Introduction

Lipid droplets are cellular organelles that act as storage sites for neutral lipids and are key regulators of cellular metabolism.[119] Lipid droplets are present in most cell types and are characterized by a monophospholipid membrane surrounding a hydrophobic lipid core.[102,119] Cells maintain energetic homeostasis and membrane formation through the regulated incorporation and release of fatty acids and lipid species from the lipid droplet core.[164-167] Importantly, lipid droplets can assume various functions during cellular stress through the sequestration of potentially toxic lipids and misfolded proteins,[138,140,168,169] maintenance of energy and redox homeostasis,[157,170] regulation of fatty acid transfer to the mitochondria for β-oxidation,[123,171] and the maintenance of endoplasmic reticulum (ER) membrane homeostasis.[139,168,172,173] Moreover, a recent study demonstrated that lipid droplets actively participate in the innate immune response[174] and, conversely, can be hijacked by infectious agents like hepatitis C virus to facilitate viral replication.[175-177] The role of lipid droplets in metabolic homeostasis and cellular stress is critical across multiple cell types and has also been increasingly implicated in cancer. For example, lipid droplets can act as a

storage pool in cancer cells after they take up lipids from extracellular sources, including adipocytes.[85,88,178]

Lipid droplets are ubiquitous across most cell types; however, they are essential to the function of adipocytes in regulating organismal energy homeostasis.[167,179] White adipocytes, which contain a large unilocular lipid droplet, can be readily labeled by lipophilic dyes.[180,181] However, in vivo imaging of lipid droplets, in adipocytes or other cell types, is currently highly limited. Understanding the dynamics of lipid droplets in vivo, rather than in fixed tissues, is important since the size of the lipid droplet can change very rapidly in response to fluctuating metabolic needs.[174,181] In mice, much of adipose tissue imaging utilizes tissue fixation and sectioning, which can fail to preserve key aspects of the tissue structure.[152,182] Whole-mount imaging approaches in mice can be combined with adipocyte-specific promoters; however, these methods still require tissue dissection and can be limited by tissue thickness.[153,183] Zebrafish offer a tractable model to address these limitations given the ease of high-throughput imaging of live animals. This is especially true with the availability of relatively transparent strains such as *casper*, which allows for detailed in vivo imaging without the need for fixation of the animal.[158] Although less well studied than other vertebrates, zebrafish adipose tissue is highly similar to mammalian white adipose tissue, and a detailed work has classified the timing, dynamics, and location of zebrafish adipose tissue development.[180] Current imaging approaches using lipophilic fluorescent dyes or analogs in vivo have advanced our understanding of lipid droplets in adipocytes and other cell types;[180,184-188] however, these methods can require extensive and repeated staining, which may restrict the ability to read out dynamic

changes over time. Furthermore, fluorescent dyes such as BODIPY and NileRed have limitations in their specificity for the lipid droplet.[189] Finally, although a probe-free imaging approach to study subcellular lipid populations has been recently described,[190] this method is restricted to early-stage zebrafish, which would fail to capture post-embryonic cell populations and tissues, including adipocytes.

Here, we report the development of an in vivo lipid droplet reporter using a -*3.5ubb:plin2-tdTomato* transgene in the *casper* strain. To date, transgenic lipid droplet reporters have been restricted to cell culture systems and invertebrate model organisms such as Caenorhabditis elegans (C. elegans) and Drosophila,[154-157] although a similar approach in zebrafish was recently described while this manuscript was in review.[191] We demonstrate that the -*3.5ubb:plin2-tdTomato* reporter faithfully marks the lipid droplet, which enables robust in vivo imaging. We show that this reporter can be applied to visualize adipocytes and to monitor adipose tissue remodeling in response to dietary and pharmacologic perturbations. Furthermore, we report the discovery of novel pharmacologic regulators of adipocyte lipolysis such as nitric oxide and demonstrate that several of these compounds can modulate adipose tissue area in our in vivo system. To facilitate the study of lipid droplets in novel contexts outside of adipocytes, we also generated a zebrafish melanoma cell line (ZMEL)[161] expressing -*3.5ubb:plin2-tdTomato* (ZMEL-LD). We confirm that this cell line can be used to monitor changes in lipid droplet production in response to both known and novel regulators of lipolysis. We anticipate that these models will be highly valuable as a high-throughput imaging platform to investigate lipid droplets in both adipose tissue biology and disease contexts such as cancer.

An in vivo lipid droplet reporter using a PLIN2-tdTOMATO fusion transgene

To create a specific fluorescent reporter for lipid droplets in zebrafish, we fused *tdTomato* to the 3' end of the *plin2* cDNA. We chose *plin2* because it is a well-known lipid droplet-associated protein that is ubiquitously expressed on lipid droplets across cell types.[101] We generated stable transgenic zebrafish expressing -*3.5ubb:plin2-tdTomato* and sought to validate whether the construct faithfully marks lipid droplets (Figure 16A). White adipocytes are fat cells known for their large unilocular lipid droplet,[192,193] so we expected expression of the PLIN2-tdTOMATO fusion protein on the surface of the adipocyte lipid droplet (Figure 16A). Since the adipocyte lipid droplet occupies the majority of space in the cell,[194] existing methods to visualize zebrafish adipocytes rely on lipophilic dyes and lipid analogs, which incorporate into the lipid droplet.[88] Thus, in addition to labeling individual lipid droplets, we reasoned that the PLIN2-tdTOMATO fusion protein can also function as a reporter for adipocytes since these cells would have the largest and unilocular lipid droplets. In adult zebrafish, subcutaneous adipocytes are known to reside proximally to the tail fin.[180] When we imaged 6-month-old adult *Tg(-3.5ubb:plin2-tdTomato)* zebrafish, we detected PLIN2-tdTOMATO expression in the zebrafish tail fin adipocytes, which colocalized with BODIPY staining (Figure 16B-C). Lipophilic dyes such as BODIPY stain the lipid-rich core of the lipid droplet while lipid droplet resident proteins, such as PLIN2, localize to the lipid droplet membrane.[88] As expected, higher magnification images of tail adipocytes revealed that PLIN2-tdTOMATO expression was on the outside of the lipid droplet, whereas the BODIPY staining was on the interior of each droplet in the adipocyte (Figure 16D).

Similarly, immunohistochemistry (IHC) on the *Tg(-3.5ubb:plin2-tdTomato)* zebrafish tail fin showed that adipocytes express tdTOMATO (Figure 16E). Taken together, this data demonstrates that the PLIN2-tdTOMATO fusion protein functions as a fluorescent lipid droplet reporter that can be applied to visualize adipocytes in vivo.

Figure 16

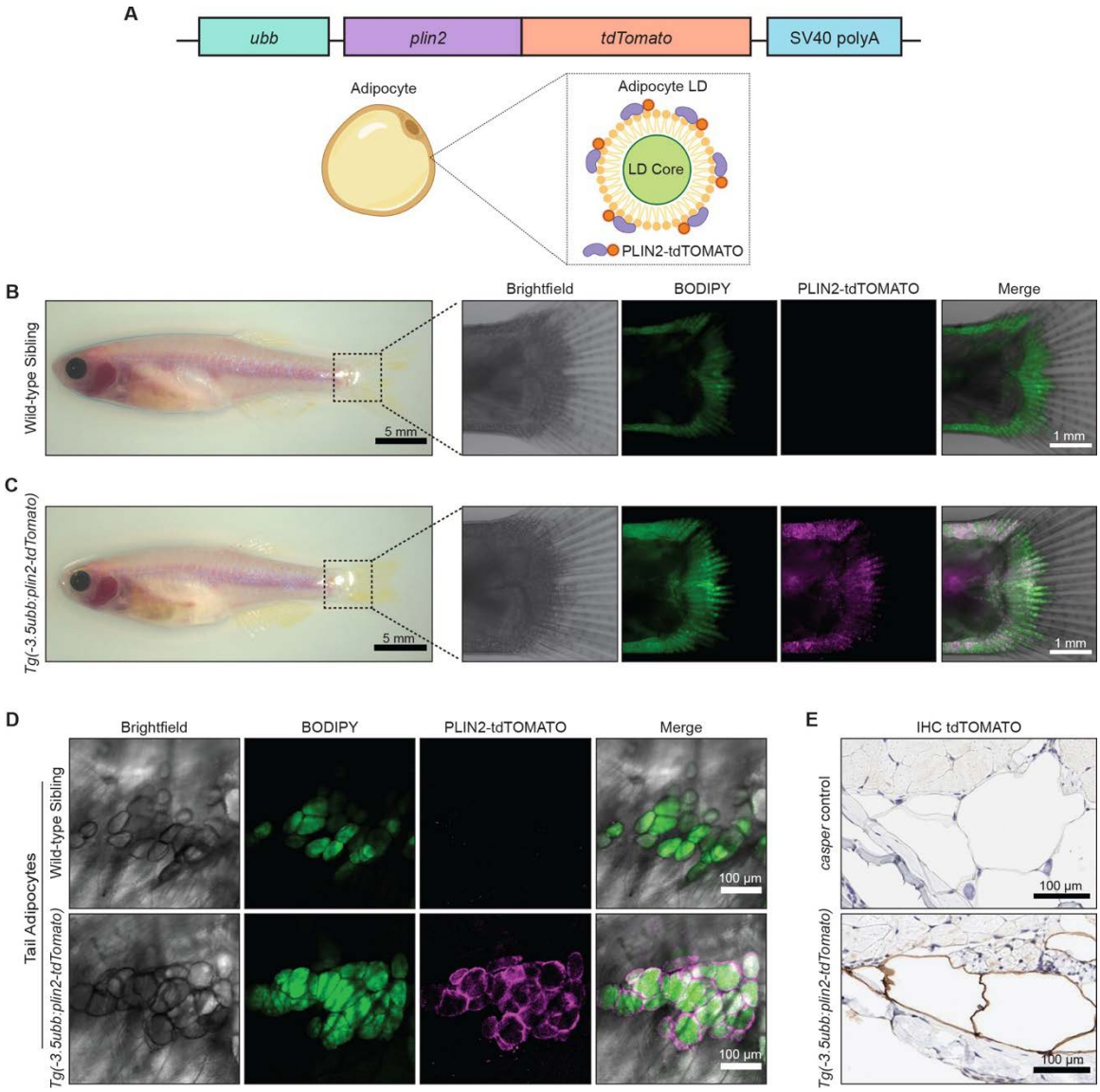

Figure 16. An in vivo lipid droplet reporter using a PLIN2-tdTOMATO fusion transgene.

(A) Schematic of ubb:plin2-tdTomato construct injected into zebrafish and an adipocyte lipid droplet labeled with PLIN2-tdTOMATO fusion protein. Widefield microscope images of adult (B) wild-type sibling and (C)Tg(-3.5ubb:plin2-tdTomato) zebrafish. Box

shows zoomed images of the fish tail with panels for brightfield, BODIPY, PLIN2-tdTOMATO, and merge. (D) Confocal images of fish tail adipocytes of adult wild-type sibling and Tg(-3.5ubb:plin2-tdTomato) zebrafish. Panels show brightfield, BODIPY, PLIN2- tdTOMATO, and merge. (E) Adult casper and Tg(-3.5ubb:plin2-tdTomato) zebrafish tails were fixed and immunohistochemistry was conducted for tdTOMATO expression of tail adipocytes.

The *Tg(-3.5ubb:plin2-tdTomato)* is an in vivo reporter for visceral adipocytes

Visceral adipose tissue, otherwise known as abdominal fat, plays an important role in metabolism and participates in pathological processes of obesity, aging, and metabolic syndromes.[195] Because PLIN2-tdTOMATO labeled subcutaneous adipocytes in the adult zebrafish tail fin, we wondered whether we could use the *Tg(-3.5ubb:plin2-tdTomato)* zebrafish to visualize other adipose depots in vivo such as visceral adipocytes. In 21 days post-fertilization (dpf) zebrafish, visceral adipose tissue is composed of abdominal and pancreatic visceral adipocytes predominantly located on the right flank near the swim bladder (Figure 17A).[180] To determine whether *Tg(-3.5ubb:plin2-tdTomato)* visceral adipocytes express PLIN2-tdTOMATO, we imaged around the swim bladder of zebrafish where we expected development of abdominal visceral adipocytes (Figure 17B). Visceral adipocytes visualized in brightfield demonstrate colocalization of PLIN2-tdTOMATO and BODIPY, as we observed for subcutaneous adipocytes (Figure 17C). IHC confirmed that the abdominal and visceral adipocytes of *Tg(-3.5ubb:plin2-Tomato)* express tdTOMATO (Figure 17G).

Previous studies have shown that overexpression of perilipin proteins alters lipid accumulation in adipocytes.[196] To test whether constitutive expression of our PLIN2-tdTOMATO transgenes altered adiposity, we compared the visceral adipose tissue of *Tg(-3.5ubb:plin2-tdTomato)* fish to their wild-type siblings. Using BODIPY staining, we did not detect differences in visceral adipose tissue area (Figure 17D). In addition to dpf,

standard length can indicate developmental progress in zebrafish.[197] Similarly, we found no difference in standard lengths between wild-type siblings and *Tg(-3.5ubb:plin2-tdTomato)* at 21 dpf (Figure 17E). We normalized visceral adipose tissue area to standard length, similar to a Body Mass Index (BMI) in mammals, and did not detect differences between wild-type and *Tg(-3.5ubb:plin2-tdTomato)* fish (Figure 17F). To comprehensively assess whether constitutive PLIN2-tdTOMATO expression alters adiposity, we imaged adipose depots of wild-type and *Tg(-3.5ubb:plin2-tdTomato)* zebrafish from 5 dpf larvae to adult fish. Using BODIPY staining to visualize adipose tissue, we observed similar development of the major adipose depots between wild-type and *Tg(-3.5:ubbplin2-tdTomato)* zebrafish (Figure 18A-B—related to Figure 17). Furthermore, we detected PLIN2-tdTOMATO expression at the corresponding time points and adipose depots within *Tg(-3.5ubb:plin2-tdTomato)* (Figure 18A-B—related to Figure 17). Thus, the *Tg(-3.5ubb:plin2-tdTomato)* zebrafish faithfully recapitulates normal adipose tissue development.

Figure 17

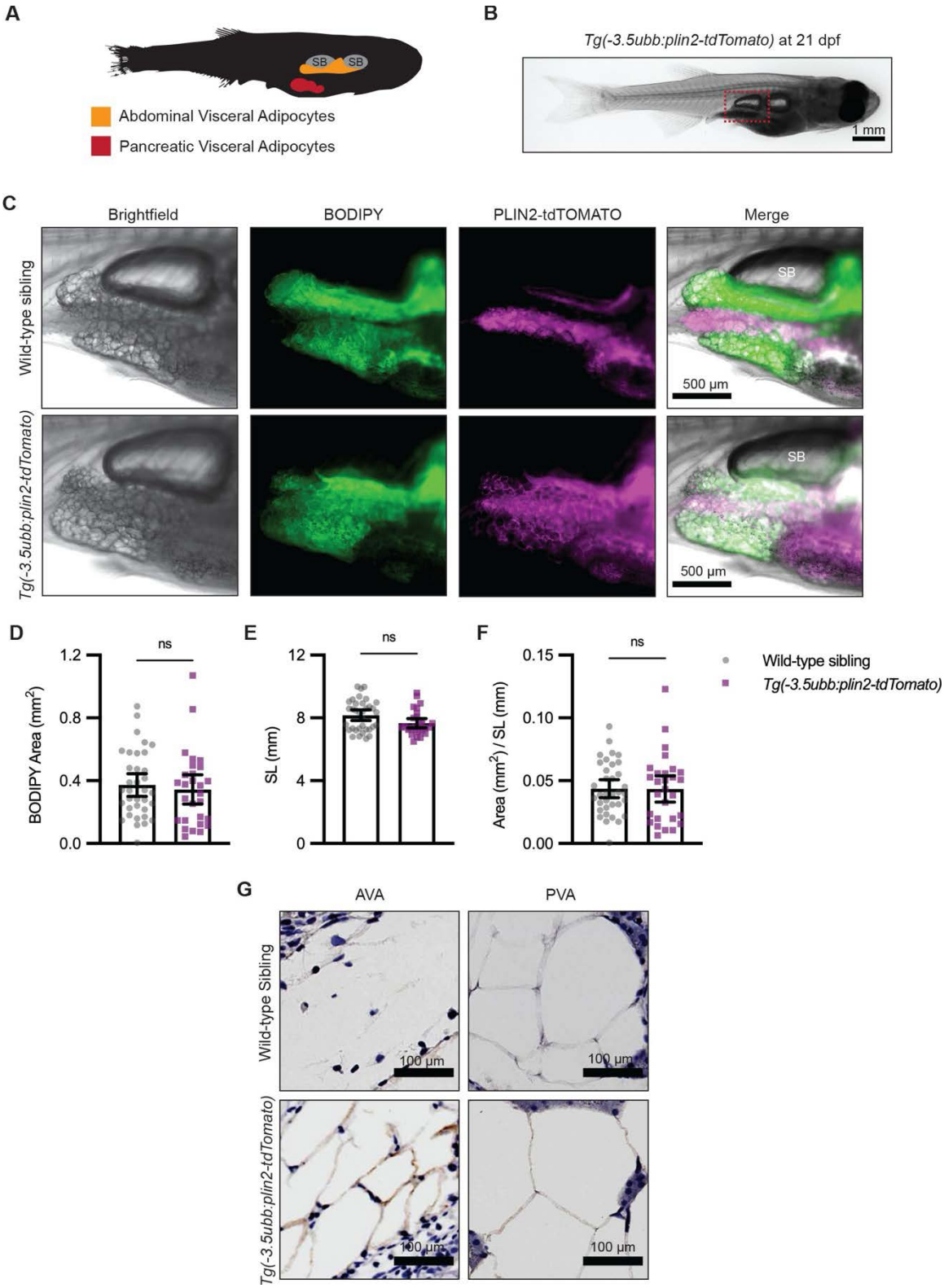

Figure 17. Tg(-3.5ubb:plin2-tdTomato) is an in vivo reporter for visceral adipocytes.

(A) Schematic of visceral adipose tissue development in the 21 days post-fertilization (dpf) zebrafish. Abdominal visceral adipocytes (orange) develop around the swim bladder (gray) and pancreatic visceral adipocytes (red) develop ventrally around the pancreas. (B) Brightfield image of Tg(-3.5ubb:plin2-tdTomato) at 21 dpf. Red box indicates position of higher magnification images to visualize abdominal visceral adipocytes. (C) Widefield microscope images of 21 dpf wild-type casper and Tg(-3.5ubb: plin2-tdTomato) visceral adipocytes around the posterior swim bladder (SB) co-stained with BODIPY. Panels show brightfield, BODIPY, tdTOMATO, and merge. BODIPY stained adipose tissue was imaged and analyzed for (D) area, (E) standard length, and (F) area/standard length. Points indicate individual fish for N= 3 independent experiments; wild-type sibling, Data values for Figure 16D-F. n=35; Tg(-3.5ubb:plin2-tdTomato), n= 28. Bars indicate mean and SEM. Significance calculated via Mann-Whitney test. (G) 21 dpf wild-type casper andTg(-3.5ubb:plin2-tdTomato)zebrafish were fixed and immunohistochemistry conducted for tdTOMATO expression of abdominal (AVA) and pancreatic visceral adipocytes (PVA).

Figure 18—Related to Figure 17

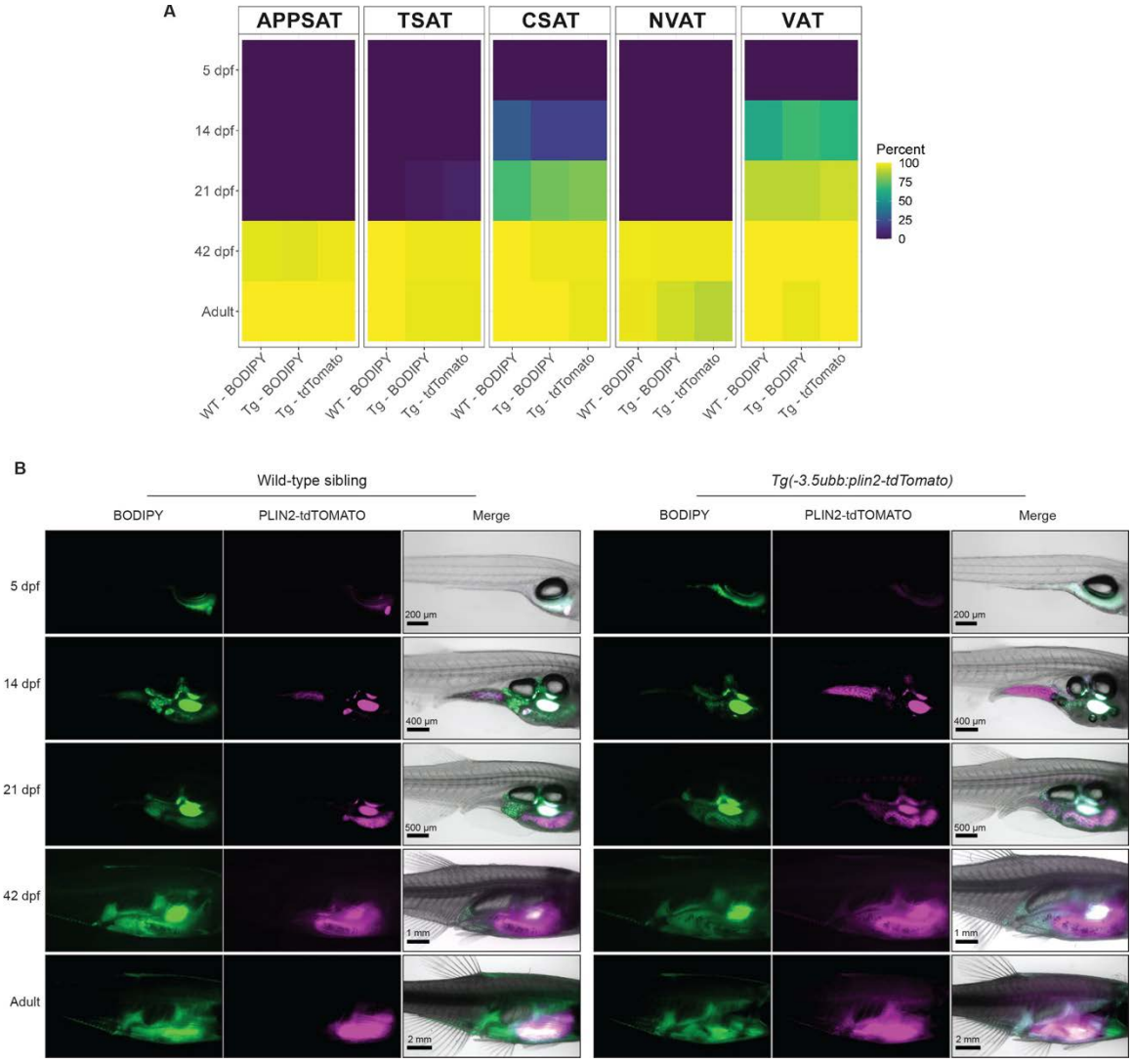

Figure 18—Related to Figure 17. Adipose tissue development in wild-type and Tg(-3.5ubb-plin2-tdTomato) zebrafish.

(A) Heatmap of adipose depot presence during zebrafish development in Tg(-3.5ubb:plin2-tdTomato) and wild-type siblings. Shown is the percent of fish scored for presence of the depot using either BODIPY GFP signal or tdTOMATO expression at each time point. (B) Representative whole-mount images demonstrating the timing of adipose tissue development in Tg(-3.5ubb:plin2-tdTomato) and wild-type siblings using visceral adipose tissue as an example. Data points are an average of N = 3 independent experiments for each time point, excluding 14 days post-fertilization (dpf), where N = 4, and the adults, where N = 5 (5 dpf WT n = 32, 5 dpf Tg(-3.5ubb:plin2-tdTomato) n = 38, 14 dpf WT n = 32, 14 dpf Tg(-3.5ubb:plin2-tdTomato) n = 48, 21 dpf WT n = 30, 21 dpf Tg(-3.5ubb:plin2-tdTomato) n = 40, 42 dpf WT n = 48, 42 dpf Tg(-3.5ubb:plin2-tdTomato) n = 43, adult WT n = 38, adult Tg(-3.5ubb:plin2-tdTomato) n = 29).

Diet and pharmacologically induced reduction in visceral adipose tissue area

After confirming that we could image visceral adipose tissue in *Tg(-3.5ubb:plin2-tdTomato)*, we wanted to test whether this could be a tractable platform to image adipose tissue remodeling. We first verified whether we could use *Tg(-3.5ubb:plin2-tdTomato)* to track reduction in visceral adiposity. Fasting is a well-known mechanism for reducing adiposity, since it will induce lipolysis and lead to a reduction in the size of the adipocyte lipid droplet.[171,198-200] To test this, wild-type and *Tg(-3.5ubb:plin2-tdTomato)* zebrafish were fed or fasted for 7 days and then imaged to measure standard length and adipose tissue area (Figure 19A). As expected, we observed a reduction in the BODIPY-stained visceral adipose tissue in both wild-type and *Tg(-3.5ubb:plin2-tdTomato)* fasted zebrafish (Figure 19B). Similarly, we measured a significant reduction in adipose tissue area, standard length, and normalized area to standard length between fed and fasted fish (Figure 19C-E). Furthermore, we did not see differences in adiposity or standard length between wild-type and *Tg(-3.5ubb:plin2-tdTomato)* fish within the same diet (Figure 19C-E). This suggests that the transgenic expression of PLIN2-tdTOMATO reflects adipose tissue remodeling consistent with wild-type fish.

Combined with the capacity for high-throughput in vivo imaging in zebrafish, we sought to use *Tg(-3.5ubb:plin2-tdTomato)* as a model to study lipid droplet dynamics in visceral adipocytes. One challenge we encountered was the autofluorescence from the zebrafish intestinal loops and gallbladder present in the tdTOMATO and GFP channels Figure 19F). To remove background fluorescence, we developed an image analysis

pipeline in MATLAB to segment the visceral adipocytes in juvenile *Tg(-3.5ubb:plin2-Tomato)* zebrafish (Figure 19F). Next, we combined our image analysis pipeline with the ability to do repeated imaging in zebrafish to more granularly quantify adipose tissue remodeling in fed or fasted *Tg(-3.5ubb:plin2-tdTomato)* fish (Figure 19G). We saw the expected increase in adipose tissue area, standard length, and normalized area to standard length over 7 days in fed *Tg(- 3.5ubb:plin2-tdTomato)* fish (Figure 19H-J). The standard lengths for fasted fish were significantly lower than those for fed fish and remained stable over 7 days, which we attribute to food restriction, disrupting zebrafish development (Figure 19I). Notably, we found that visceral adiposity was not reduced until after 2 days of fasting (Figure 19H,J).

In addition to fasting as a dietary perturbation, we also pharmacologically reduced adipose tissue. To achieve this, we used Forskolin, a drug that is known to induce lipolysis through cAMP signaling.[201] We treated juvenile zebrafish for 24 hr with either dimethyl sulfoxide (DMSO) or 5 mM Forskolin and imaged the adipocytes (Figure 20A—related to figure 19). We detected a reduction in both the adipose tissue area and normalized area to standard length in the Forskolin-treated fish,

Figure 19

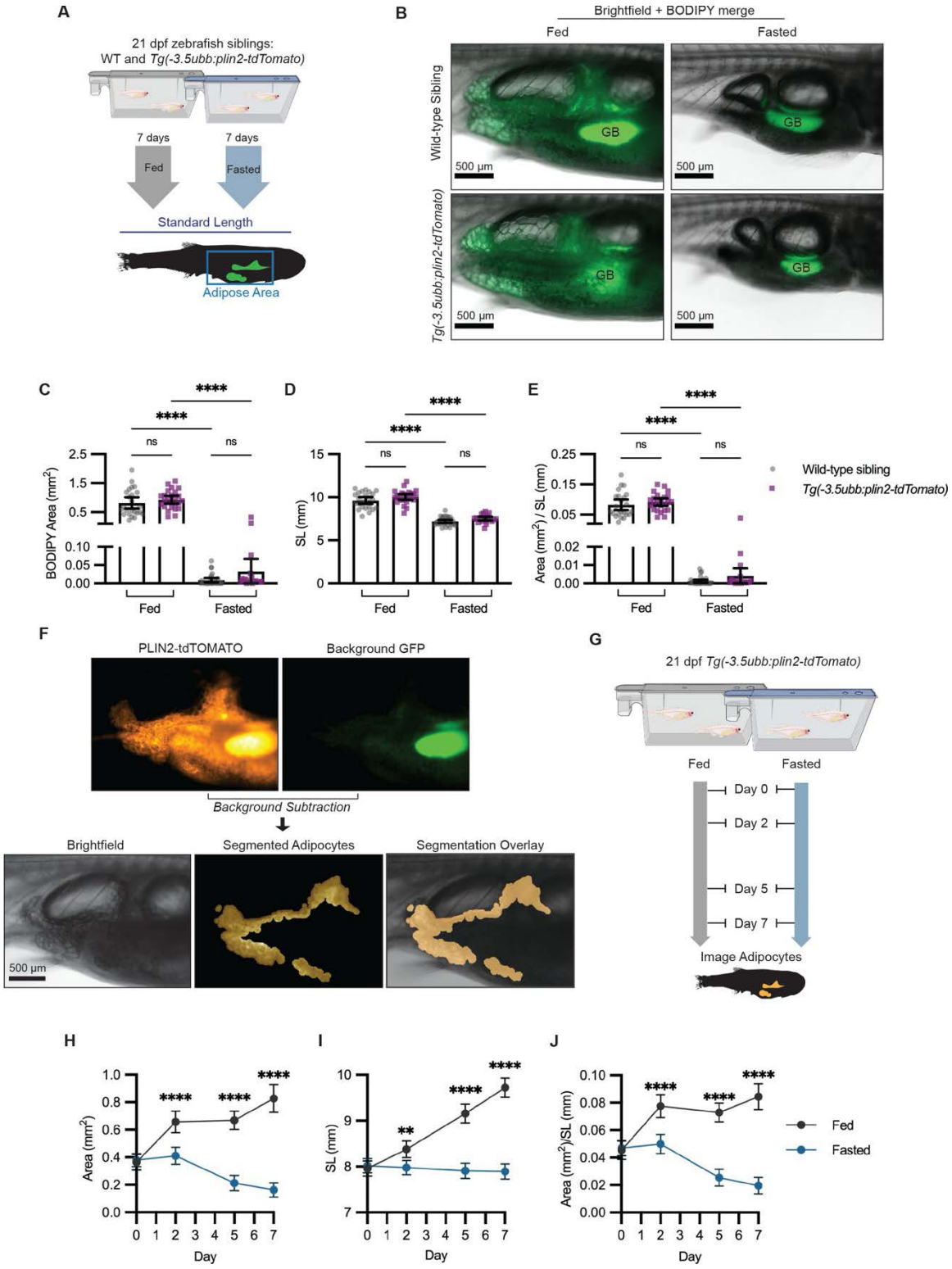

Figure 19. Fasting reduces visceral adipose tissue area. (A) Schematic of experimental set-up for fasting experiment.

21 days post-fertilization (dpf) wild-type casper and Tg(-3.5ubb:plin2-tdTomato) zebrafish were fed or fasted for 7 days and imaged to measure standard length and adipose area. (B) Representative images of zebrafish fed or fasted after 7 days. Panels show merged images of brightfield and BODIPY-stained visceral adipose tissue. BODIPY-stained adipocytes were imaged to measure (C) area, (D) standard length, and (E) area/standard length. Data points indicate individual fish for N = 3 independent experiments; bars indicate mean and 95% CI. Fed wild-type n = 24; fed Tg(-3.5ubb:plin2-tdTomato) n = 24; fasted wild-type n = 29; fasted Tg(-3.5ubb:plin2-tdTomato) n = 20. Significance calculated via Kruskal-Wallis with Dunn's multiple comparisons test; ****p<0.0001. (F) Representative image of computational segmentation of Tg(-3.5ubb:plin2-tdTomato) adipocytes. PLIN2-tdTOMATO was background subtracted with GFP fluorescence. Bottom panels show brightfield, segmented adipocytes, and segmentation overlaid on brightfield. (G) Schematic of experimental set-up for repeated imaging of 21 dpf Tg(-3.5ubb:plin2-tdTomato) zebrafish, which were fed or fasted for 7 days. Adipose tissue was imaged and analyzed for (H) area, (I) standard length, and (J) area/standard length. Points indicate mean and error bars indicate 95% CI for N = 3 independent experiments; by day 7, fed n = 46 and fasted n = 57. Significance calculated via Mann-Whitney test; **p<0.01, ****p<0.0001.

Figure 20—Related to Figure 19

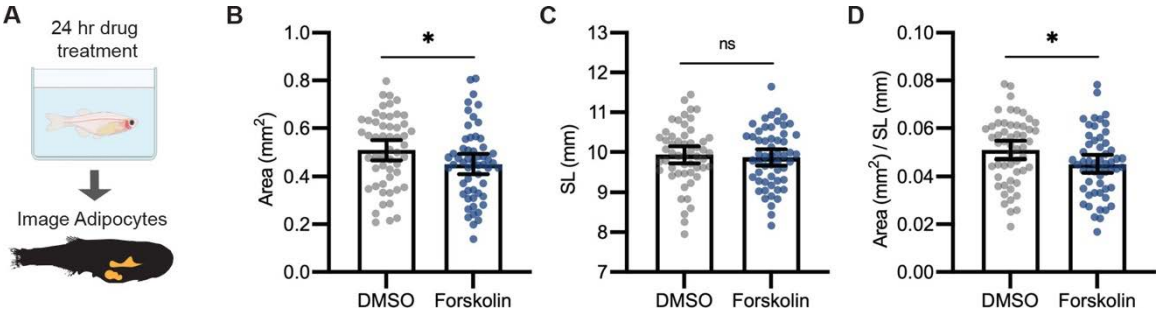

Figure 20—Related to Figure 19. Forskolin reduces visceral adipose tissue area.

(A) Schematic of experimental set-up for Forskolin drug treatment. 21 days post-fertilization (dpf) Tg(-3.5ubb:plin2-tdTomato) zebrafish were individually placed in six-well plates with either dimethyl sulfoxide (DMSO) or 5 µM Forskolin for 24 hr. Adipose tissue was imaged and analyzed for (**B**) area, (**C**) standard length, and (**D**) area/standard length. Points indicate individual fish for N = 5 independent experiments; DMSO, n = 53; Forskolin, n = 55. Bars indicate mean and SEM. Significance calculated via Mann-Whitney test; *p<0.05.

but no differences in standard length (Figure 19B-D—Related to Figure 18). Thus, *Tg(-3.5ubb:plin2-tdTomato)* can be used as an in vivo model to visualize adipocytes, with the benefits of avoiding staining steps and allowing for repeated imaging with high-

throughput image analysis in zebrafish.

High-fat diet leads to specific enlargement of visceral adipose tissue

Having shown that we could use *Tg(-3.5ubb:plin2-tdTomato)* to image and measure reduction in adipose tissue, we tested whether we can use our model to detect an increase in adiposity. Zebrafish have been used as a model for diet-induced obesity and share pathophysiological perturbations seen in mammals, but few studies have focused on architectural changes of visceral adipose tissue.[202-204] We sought to determine if we could detect increases in visceral adiposity from a high-fat diet (HFD). We fed juvenile zebrafish with either control feed (12% crude fat) or HFD (23% crude fat) for 7 days and subsequently imaged the adipose tissue (Figure 21A,B). After a week of HFD feeding, we observed that HFD-fed fish developed significantly increased visceral adiposity compared to the fish fed with control feed (Figure 21C,E). Although less dramatic between 7 and 14 days of HFD, we found that significantly greater visceral adiposity persisted after 2 weeks of HFD (Figure 21C,E). Interestingly, we did not detect differences in the standard lengths of the control and HFD-fed fish, suggesting that this formulation of HFD leads to specific enlargement of visceral adipose tissue (Figure 21E). Our results demonstrate that *Tg(-3.5ubb:plin2-tdTomato)* is an effective and unique tool to visualize visceral adipose tissue remodeling induced by HFD, which can be widely applied to study obesity.

Figure 21

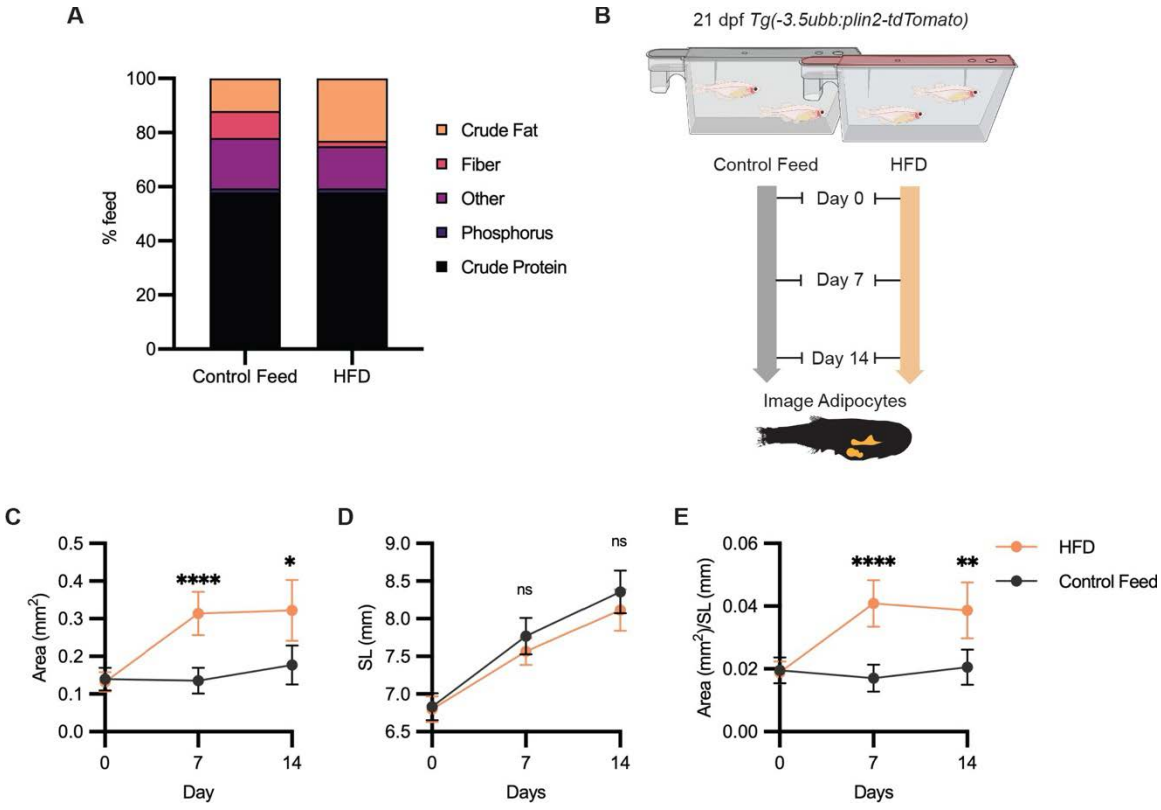

Figure 21. High-fat diet leads to specific enlargement of visceral adipose tissue.

(A) Percent breakdown of nutritional content for control feed and high-fat diet (HFD). (B) Schematic of experimental set-up for HFD experiment. 21 days post-fertiization (dpf) Tg(-3.5ubb:plin2-tdTomato) zebrafish were fed control feed or HFD for 14 days and imaged to measure standard length and adipose area. Image analysis pipeline resulted in measurements of adipose tissue (C) area, (D) standard length, and (E) area/standard length. Points indicate mean and error bars indicate 95% CI for N = 3 independent experiments; by day 14, control feed n = 57; HFD n = 61. Significance calculated via Mann-Whitney test; *p<0.05, **p<0.01, ****p<0.0001.

A screen to discover novel compounds that modulate lipolysis and lipid droplets in vivo

To meet fluctuating nutritional needs of the cell, lipid droplets are remodeled through lipolysis to regulate lipid mobilization and metabolic homeostasis.[101,205,206] As a major lipid depot for the body, white adipose tissue is critical to lipid availability and cycles through lipolytic flux in response to energy demands.[207] In disease contexts such as

cancer, adipocytes undergoing lipolysis act as a lipid source for neighboring cancer cells.[208] Adipocyte-derived lipids have been directly shown to promote cancer progression in ovarian,[85] breast,[209] and melanoma cancer cells.[88] Due to growing evidence of adipocyte and cancer cell cross-talk as a metabolic adaptation for tumor progression, there is significant interest in disrupting lipid transfer between adipocytes and cancer cells.

Leveraging our model to visualize lipid droplets in adipocytes, we became interested in identifying novel compounds that remodel adipocyte lipid droplets through lipolysis. In mammalian systems, the most commonly used cell line to study lipolysis is 3T3-L1 cells, which can be differentiated in vitro to resemble adipocytes.[210] We first used the 3T3-L1 system to rapidly identify lipolysis inhibitors at high throughput and then test those hits using our zebrafish lipid droplet reporter. We reasoned that compounds that inhibit lipolysis in vitro would cause an increase in the size of the lipid droplets in vivo. To achieve this, we differentiated mouse 3T3-L1 fibroblast cells into adipocytes and conducted a chemical screen for compounds that inhibit lipolysis (Figure 22A), measured by quantifying glycerol in the media, a gold standard readout of lipolysis in this system.[211] As a positive control, we used Atglistatin, an inhibitor of adipose triglyceride lipase (ATGL) that is known to be the rate-limiting step of lipolysis and has been shown to inhibit lipolysis in cell lines and mouse models.[212,213] We confirmed that Atglistatin potently inhibits lipolysis in 3T3-L1 adipocytes (Figure 22B). We then screened through a library of 1280 compounds of diverse chemical structures to find novel inhibitors of lipolysis. Overall, we found 29 out of 1280 compounds that led to at least a 40% reduction in

lipolysis as measured by glycerol release into the media. Looking more closely at the top 10 hits from this screen, we noted that 2 of the top 10 hits (Auranofin and JS-K) modulated nitric oxide (Figure 22A). Nitric oxide can be used for post-translational modification of proteins via S-nitrosylation.[214] A previous study has shown that increased nitric oxide has a suppressive role on lipolysis, and Auranofin, a thioredoxin reductase inhibitor that promotes S-nitrosylation, can inhibit lipolysis in 3T3-L1 cells.[215] Similarly, JS-K is a nitric oxide donor purported to promote S-nitrosylation, but it has not been shown to play a role in lipolysis.[216,217] Given that both of these top hits were in the same pathway, we chose these for in vivo validation.

Next, we asked whether these drugs could modulate lipid droplet size and lead to increased adiposity in zebrafish. We first established the maximal tolerated doses of Atglistatin, Auranofin, and JS-K in vivo (Figure 23A-C—related to Figure 22), and then tested their effects on adipose tissue in the Tg(-3.5ubb:plin2-tdTomato) fish (Figure 22D-F). As expected, treatment of juvenile zebrafish for 24 hr with Atglistatin caused a significant increase in adipose tissue area without affecting standard length or fish viability at the maximally tolerated dose. Consistent with our screen results, we found that JS-K also significantly increased adiposity (Figure 22C,E). These effects were specific to the adipose tissue as standard length was not affected (Figure 22D). These data indicate that modulators of nitric oxide can inhibit lipolysis in cell lines and lead to increased adiposity in vivo in zebrafish. Moreover, this approach demonstrates the power of this system to dissect the relationship between novel modulators of lipolysis (i.e., nitric oxide) and adiposity in vivo.

Figure 22

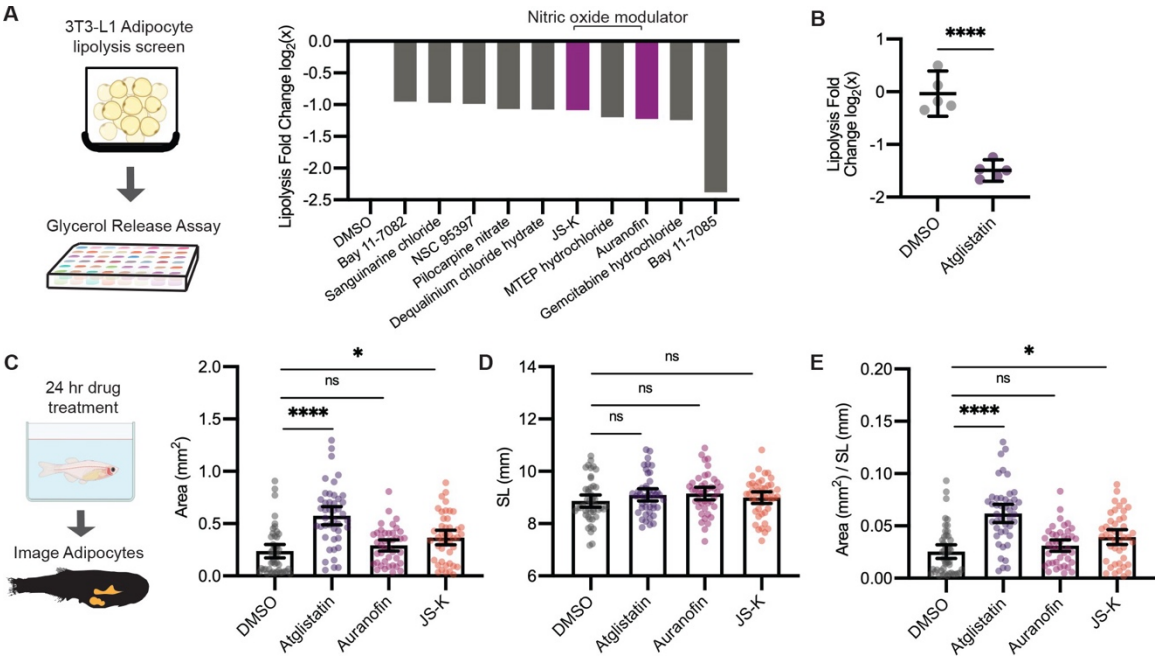

Figure 22. A screen to discover novel compounds that modulate lipolysis and lipid droplets in vivo.

(A) Schematic of pharmacologic lipolysis screen in 3T3-L1 adipocytes using a glycerol release assay. Normalized log_2 transformed values for top 10 drugs that inhibit lipolysis are shown. Magenta indicates compounds that modulate nitric oxide. (B) Normalized log_2 transformed values for lipolysis inhibition in 3T3-L1 adipocytes using either dimethyl sulfoxide (DMSO) or 100 μM Atglistatin. N = 5 independent experiments. Bars indicate mean and SEM. Significance calculated via Welch's t-test; ****p<0.0001. (C) Schematic of experimental set-up for drug treatment. 21 days post-fertilization (dpf) Tg(-3.5ubb:plin2-tdTomato) zebrafish were individually placed in six-well plates with either DMSO, 40 μM Atglistatin, 1 μM Auranofin, or 1 μM JS-K for 24 hr. Adipose tissue was imaged and analyzed for (C) area, (D) standard length, and (E) area/standard length. Data points indicate individual fish for N = 4 independent experiments; DMSO n = 47; Atglistatin n = 44; Auranofin n = 42; JS-K n = 44. Bars indicate mean and SEM. Significance calculated via Kruskal-Wallis with Dunn's multiple comparisons test; *p<0.05, ****p<0.0001.

Figure 23—Related to Figure 22

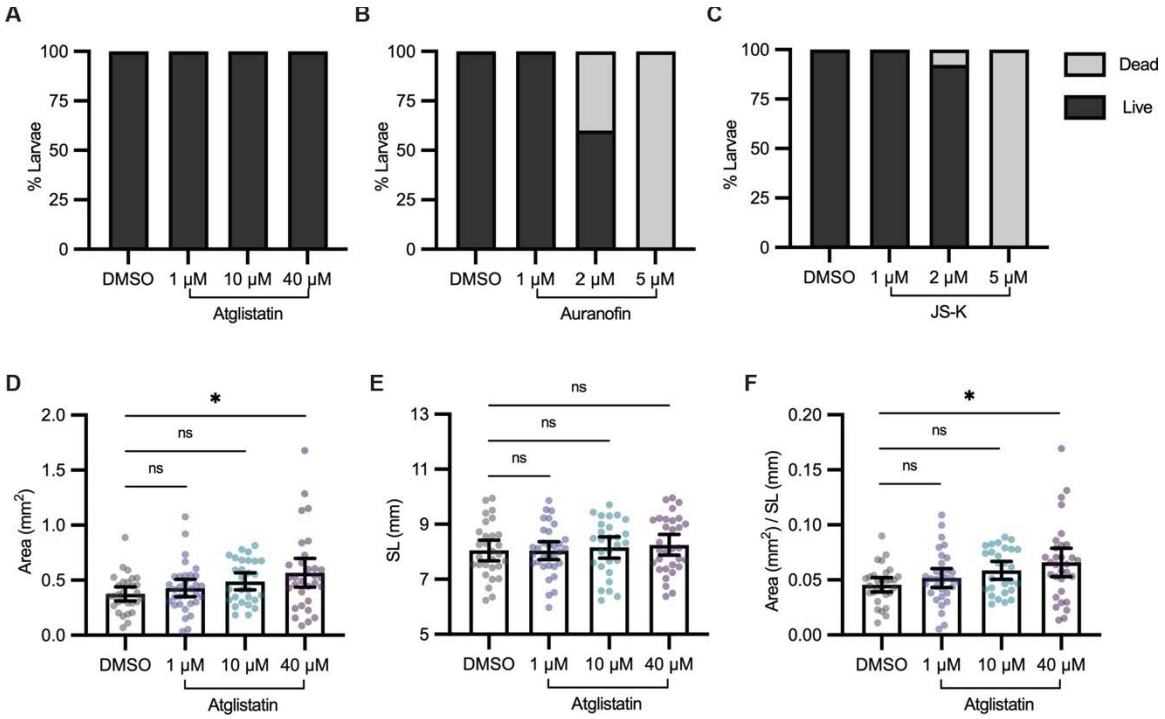

Figure 23—Related to Figure 22. Atglistatin, Auranofin, and JS-K in vivo dose titration.

Viability of 21 days post-fertilization (dpf) Tg(-3.5ubb:plin2-tdTomato) zebrafish was measured after 24 hr of treatment with dimethyl sulfoxide (DMSO) or increasing concentrations of (**A**) Atglistatin, (**B**) Auranofin, or (**C**) JS-K. Percent larval viability measured from N = 3 independent experiments. After 24 hr of drug treatment, 21 dpf zebrafish were imaged to measure (**D**) area, (**E**) standard length, and (**F**) area/standard length. Data points indicate individual fish for N = 5 independent experiments; DMSO n = 29; 1 µM n = 32; 10 µM n = 28; 40 µM n = 31. Bars indicate mean and SEM. Significance calculated via Kruskal-Wallis with Dunn's multiple comparisons test; *p<0.05.

Lipolysis modulators also inhibit lipid droplet loss in melanoma cells

Upon uptake of adipocyte-derived lipids, cancer cells can store excess lipids in lipid droplets.[208] Accumulation of lipid droplets in melanoma cells has been associated with increased metastatic potential and worse clinical outcomes.[88,194] The mechanisms regulating subsequent lipolysis from the lipid droplets in cancer cells are not well understood, but we reasoned that some of the same mechanisms (i.e., ATGL, nitric oxide) used in adipocytes might also be used in cancer cells. To test this, we created a stable

zebrafish melanoma cell line (ZMEL) that expressed the -3.5ubb:plin2-tdTomato construct[161] to generate the ZMEL-LD (lipid droplet) reporter cell line (Figure 24A). Because melanoma cells at baseline only have few small lipid droplets, we induced their formation via extrinsic addition of oleic acid, a key fatty acid that can be transferred from the adipocyte to the melanoma cell.[88] We found that after a pulse of oleic acid for 24 hr, we could easily detect PLIN2-tdTOMATO expression surrounding lipid droplets marked by the lipid droplet dye Monodansylpentane (MDH) (Figure 24B), similar to what we saw in the adipocytes (Figure 16). Similar to what we did in the whole fish, we wanted to be sure that the PLIN2-tdTOMATO transgene itself did not alter lipid droplets, so we compared lipid droplet formation in ZMEL-LD and parental cell line (ZMEL-GFP) via imaging and flow cytometry (Figure 25A,B—Related to Figure 24). Using the lipid droplet dye Lipidtox as a proxy for lipid droplet content, we pulsed the cells with increasing amounts of oleic acid and found no difference in Lipidtox median fluorescence intensity (MFI) between the two cell lines (Figure 25B—related to Figure 24), indicating that the transgene was not having any unexpected effect. Next, we assessed the sensitivity of the PLIN2-tdTOMATO transgene versus Lipidtox in reporting changes in lipid droplets of ZMEL-LD. While both PLIN2-tdTOMATO and Lipidtox expression increased accordingly with oleic acid, PLIN2-tdTOMATO expression provided a much greater dynamic range (Figure 25C-F—Related to Figure 24), highlighting its advantages over standard lipid dyes like Lipidtox.

To validate whether the lipolysis-inhibiting compounds we identified above could modulate lipid droplets in ZMEL-LD cells, we utilized the same flow cytometry assay to measure PLIN2-tdTOMATO expression. We treated ZMEL-LD cells for 72 hr with either BSA or oleic acid as controls for low- or high-lipid droplet cell populations

(Figure 24C). We then tested the effects of the lipolysis inhibitors Atglistatin, Auranofin, and JS-K. We pulsed the ZMEL-LD cells with oleic acid for 24 hr (to induce lipid droplets) and then measured the subsequent decay in signal over the ensuing 48 hr, which is expected to decrease due to gradual lipolysis of the lipid droplets. Compared to cells with oleic acid pulse and DMSO, cells given JS-K did not differ in the percent of lipid droplet-positive cells (Figure 24D,E). In contrast, cells treated with Atglistatin and Auranofin demonstrated significantly higher lipid droplet-positive cells (Figure 24D,E). These data indicate that similar to adipocytes, ATGL is a key regulatory step in lipolysis in melanoma cells. Moreover, we found that nitric oxide, which was identified in our adipocyte screen, is similarly a modulator of lipolysis in the melanoma context and can be utilized for future studies to target adipocyte-melanoma cell cross-talk. We do not yet understand why different nitric oxide donors are more or less potent in adipocytes (where JS-K is a better inhibitor in vivo) versus melanoma cells (where Auranofin is a better inhibitor), but this could reflect differences in pharmacokinetics or cell-type-specific lipid droplet regulation.

Figure 24

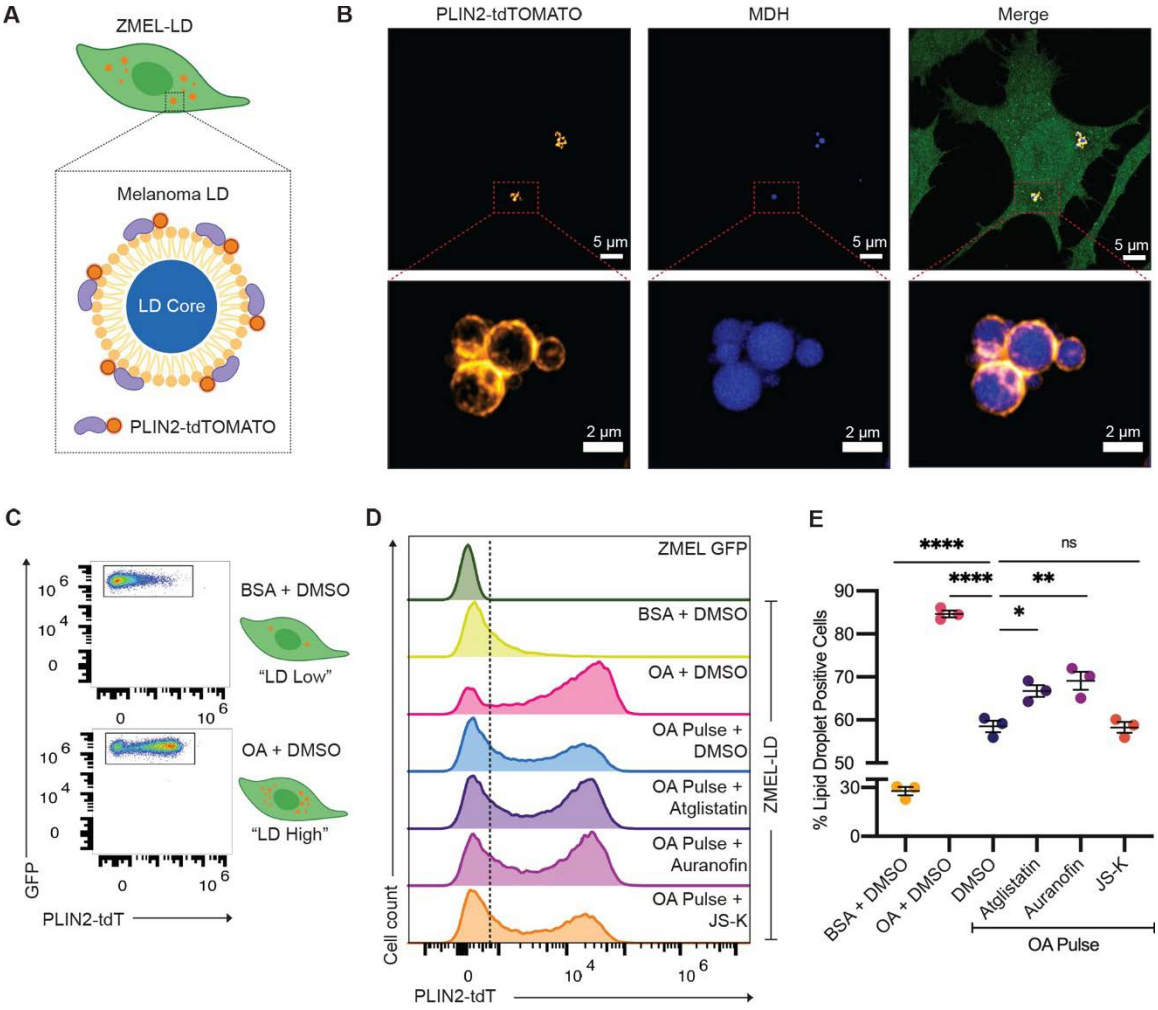

Figure 24. Lipolysis modulators also inhibit lipid droplet loss in melanoma cells.

(A) Schematic of zebrafish melanoma cell line with lipid droplet reporter (ZMEL-LD) with lipid droplet labeled by PLIN2-tdTOMATO. (B) Confocal images of ZMEL-LD cells after 24 hr of oleic acid treatment. Panels show fluorescence signals in PLIN2-tdTOMATO, MDH (lipid droplet dye) staining, and merge of images with cytoplasmic GFP. Red box indicates position of higher magnification image of lipid droplets. (C) ZMEL-LD cells were treated with either bovine serum albumin (BSA) or oleic acid with dimethyl sulfoxide (DMSO) for 72 hr and then analyzed by Fluorescence Activated Cell Sorting (FACS) for PLIN2-tdTOMATO expression. (D) Representative histogram of PLIN2-tdTOMATO expression of ZMEL-GFP and GFP+ZMEL-LD cells with indicated drugs. Dashed line shows threshold for PLIN2- tdTOMATO expression. (E) Quantification of percent of GFP+ZMEL-LD cells with lipid droplets. Lipid droplet low and high controls were ZMEL-LD cells treated with BSA or oleic acid for 72 hr. For drug treatments, ZMEL-LD cells were pulsed with oleic acid for 24 hr and then given DMSO, 40 µM Atglistatin, 0.5 µM Auranofin, or 0.5 µM JS-K for 48 hr. N = 3 independent

experiments. Bars indicate mean and SEM. Significance calculated via one- way ANOVA with Dunnett's multiple comparisons test; *p<0.05, ***p<0.001, ****p<0.0001.

Figure 25—Related to Figure 24

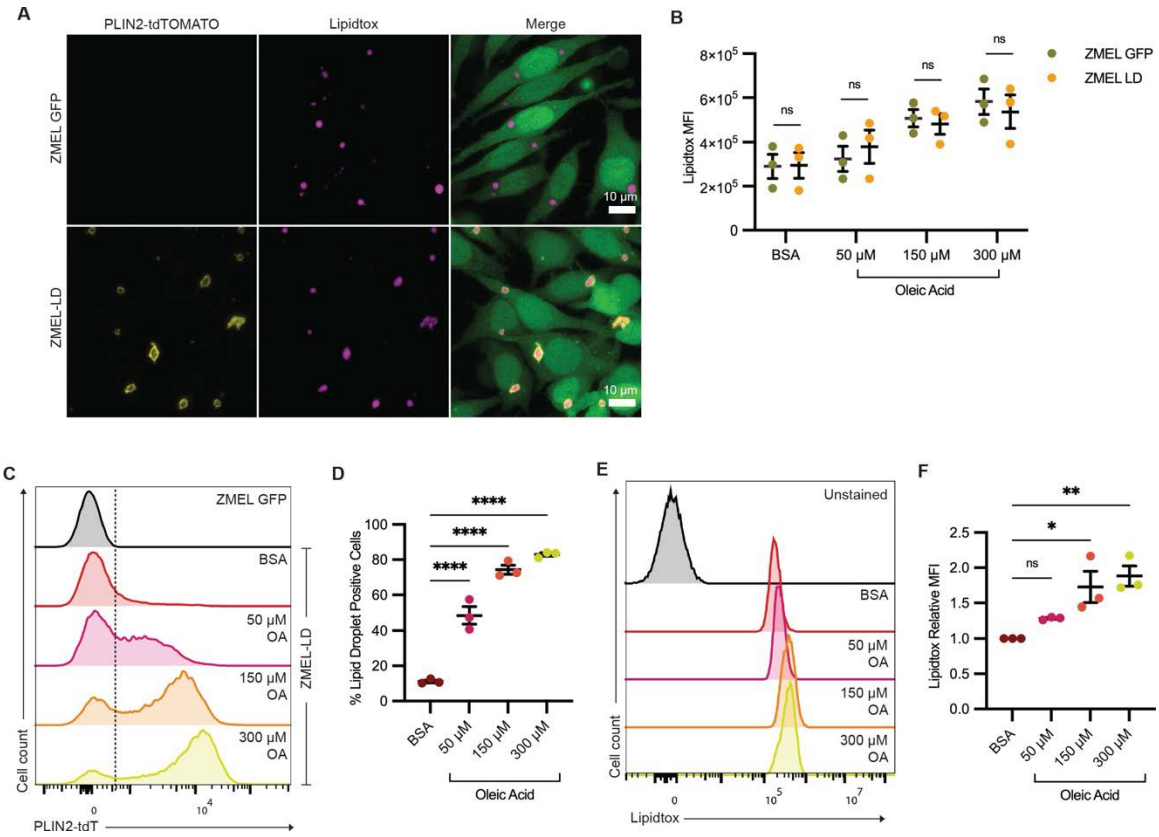

Figure 25—Related to Figure 24. Lipid droplet production is equivalent between ZMEL-GFP and ZMEL-LD.

(A) Confocal images of ZMEL-GFP and ZMEL-LD after 24 hr of 150 µM oleic acid treatment. Cells were fixed and stained, with panels showing fluorescence signals for PLIN2-tdTOMATO, Lipidtox (lipid droplet dye), and merge of images with cytoplasmic GFP. ZMEL-GFP and ZMEL-LD cells were treated with bovine serum albumin (BSA) or increasing concentrations of oleic acid for 24 hr and then analyzed by FACS. (**B**) Comparison of Lipidtox median fluorescence intensity (MFI) between ZMEL-GFP and ZMEL-LD. Significance calculated via Welch's t-test with Bonferroni correction. (**C**) Representative histogram of PLIN2-tdTOMATO expression of ZMEL-GFP and ZMEL-LD cells. Dashed line shows the threshold for PLIN2-tdTOMATO expression. (**D**) Quantification of percent of GFP+ ZMEL-LD cells with lipid droplets. Significance calculated via one-way ANOVA with Dunnett's multiple comparison test. (**E**) Representative histogram of Lipidtox expression of ZMEL-LD cells. (**F**) Quantification of Lipidtox MFI relative to BSA control of GFP+ZMEL-LD cells. Significance calculated via one-way ANOVA with Dunnett's multiple comparison test. N = 3

independent experiments. Bars indicate mean and SEM. *p<0.05, **p<0.01, ****p<0.0001.

Discussion

Lipid droplets are cytosolic storage organelles for cellular lipids, which are dynamically regulated in response to metabolic and oxidative perturbations.[145] Changes in the lipid droplet content of a cell can occur in response to a variety of factors, including hypoxia, reactive oxygen stress, ER stress, and alterations in nutrient availability.[139-141,168,173,218,219] However, the regulatory mechanisms driving these processes remain incompletely understood. Furthermore, lipid droplets are highly heterogeneous, and the pathways that regulate lipid droplet dynamics in specific cell types warrant investigation.

To address such questions, we report the first lipid droplet reporter in a vertebrate model organism. We show that our *plin2-tdtomato* reporter faithfully marks the lipid droplet in vivo. As a further validation of our approach, while our manuscript was in review, a similar approach using knock-in at the endogenous plin2 promoter was recently described.[191] The combination of our reporter with the in vivo system of the casper zebrafish enables flexible and robust imaging approaches to examine lipid droplet regulation and function. In particular, the ease of chemical and genetic manipulation of the zebrafish combined with high-throughput imaging approaches enables interrogation of relevant pathways in a cell type-specific manner. Furthermore, the capacity for intravital imaging creates the opportunity to conduct longitudinal analysis of lipid droplet dynamics across developmental time and in disease contexts between single animals.

Here, we demonstrate the capabilities of the *Tg(-3.5ubb:plin2-tdTomato)* line by taking advantage of the fact that white adipocytes are readily labeled by PLIN2-tdTOMATO expression. This labeling enables the study of individual adipocytes and adipose tissue in adult and juvenile zebrafish. We show that the *Tg(-3.5ubb:plin2-tdTomato)* reporter can be used as an alternative to lipophilic fluorescent dyes to study adipose tissue across zebrafish developmental stages while preserving normal adipose tissue development.

We establish the utility of this transgenic line to study the regulation of adipose tissue by both diet and pharmacologic perturbations. We focused on visceral adipose tissue due to its role as an endocrine organ and the central regulator of organismal metabolism.[220-222] We show that our *Tg(-3.5ubb:plin2-tdTomato)* line is sensitive enough to capture quantitative changes in visceral adipose tissue after short-term pharmacologic treatments with known regulators of adipocyte lipolysis. Furthermore, by combining top hits from a large-scale in vitro chemical screen in 3T3-L1 adipocytes with our reporter we uncovered a novel role for nitric oxide in modulating adipocyte lipolysis and adipose tissue dynamics.

Beyond pharmacologic perturbations, we also demonstrate the power of this line to perform longitudinal analyses of diet-induced perturbations on adipose tissue area across multiple time points. This work yielded compelling insights into the dynamics of adipose tissue response to both prolonged fasting and high-fat diet. Differences in the kinetics of each response suggest a complex relationship between

adipose tissue development and the nutritional and energetic requirements of the developing organism, which merits future investigation. Collectively, these data illustrate the potential of our model to yield novel insights into the regulation of visceral adipose tissue, including the context of obesity.

While our studies show that this tool can be used to increase our understanding of adipocyte biology, it can also be utilized to study lipid droplets in other contexts as well. Lipid droplets are ubiquitous across almost all cell types. Therefore, this model could be applied to study the regulation of lipid droplets in the development and function of other adipose depots and additional cell types, such as muscle and hepatocytes.[223,224] In the disease context, we focused on the role of lipid droplets in cancer, since tumor cells can take up lipids from adipocytes and then package them into lipid droplets.[85,88,208,209] This transfer of lipids has been linked to disease progression, making the regulation of lipid release from the lipid droplet through subsequent lipolysis in the tumor cell of particular interest. We found that regulation of lipolysis by ATGL and nitric oxide pathways is conserved between adipocytes and melanoma cells although phenotypes downstream of nitric oxide may be cell type specific. Collectively, this underscores the complexity of lipid droplet regulation and emphasizes the importance of studying these processes in multiple cell types. We believe that our model will serve as a powerful tool to study cell type-specific regulation of lipid droplet biogenesis and function while preserving the endogenous structural and metabolic environment of an in vivo system.

2.3 Authorship contributions

Eleanor Johns performed the experiments shown in Figure 18, Figure 20, Figure 22C-E, and Figure 23.

Dianne Lumaquin developed the model and performed the experiments displayed in Figures 16-18 and Figure 24, 20, and Figure 25.

Emily Montal performed the experiments shown in Figure 21.

Joshua M. Weiss and David Ola performed the experiments shown in Figure 22A-B.

Abderhman Abuhashem performed experiments in Figure 16D.

Eleanor Johns, Dianne Lumaquin, and Richard White wrote and revised the manuscript.

2.4 Methods

Cloning of -3.5ubb:plin2-tdtomato

To clone the *plin2* cDNA, tissue from the muscle and heart of adult *casper* zebrafish was dissected, pooled, and then RNA was isolated using the Zymogen Quick RNA Miniprep Kit (Zymo Research, Irvine, USA; catalog #R1054) according to manufacturer's instructions. The Invitrogen SuperScriptIII First-Strand Synthesis SuperMix Kit (Thermo Fisher, Waltham, USA; catalog #18080400) was used according to manufacturer's instructions to produce cDNA. CloneAmp HiFi PCR Premix (Takara, Mountain View, USA; catalog #639298) was used to PCR amplify the PLIN2 cDNA and gel purified via NucleoSpin Gel and PCR Clean Up (Takara, Mountain View, USA; catalog #740609.50). To generate pME-PLIN2-tdTOMATO, the PLIN2 cDNA was inserted on the 5' end of pME-tdTOMATO using In-Fusion HD Cloning Plus (Takara, Mountain View, USA; catalog #638920). Gateway cloning using the Gateway LR Clonase Enzyme mix (Thermo Fisher, Waltham, USA; catalog #11791019) was

employed to create the *-3.5ubb:plin2-tdTomato* construct with p5E-ubb, pME-PLIN2-tdTOMATO, and p3E-polyA into pDestTol2pA2-blastocidin (cells)[161] or pDestTol2CG2 (zebrafish).[225]

Zebrafish husbandry

All zebrafish experiments were carried out in accordance with institutional animal protocols. All zebrafish were housed in a temperature- (28.5˚C) and light-controlled (14 hr on, 10 hr off) room. Fish were initially housed at a density of five fish per liter and fed three times per day using rotifers and pelleted zebrafish food. Anesthesia was done using Tricaine (Western Chemical Incorporated, Fern- dale, USA) with a stock of 4 g/l (protected for light) and diluted until the fish was immobilized. All procedures were approved by and adhered to Institutional Animal Care and Use Committee (IACUC) protocol #12-05-008 through Memorial Sloan Kettering Cancer Center.

Generation of Tg(-3.5ubb:plin2-tdTomato)

The *ubb:plin2-tdTomato* plasmid was injected into *casper* embryos with Tol2 mRNA to introduce stable integration of the *ubb:plin2-tdTomato* cassette. Fish with GFP+ hearts (due to pDestTol2CG) were selected and outcrossed with *casper* fish to produce the F1 generation. F1 zebrafish with GFP+ hearts and validated PLIN2-tdTOMATO-expressing adipocytes were outcrossed to generate F2 and F3 generation zebrafish for experiments.

Zebrafish imaging and analysis

Zebrafish were imaged using an upright Zeiss AxioZoom V16 Fluorescence Stereo Zoom Microscope with a x0.5 (for adult fish) or x1.0 (for juvenile fish) adjustable objective lens equipped with a motorized stage, brightfield, and Cy5, GFP, and tdTomato filter sets. To acquire images, zebrafish were lightly anesthetized with 0.2%

Tricaine. Images were acquired with the Zeiss Zen Pro v2 and exported as CZI files for visualization using FIJI or analysis using FIJI (to manually quantify standard length) and MATLAB (Mathworks, Natick, USA).

Our adipocyte segmentation approach utilized the Image Processing Toolbox within MATLAB. Because the zebrafish gut is highly autofluorescent, we chose a threshold for the GFP channel to categorize as background signal and subtracted it from a determined threshold for the tdTOMATO channel. We used a set size to crop images around the tdTOMATO-positive signal and created a mask for the adipose tissue. Within the masked area, we applied a higher tdTOMATO threshold to segment the fluorescent signal from the adipocytes. Finally, we quantified the number of pixels above the threshold to quantify adipose tissue area. MATLAB code is available for download at https://github.com/dlumaquin/PLIN2-tdT-Adipo-Quant.git

To quantify BODIPY-stained adipose tissue, we utilized FIJI to autothreshold GFP signal. We removed background autofluorescence by subtracting Cy5 autothresholded signal. We used the polygon tool to outline and quantify the resulting segmented adipose area. For visualization purposes, the segmented images were color filtered on Adobe Photoshop from grayscale to gold color scale.

BODIPY staining of zebrafish

Adult zebrafish were placed in tanks with 10 ng/ml BODIPY 493/503 (Thermo Fisher, Waltham, USA; catalog #D3922) for 30 min in the dark. Fish were washed and then placed in new tanks with fresh water for 2 hr. Fish were washed again to remove any residual BODIPY, then anesthetized and imaged as indicated above for whole

adipose tissue.

Higher resolution images of zebrafish adipocytes were acquired using the Zeiss LSM 880 inverted confocal microscope using a x10 objective. Zebrafish were lightly anesthetized with 0.2% Tricaine and mounted on a glass bottom dish (MatTek, Ashland, USA; catalog #P35G-1.5–20 C) with 0.1% low gelling agarose (Sigma-Aldrich, St. Louis, USA; catalog #A9045-25G).

Staining to track adipose depot development

For BODIPY staining, 5, 14, and 21 dpf fish were incubated with 5 ng/*m*l BODIPY 493/503 in dishes for 30 min in the dark. Fish were washed with fresh E3 every 45 min for 1.5 hr, then anesthetized and imaged as indicated above for whole adipose tissue. 42 dpf and adult zebrafish were stained in p1000 tip boxes for 30 or 15 min, respectively, in the dark. Fish were then placed back on system to wash with fresh water for 1.5 hr and then anesthetized and imaged as indicated below for whole adipose tissue.

Image analysis to track adipose depot development

To track adipose depot development across multiple stages, F2 (-3.5ubb:plin2-tdTomato) zebrafish were outcrossed with *caspers* to generate F3 fish expressing the transgene and control siblings. Control and *Tg(-3.5ubb:plin2-tdTomato)* fish were raised to a standard density of 25 fish per 2.8 l tank. At the appropriate time points, 5, 14, 21, and 42 dpf or adult-stage zebrafish were removed from the tank and stained for BODIPY as described above.

Images were acquired in three segments per fish along the anterior to posterior axis to capture the entire body of the fish. Adipose depots were classified based on the previously described system.[180] To determine the presence of each adipose depot,

images were thresholded in FIJI for GFP (BODIPY493/503) or tdTomato (-*3.5ubb:plin2-tdTomato*) using control fish as the reference. A depot was scored as present based on positive signal corresponding to the presence of adipocytes for at least one sub-depot in the appropriate anatomic location.

IHC for tdTOMATO

Zebrafish were sacrificed in an ice bath for at least 15 min. For adults, zebrafish tails were dissected. For juvenile zebrafish, the entire fish was used for fixation. Selected zebrafish were fixed in 4% paraformaldehyde for 72 hr at 4˚C, washed in 70% ethanol for 24 hr, and then paraffin embedded. Fish were sectioned at 5 *m*m and placed on Apex Adhesive slides, baked at 60˚C, and then stained with antibodies against tdTomato (1:500, Rockland, #600-401-379). Histology was performed and stained by Histowiz.

Zebrafish fast

Tg(-3.5ubb:plin2-tdTomato) F2 fish were outcrossed with *caspers* to generate the F3 generation. F3 fish were raised at a standard density of 25 fish per 2.8 l tank. For BODIPY staining experiments, 21 dpf fish were separated into new tanks that received standard feed or were fasted for 7 days. Prior to imaging, food was withheld for 3–6 hr to clear the gut. Fish were anesthetized with Tricaine and imaged as described above to quantify BODIPY-stained visceral adipose tissue area and standard length. For the time course fast, 21 dpf *Tg(-3.5ubb:plin2-tdTomato*) fish were separated into new tanks that received standard feed or fasted. Prior to imaging, food was withheld for 3–6 hr to clear the gut. Fish were anesthetized with Tricaine and imaged on days 0, 2, 5, and 7 to quantify PLIN2- tdTOMATO-positive visceral adipose tissue area and standard length.

High-fat diet feeding

Tg(-3.5ubb:plin2-tdTomato) F3 zebrafish were raised at a standard density of 25 fish per 2.8 l tank. At 21 dpf, the zebrafish were placed in 0.8 l tanks and fed either a high-fat or control diet (Sparos, Portugal) for up to 14 days. Fish were then imaged for PLIN2-tdTOMATO expression at days 0, 7, and 14 after the start of diet. Prior to imaging, fish were put in a new tank and food withheld for ~16 hr. Zebrafish were at equal density for control and experimental groups, ranging from 15 to 30 fish per tank. Fish were fed 0.1 g feed per tank per day split over two feedings. The high-fat and control diets were customized and produced at Sparos Lda (Olhao, Portugal), where powder ingredients were initially mixed according to each target formulation in a double-helix mixer, and thereafter ground twice in a micropulverizer hammer mill (SH1; Hosokawa-Alpine, Germany). The oil fraction of the formulation was subsequently added and diets were humidified and agglomerated through low- shear extrusion (Dominioni Group, Italy). Upon extrusion, diets were dried in a convection oven (OP 750-UF; LTE Scientifics, United Kingdom) for 4 hr at 60˚C, and subsequently crumbled (Neuero Farm, Germany) and sieved to 400 *m*m. Experimental diets were analyzed for proximal composition. The Sparos control diet contains 30% fishmeal, 33% squid meal, 5% fish gelatin, 5.5% wheat gluten, 12% cellulose, 2.5% soybean oil, 2.5% rapeseed oil, 2% vitamins and minerals, 0.1% vitamin E, 0.4% antioxidant, 2% monocalcium phosphate, and 2.2% calcium silicate. The Sparos HFD contains 30% fishmeal, 33% squid meal, 5% fish gelatin, 5.5% wheat gluten, 12% palm oil, 2.5% soybean oil, 2.5% rapeseed oil, 2% vitamins and minerals, 0.1% vitamin E, 0.4% antioxidant, 2% monocalcium phosphate, and 2.2% calcium silicate.

3T3-L1 cell culture

3T3-L1 cells were acquired from ZenBio and their differentiation protocol was followed. Cells were received at passage 8 and split to a maximum of passage 12 as per the recommendations of the company. 96-well plates were coated with fibronectin (EMD Millipore, Burlington, USA; catalog #FC010) diluted 1:100 in phosphate-buffered saline (PBS) for at least 30 min to promote improved adherence of cells to the dish. 3T3-L1 cells were first cultured in PM-1-L1 Preadipocyte Medium and allowed to grow to 100% confluence. PM-1-L1 medium was changed every 48–72 hr. 48 hr after reaching 100% confluence, cells were changed to DM-1-L1 Differentiation Medium for 72 hr and then changed to AM-1-L1 Adipocyte Medium. AM-1-L1 Adipocyte Medium was changed every 48-72 hr. Once in AM-1-L1, the medium was changed gently with a multichannel pipette, and only 150 µl of the 200 µ1 was replaced to prevent touching the bottom of the well with the pipette tip. After 2–3 weeks in AM-1-L1, the 3T3-L1 developed significantly large lipid droplets and were used in the screen.

LOPAC library screen

The LOPAC library includes 1280 clinically relevant compounds with annotated targets or pathways. The workflow of the screen involved drug or vehicle control of the 3T3-L1 adipocytes for 24 hr in serum-free media. After 24 hr, 100 µl of the media supernatant was collected to measure secreted glycerol using the Free Glycerol Reagent (Sigma-Aldrich, St. Louis, USA; catalog F6428) following the associated glycerol assay protocol.

The medium (screen media) used for drug treatment was phenol-free DMEM supplemented with 0.2% BSA FFA-free (Sigma-Aldrich, St. Louis, USA; catalog 9048-

46-8). The 1280 compounds were aliquoted as 2 l at µ1 mM into 16 x 96-well plates and stored at -20˚C. Upon thawing, 198 µl of screen media was added to the well, bringing the final drug concentration for all compounds in the screen to 10 µM. Control vehicle was 1% DMSO served as a negative control and 1 µM isoproterenol served as a positive control in the screen. This medium containing LOPAC drugs, DMSO, and isoproterenol was transferred to 3T3-L1 cells and incubated for 24 hr.

To measure glycerol release as a readout for lipolysis, 100 µl of Free Glycerol Reagent was aliquoted per well of a 96-well plate. 10 µl of supernatant media from 3T3-L1 adipocytes was then added to each well. A standard curve was produced by using Glycerol Standard Solution (Sigma-Aldrich, St. Louis, USA; catalog G7793). The plate was incubated at 37˚C for 5 min and then developed with a plate reader set to detect absorbance at 540 nm. Using the standard curve, a fit equation was developed in Excel to convert the absorbance values into glycerol concentrations. To take into account differences that occur in wells on the edge versus middle of the plate, all well positions across all plates in the screen were averaged to create a normalization factor for any given position on the plate. These normalized values were then used to determine top hits for compounds that block lipolysis.

Glycerol release assay with Atglistatin

3T3-L1s were differentiated on a fibronectin-coated 96-well dish. At the start of the lipolysis experiment, 3T3-L1s were changed to serum-free DMEM supplemented with 0.2% BSA FFA-free (Sigma- Aldrich, St. Louis, USA; catalog 9048-46-8). The medium was supplemented with 1% DMSO for negative control or 1 µM isoproterenol to induce lipolysis or ±100 µM Atglistatin (Sigma-Aldrich, St. Louis, USA; catalog

SML1075) to block lipolysis and cells were incubated for 24 hr.

To measure glycerol release, 100 μl of Free Glycerol Reagent was aliquoted per well of a new 96-well plate. 10 μl of supernatant media from 3T3-L1 adipocytes was then added to each well. A standard curve was produced by using Glycerol Standard Solution (Sigma-Aldrich, St. Louis, USA; cata- log G7793). The plate was incubated at 37˚C for 5 min and then developed with a plate reader set to detect absorbance at 540 nm. Using the standard curve, a fit equation was developed in Excel to convert the absorbance values into glycerol concentrations.

Zebrafish drug treatments

Tg(-3.5ubb:plin2-tdTomato) zebrafish were outcrossed with *caspers* to generate the F2 or F3 gener- ation. F2 or F3 fish were raised at a standard density of 50 fish per 6.0 l tank. For drug treatment, fish were removed from the system at 21 dpf and placed at a density of one fish per well in a six- well plate with 10 ml of E3 per well. To evaluate viability, fish were treated for 24 hr and quantified for live and dead larvae. After a 24 hr incubation with the drug, fish were anesthetized with Tricaine and imaged using the described protocol to quantify (1) standard length and (2) area of PLIN2-tdTOMATO expression corresponding to visceral adipose tissue area. Fish were treated with Forskolin (Sigma-Aldrich, St. Louis, USA; catalog #F6886), Auranofin (Sigma-Aldrich, St. Louis, USA; catalog #A6733), JS-K (Sigma-Aldrich, St. Louis, USA; catalog #J4137), or Atglistatin (Sigma-Aldrich, St. Louis, USA; catalog #SML1075[1]), which were all dissolved in DMSO.

Generation of ZMEL-LD cell line

The ZMEL zebrafish melanoma cell line was derived from a tumor of a

mitfa:BRAF^{V600E}*/p53*$^{-/-}$ zebra- fish as described previously.[161] ZMEL cells constitutively express eGFP driven by the *mitfa* promoter.[161] ZMEL cells were grown at 28˚C in a humidified incubator in DMEM (Gibco, Waltham, USA; catalog #11965) supplemented with 10% fetal bovine serum (FBS) (Gemini Bio, #100–500), 1x penicillin/streptomycin/glutamine (Gibco, Waltham, USA; catalog #10378016), and 1x GlutaMAX (Gibco, Waltham, USA; catalog #35050061). To generate the ZMEL-LD cells, ZMEL cells were nucleofected with the *ubb:plin2-tdtomato* plasmid using the Neon Transfection System (Thermo Fisher, Waltham, USA; catalog #MPK10096), selected for 2 weeks in blasticidine-supplemented media at 4 *m*g/*m*l (Sigma-Aldrich, St. Louis, USA; catalog #15205–25 MG), and FACS sorted for GFP and tdTOMATO double-positive cells. ZMEL and ZMEL-LD cells underwent routine *Mycoplasma* testing, most recently in January 2021.

ZMEL-GFP and ZMEL-LD imaging

Eight-well Nunc Lab-Tek Chambered Coverglass was coated with 1:100 dilution of fibronectin in Dulbecco's Phosphate Buffered Saline (DPBS) (Millipore Sigma, Burlington, USA; catalog #FC010-5MG) for 30 min and then washed with DPBS (Thermo Scientific, Waltham, USA; catalog #14190–250). ZMEL-GFP or ZMEL-LD cells were seeded at 30,000 cells per well and left to adhere for 24 hr. A medium supplemented with oleic acid (Sigma-Aldrich, St. Louis, USA; catalog #O3008-5ML) was added for 24 hr. Cells were fixed with 2% paraformaldehyde (Santa Cruz Biotechnology, Santa Cruz, USA; catalog #sc-281692) for 45 min and washed with DPBS. For MDH staining, cells were permeabilized with 0.1% Triton-X (Thermo Fisher, Waltham, USA; catalog #PI85111) for 30 min at room temperature, washed, and stained with 1:500 MDH (Abcepta, San Diego, USA; catalog #SM1000a) for 15 min.

Cells were imaged on the Zeiss LSM 880 inverted confocal microscope with AiryScan using a x63 oil immersion objective. For Lipid staining, cells were stained with 1:500 Lipidtox Deep Red (Thermo Fisher, Waltham, USA; catalog #H34477) and 1:2000 Hoechst 33342 (Thermo Fisher, Waltham, USA; catalog #H3570) for 30 min. Cells were imaged on the Zeiss LSM 880 inverted confocal microscope using a x40 oil immersion objective. Confocal stacks were visualized via FIJI, and 3D reconstruction was created using Imaris (Bitplane Inc, Concord, USA).

ZMEL-LD FACS analysis

ZMEL Dark (no fluorescence), ZMEL-GFP, and ZMEL-LD cells were plated on fibronectin-coated six-well plates at a density of 500,000 cells in 1 ml of media per well. At 24 hr after plating, cells were given either 150 *m*M of BSA or oleic acid with 1 *m*l of DMSO. At 48 and 72 hr after plating, lipid droplet low and high controls were switched to fresh media with 150 μM of BSA or oleic acid with 1 μl of DMSO. Cells pulsed with oleic acid received fresh media with 150 μM of BSA with either 40 μM Atglistatin, 0.5 μM Auranofin, or 0.5 μM JS-K. At 96 hr after plating, cells were trypsinized, washed with DPBS, and resuspended in DMEM supplemented with 2% FBS, 1x penicillin/streptomycin/gluta- mine, and 1x GlutaMAX. Cells were stained for viability with 1:1000 DAPI and strained through the Falcon FACS Tube with Cell Strainer Cap (Thermo Fisher, Waltham, USA; catalog #08-771-23). For Lipidtox comparison, cells were given either BSA or indicated concentrations of oleic acid for 24 hr. Cells were trypsinized, washed with DPBS, stained with 1:250 Lipid Deep Red and 1:1000 DAPI for 10 min, and strained through the Falcon FACS Tube with Cell Strainer Cap. Data was acquired via the Beckman Coulter CytoFLEX

Flow Cytometer (Beckman Coulter, Miami, USA) and analyzed using FlowJo software (BD Biosciences, San Jose, USA).

Schematics

Schematics and illustrations were generated using Biorender on biorender.com.

Statistics

All statistical analyses were performed using GraphPad Prism 8 (Graphpad, San Diego, USA). Data are presented as mean ± 95% confidence interval (CI) or standard error of the mean (SEM). $p<0.05$ was considered statistically significant. Statistical tests used are noted in the figure legend. All experiments were done with at least three independent replicates. For in vivo experiments, N denotes the number of independent experiments while n denotes the number of individual fish. Imaging analyses utilized FIJI, Imaris, and MATLAB software.

Availability of resources

All zebrafish cell lines and transgenic lines are available upon request. In addition, the *Tg(-3.5ubb: plin2-tdTomato)* zebrafish will be deposited at the Zebrafish International Resource Center.

Acknowledgements

We thank members at the Memorial Sloan Kettering Cancer Center Aquatics Core, Molecular Cytology Core, and Flow Cytometry Core for their contributions to this work. We thank Dr. Mohita Tagore and Dr. Ting-Hsiang (Richard) Huang for comments on the project and manuscript.

Funding Sources

DL was supported by F30 CA254152 from the NCI. DL, JMW, and AA were supported

by T32GM007739-42 from the NIH. AA was supported by F30 HD 103398 from the NIH. EJ was supported by F31 AR079215 from NIAMS. David Ola was supported by R25CA020449 from the NIH. RMW was supported by the following grants: Melanoma Research Alliance, R01CA229215 from the NIH, R01CA238317 from the NIH, DP2CA186572 from the NIH, The Pershing Square Foundation, The Mark Foundation for Cancer Research, Harry J. Lloyd Charitable Trust, P30 CA008748 from the NIH, Consano, SCC and the American Cancer Society.

Ethics

Animal experimentation: This study was performed in strict accordance with the recommendations in the Guide for the Care and Use of Laboratory Animals of the National Institutes of Health. All of the animals were handled according to approved institutional animal care and use committee (IACUC) protocols (#12-05-008) of Memorial Sloan Kettering Cancer Center. The protocol was approved by the Committee on the Ethics of Animal Experiments of Memorial Sloan Kettering Cancer Center (Permit Number: D16-00199). Every effort was made to minimize suffering.

Competing interests

Richard White: Senior editor, eLife. Is a paid consultant to N-of-One Therapeutics, a subsidiary of Qiagen. Is on the scientific advisory board of Consano, but receives no income for this. Receives royalty payments for the use of the casper zebrafish line from Carolina Biologicals. All other authors declare no competing interests.

CHAPTER 3: THE LIPID DROPLET PROTEIN DHRS3 IS A REGULATOR OF MELANOMA CELL STATE

This chapter is based on the following manuscript in preparation:

Johns E, Ma Y, Louphrasitthipol P, Peralta C, Hunter MV, Raymond JH, Molina H, Goding CR, White RM. The lipid droplet protein DHRS3 is a regulator of melanoma cell state.

3.1 Abstract:

Lipid droplets are fat storage organelles composed of a protein envelope and lipid rich core. Regulation of this protein envelope underlies differential lipid droplet formation and function. In melanoma, lipid droplet formation has been linked to tumor progression and metastasis, but it is unknown whether lipid droplet proteins play a role. To address this, we performed proteomic analysis of the lipid droplet envelope in melanoma. We found that lipid droplet proteins were differentially enriched in distinct melanoma states; from melanocytic to undifferentiated. DHRS3, which converts all-trans-retinal to all-trans-retinol, is upregulated in the $MITF^{LO}$/undifferentiated/neural crest-like melanoma cell state and reduced in the $MITF^{HI}$/melanocytic state. Increased DHRS3 expression is sufficient to drive $MITF^{HI}$/melanocytic cells to a more undifferentiated/invasive state. These changes are due to retinoic acid mediated regulation of melanocytic genes. Our data demonstrate that melanoma cell state can be regulated by expression of lipid droplet proteins which affect downstream retinoid signaling.

3.2 Main Text

Introduction

Cell plasticity is one of the defining features of melanoma, with significant differences in clinical outcomes associated with phenotype switching.[3,54,56] Melanoma cells can reversibly move between different transcriptional states, each of which is associated with distinct phenotypes. These different cell states can have important implications in disease progression, metastasis, and drug resistance.[3,57,59,226] Numerous studies have attempted to define transcriptomic signatures that identify these diverse melanoma cell states, which have begun to converge on at least 4 distinct classifications: undifferentiated, neural crest-like, transitory, and melanocytic.[54,57-59] What drives each and what allows cells to move between states, remain significant open questions.

Across a multitude of tumor types, uptake of fatty acids has been shown to support a variety of tumor metabolic needs which can facilitate tumor formation, cancer cell survival, and metastasis.[84,227,228] Lipid droplets, which are associated with excess fatty acid levels, have long been studied for their roles in fatty acid and lipid storage, particularly in specialized cells such as adipocytes. However, there is increasing interest in understanding the complex role of lipid droplets in cellular metabolism across a diversity of cell types and disease states. Recent research has clearly demonstrated the importance of lipid droplet formation and function in melanoma,[88,93,151] however we do not fully understand how lipid droplet formation affects disease progression. Furthermore, the dynamic regulation of the lipid droplet in this lineage remains an open area of investigation.

Previous work from our laboratory has demonstrated that formation of lipid droplets is associated with changes in cell state. During melanoma development, tumor cells take up diverse species of fatty acids from nearby adipocytes and readily form lipid droplets.[88] Uptake of saturated fatty acids is linked to a more undifferentiated, invasive cell state.[229] Conversely, melanocytic melanoma cells, which are more oxidative, rely on increased lipid droplet content to support unsaturated fatty acid flux through the mitochondria.[93] These observations imply that the regulation and function of lipid droplets is highly dependent on cellular context and substrate availability. Furthermore, they suggest that lipid droplets may be linked to distinct transcriptional cell states.

While significant work has focused on the lipid components of the droplet, many studies also focus on the protein coat which surrounds the lipid rich core.[116] Differential localization of proteins to the lipid droplet membrane can have dramatic effects on lipid droplet function as well as cellular metabolism.[118,120,124] Numerous proteomic studies have been conducted to better understand the role of these lipid droplet proteins in a variety of contexts.[122,124,133,135,137] These observations led us to hypothesize that proteins in the lipid droplet coat might be determinants of melanoma cell state.

To better understand the potential role of lipid droplets in determining melanoma phenotypic identity we used APEX2 proximity labeling[135,136] to define the melanoma lipid droplet proteome. Using a combination of transcriptomic and biochemical approaches, we demonstrate that a particular lipid droplet protein, DHRS3, plays a critical role in supporting the undifferentiated/neural crest-like melanoma cell state.

Proximity labeling of the melanoma lipid droplet proteome

We hypothesized that a key determinant of the effect of lipid droplet accumulation in melanoma would be due to the dynamic composition of the lipid droplet protein coat. As no previous study had examined the melanoma lipid droplet proteome, we adapted lipid droplet targeted APEX2 proximity labeling[135,136] for our cell type of interest. This approach utilizes a lipid droplet specific APEX2 (by fusion to the lipid droplet protein Perilipin 2 (PLIN2). We introduced an inducible lipid droplet targeted PLIN2-V5-APEX2 construct along with a cytosolic, Cyto-V5-APEX2 control to A375 human melanoma cells (Figure 26A). Titration of doxycycline for 48 hours showed dose responsive expression of the APEX2 fusion constructs (Figure 26B). In addition, treatment with biotin phenol and H_2O_2 demonstrated robust, inducible biotinylation of proteins in both conditions (Figure 26B, Figure 27C). To collect the large numbers of lipid droplets necessary for proteomics,[135] we treated cells with 200 μM Oleic Acid for 24 hours (Figure 27A-B). Imaging of the PLIN2-V5-APEX2 and Cyto-V5-APEX2 cell lines showed clear localization of APEX2 to the lipid droplet combined with an enrichment of biotinylated proteins around the lipid droplet in PLIN2-V5-APEX2 cells only (Figure 26C).

Given that we observed labeling of cytosolic proteins in PLIN2-V5-APEX2 cells, as has been previously reported,[135] we performed a further enrichment of lipid droplets by combining the proximity labeling approach with gradient ultracentrifugation (Figure

26D).[135] Using this method, we were able to isolate intact lipid droplets relatively devoid of common contaminants (Figure 26E, Figure 27D).

Figure 26

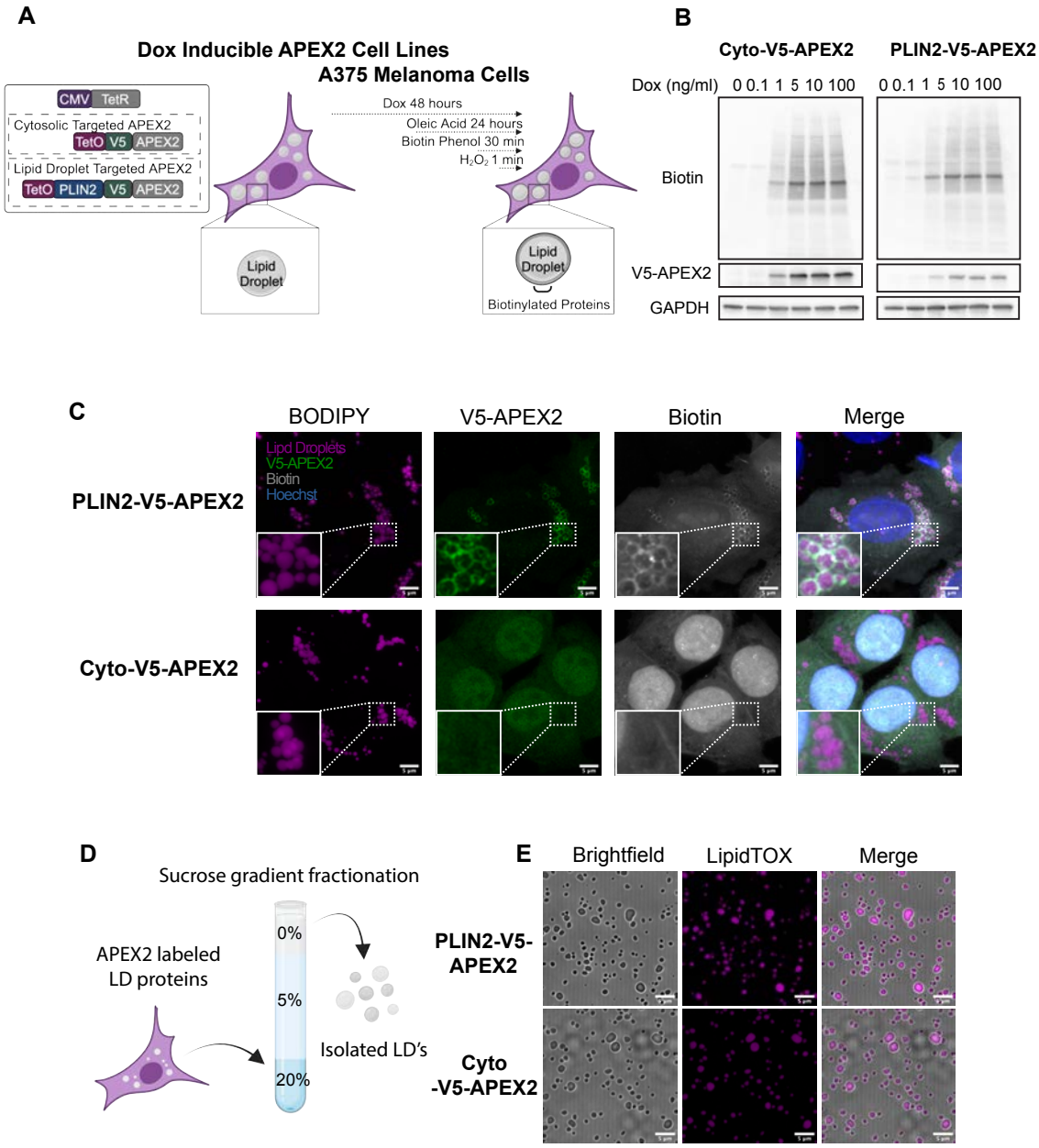

Figure 26. Proximity labeling of the melanoma lipid droplet proteome

A. Schematic of the APEX2 expressing cell lines used in this study B. Western blot of cells treated with indicated doses of doxycycline for (48 hours) and 200 μM Oleic Acid (24 hours) followed by 30 minutes of biotin phenol (500 μM) and 1 minute of H_2O_2 (1 mM). C. Immunofluorescence imaging of APEX2 expressing cells treated as in B followed by fixation and staining for lipid droplets (BODIPY), PLIN2-V5-APEX2 (V5

antibody) and biotin (Streptavidin antibody). Representative high-resolution images from n = 18 images taken from n = 3 independent experiments. Shown as max intensity projections. Scale bars are 5 μm. D. Simplified schematic of gradient ultracentrifugation to isolate lipid droplets (see methods). E. Confocal imaging of lipid droplets stained with the lipid droplet dye LipidTOX after isolation. All data are representative of at least n = 3 independent experiments. Scale bars are 5 μm. Diagrams made with Biorender.com

Figure 27—Related to Figure 26

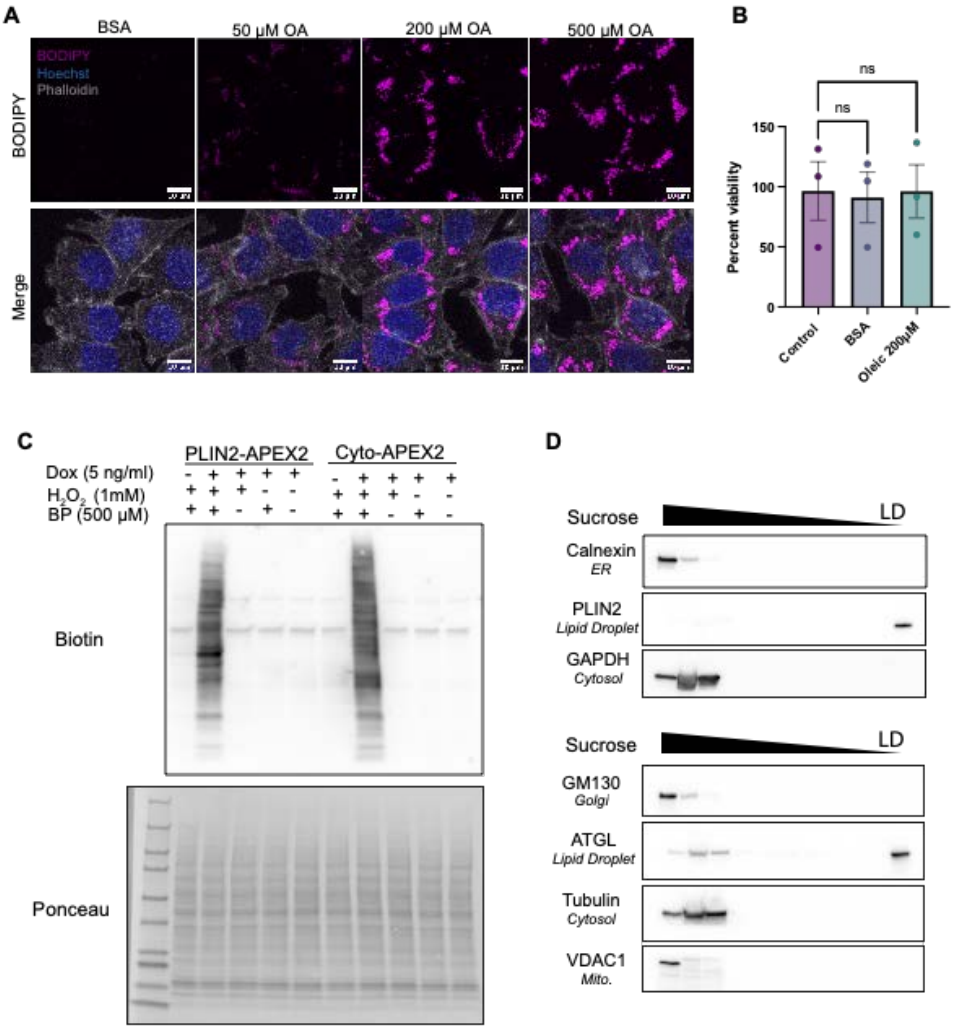

Figure 27—Related to Figure 26. Validation of lipid droplet isolation with APEX2 and gradient ultracentrifugation.

A. Titration of Oleic Acid in A375 cells for 24 hours followed by fixation and imaging. Scale bars are 5 μm. B. Cyquant to measure cell viability after 24-hour treatment with 200 μM Oleic Acid. Data are normalized to the average of the control. Significance measured with One way ANOVA with Dunnett's Multiple Hypothesis Correction. Data are presented as mean +/- SD. C. Western blot of Cyto-V5-APEX2 and PLIN2-V5-APEX2 cell lines treated +/- H_2O_2 for 1 min, +/- Biotin Phenol for 30 min, and

Doxycycline for 48 hours at the indicated doses D. Representative western blot results for fractionation of lipid droplets from wild-type A375 cells (following 24-hour treatment with Oleic Acid). Fractions were loaded in equal percent by volume. Data in A-D are representative of 3 independent experiments.

Identification of the melanoma lipid droplet proteome

To characterize the lipid droplet proteome in melanoma cells we performed mass spectrometry. We induced APEX2 activity followed by gradient ultracentrifugation to isolate biotinylated lipid droplet fractions. Western blotting demonstrated effective isolation of a biotinylated fraction in PLIN2-V5-APEX2 cells treated with H_2O_2 (Figure 28A), but not in Cyto-V5-APEX2 (Figure 28B) or no H_2O_2 controls (Figure 28C). After isolation of lipid droplet fractions, we used streptavidin immunoprecipitation to enrich for the biotinylated proteins followed by LC-MS/MS (Figure 28D). Analysis revealed clear differentiation between samples depending on condition (Figure 29) and enrichment of canonical lipid droplet proteins (Figure 28E, Figure 30).

To generate a list of lipid droplet proteins, we used label free quantification based on the Intensity Based Absolute Quantification (iBAQ) value for each protein. To account for the cytosolic background and nonspecific binding to the beads we subtracted the average Cyto-V5-APEX2 iBAQ values from the PLIN2-V5-APEX2 iBAQ values to generate a normalized iBAQ value.[136] To determine a high confidence list of lipid droplet proteins, we set a cut-off such that 60% of previously validated lipid droplet proteins were identified[135] (Table 1), which yielded a total of 96 proteins (Figure 28E, Table 2). Analysis of this list with gProfiler demonstrated enrichment of lipid droplet genes as the top pathway (Figure 28F-G). We were therefore able to determine a robust list of 96 lipid droplet proteins in melanoma.

Figure 28

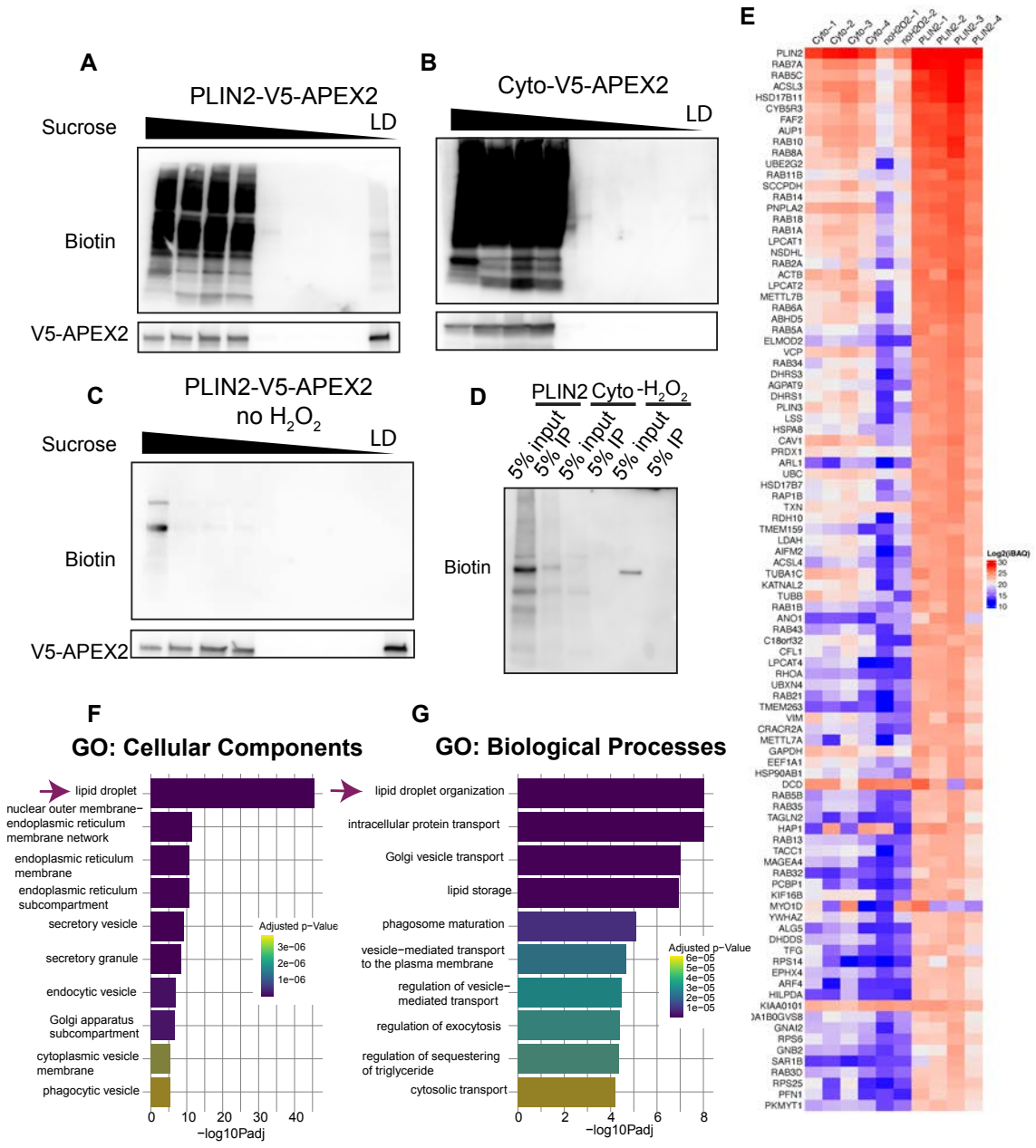

Figure 28. Identification of the melanoma lipid droplet proteome

A-C. Representative western blots (from n = 4 independent experiments) of equal percent by volume of each fraction after APEX2 labeling and gradient ultracentrifugation as described in Methods. D. Representative western blot of streptavidin immunoprecipitation of isolated lipid droplet proteins from the indicated conditions which were used for LC-MS/MS E. Heatmap of the log_2iBAQ values for the top 96 lipid

droplet proteins identified by LC-MS/MS. F-G. Top 10 pathways as identified using gProfiler. Data are representative of 4 independent experiments (Cyto and PLIN2-APEX2) and 2 independent experiments for -H_2O_2.

Figure 29—Related to Figure 28

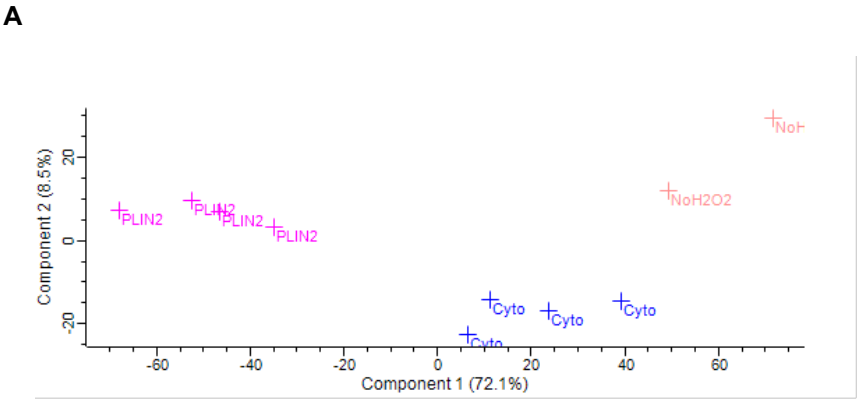

Figure 29—Related to Figure 28. Analysis of LC-MS/MS results.

PCA plot of the 10 conditions submitted for LC-MS/MS. Each condition clusters separately indicating true differences between the proteins identified with each.

Figure 30—Related to Figure 28

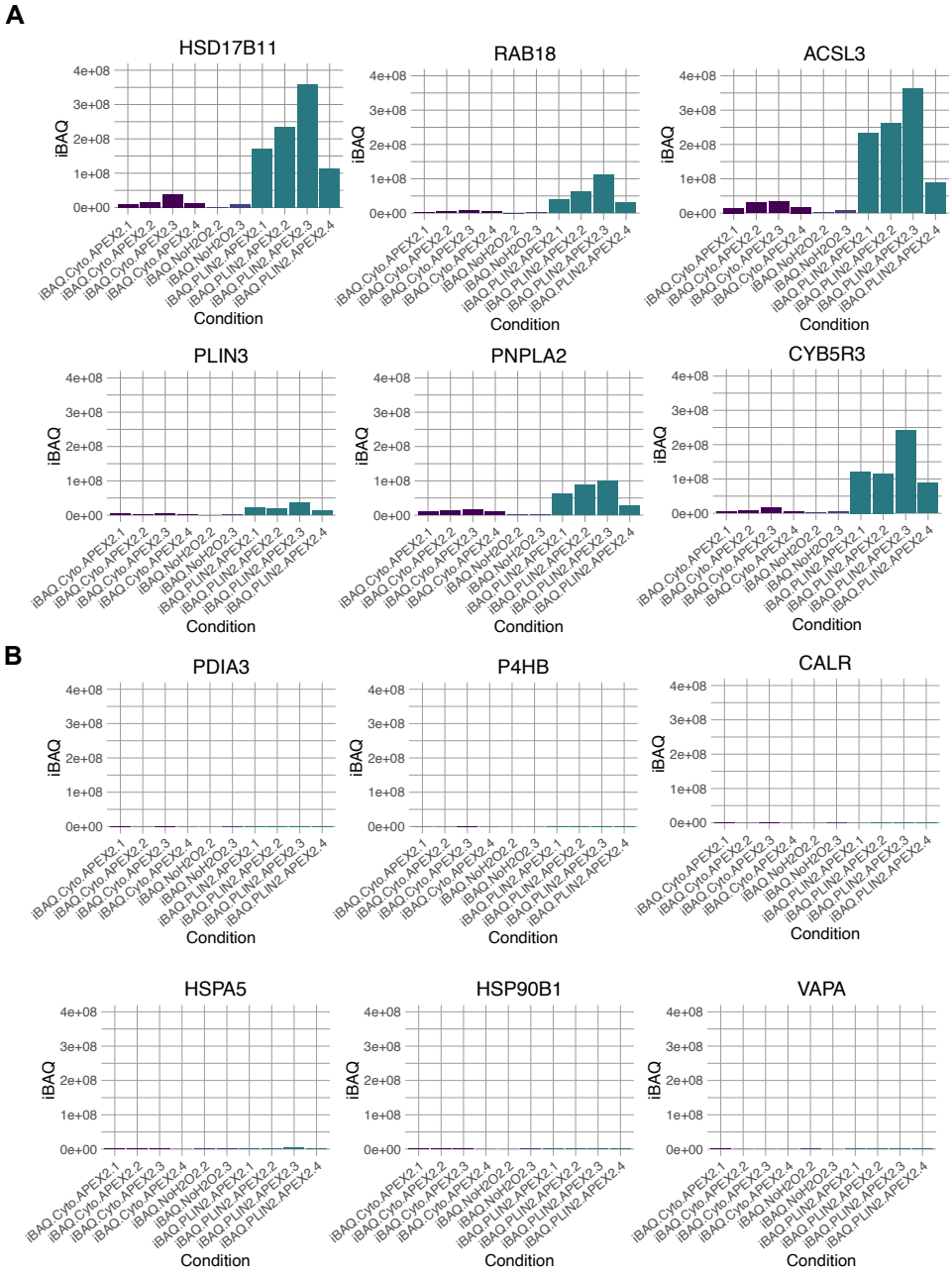

Figure 30—Related to Figure 28. Quality control of lipid droplet proteomic data.

A-B. iBAQ values of commonly identified lipid droplets (A) and common contaminants (B).

DHRS3 is a lipid droplet protein enriched in the undifferentiated/neural crest versus melanocytic cell state

We next sought to better understand the function of these lipid droplet proteins in melanoma. We were most interested in lipid droplet proteins that might have a function in specific melanoma phenotypes, as opposed to general functions that occur in most cell types. Because it is now well-recognized that human melanomas exist in at least 4 distinct transcriptional states (Figure 31A), we asked whether any of the identified proteins were specifically enriched in certain states. To do this, we compared our proteomics data to published melanoma transcriptional cell state signatures which have been linked to these phenotypic states: undifferentiated, neural crest-like, transitory, and melanocytic.[57] We decided to focus on one protein, DHRS3, for further downstream functional analysis. DHRS3 is the enzyme that converts all-trans-retinal to all-trans-retinol[230,231] (Figure 31B, Figure 33A). This was especially intriguing to us given the known role of retinoid signaling in melanocyte differentiation[232,233] as well as previous data which identified Retinoid X Receptors (RXRs) as a therapeutic vulnerability of the neural crest-like melanoma cell state.[3] We found that *DHRS3* was markedly enriched in the undifferentiated and neural crest-like melanoma cells (Figure 31C-D) compared to the melanocytic/pigmented state, where it is minimally expressed. This made it a good candidate for studying its functional role in these very different phenotypic cell states. As we generally see similar trends in DHRS3 levels between the undifferentiated and neural crest-like states vs. the melanocytic state, we will be referring to this less differentiated group as undifferentiated/neural crest-like for the rest of the paper. Confirming the link between upregulation of *DHRS3* mRNA and protein, DHRS3 protein was also

upregulated in neural crest-like cells in the CCLE proteomics dataset (Figure 31E).[234] We also analyzed a previously published human melanoma single cell RNA-seq dataset[59] composed of expression data from patient-derived cell lines classified as either 'mesenchymal', 'intermediate' or 'melanocytic'. Similar to what we observed in the TCGA and CCLE bulk RNA-seq datasets, *DHRS3* was highly expressed in mesenchymal/intermediate-like cell lines and downregulated in melanocytic cell lines (Figure 31F). Taken together, our data suggests that DHRS3 mRNA and protein expression is associated with the undifferentiated/neural crest-like cell state in melanoma, raising the question of whether it plays a functional role.

Figure 31

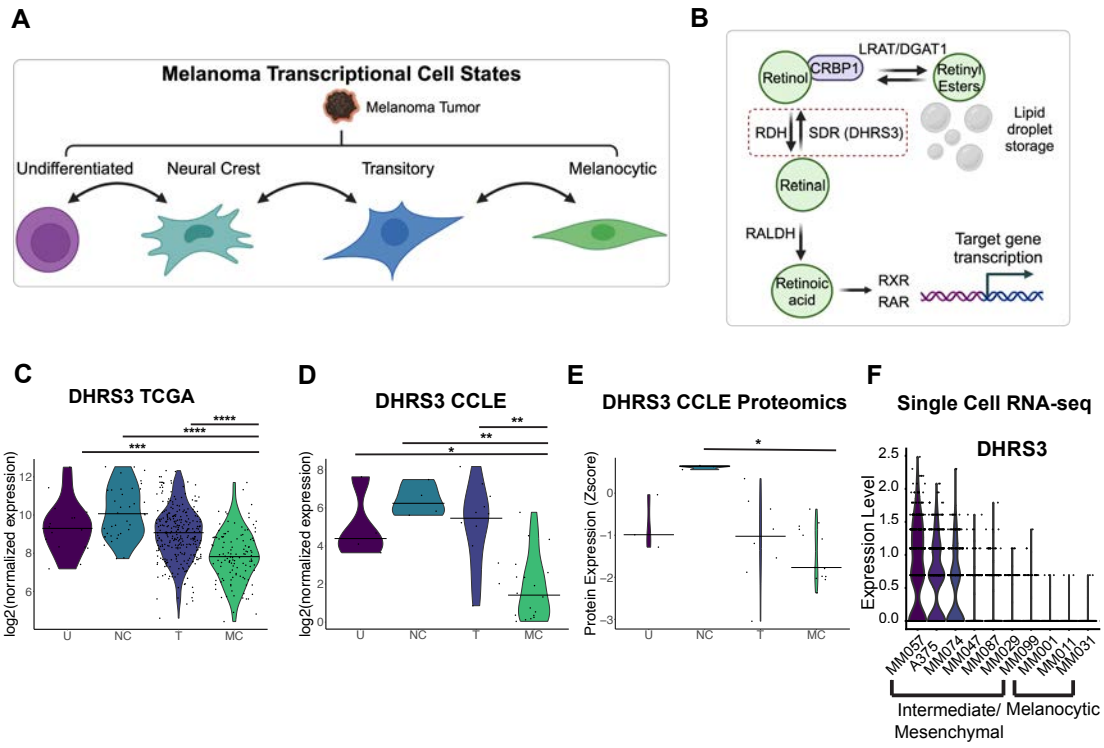

Figure 31. DHRS3 is a lipid droplet protein enriched in the undifferentiated/neural crest versus melanocytic cell state

A. Diagram of the four melanoma transcriptional cell states as in[57] B. Simplified diagram of retinoic acid metabolism, highlighting the known function of DHRS3[231]. C-D. Violin plots of analysis of the CCLE and TCGA transcriptomic databases (bar = median, dots

represent each sample or cell line.). Data was grouped by the Tsoi cell state classifiers which have been previously annotated for this data [57]. Statistics were generated with two-sided Wilcoxon rank sum test with Holm correction. * $p < 0.05$ **, $p < 0.01$, *** $p < 0.001$, **** $p < 0.0001$. U = Undifferentiated, NC = Neural Crest-like, T = Transitory, M = Melanocytic E. Analysis of the CCLE proteomics database. Data was grouped by Tsoi cell state classifiers. Statistics were generated with two-sided Wilcoxon rank sum test with Holm correction. * $p < 0.05$. F. Normalized expression of DHRS3 in scRNA-seq of patient derived melanoma cell lines. Cell lines are grouped by cell states identified in the manuscript [59].

DHRS3 is an effector of melanoma cell state

DHRS3 has been previously identified in lipid droplets,[124,235,236] but its functional role remains incompletely understood, particularly in the context of melanoma. We first confirmed our proteomic results by immunofluorescence. Consistent with our data, we found that DHRS3 exclusively localizes to the lipid droplet in A375 cells in both normal media and media with oleic acid (Figure 32A).

To study the functional relationship between DHRS3 expression and melanoma cell state, we sought to use an isogenic cell line system that represented these different states. A unique resource in melanoma are the IGR37/IGR39 cell lines. These are two cell lines that come from the same melanoma patient but have markedly different characteristics. The IGR37 line is melanocytic, with high levels of *MITF*, and the cells readily pigment. The IGR39 line is undifferentiated, does not express *MITF*, and is unpigmented. Furthermore, IGR37 cells are sensitive to BRAF inhibition while IGR39 cells are resistant and invasive.[72] This pair of lines best represents the melanocytic and undifferentiated cell states respectively[57] (Figure 32B). At both the RNA and protein level, DHRS3 is markedly higher in the IGR39 ($MITF^{LO}$, undifferentiated) cells compared to the IGR37 ($MITF^{HI}$, melanocytic) cells (Figure 32C-E), consistent with our

TCGA/CCLE analysis above. Moreover, when we compared the top 30 proteins we found at the lipid droplet by proteomics, DHRS3 is the sole protein that reliably distinguishes the IGR37 vs. IGR39 cell line (Figure 32C-D). Consistent with this, when we treated cells with oleic acid, DHRS3 was enriched at the lipid droplet in IGR39 cells but not IGR37 cells (Figure 32F). To extend this observation to other cell lines, we performed imaging of additional undifferentiated/neural crest-like cell lines, which revealed a similar localization of DHRS3 to the lipid droplet (Figure 33B-C).

Figure 32

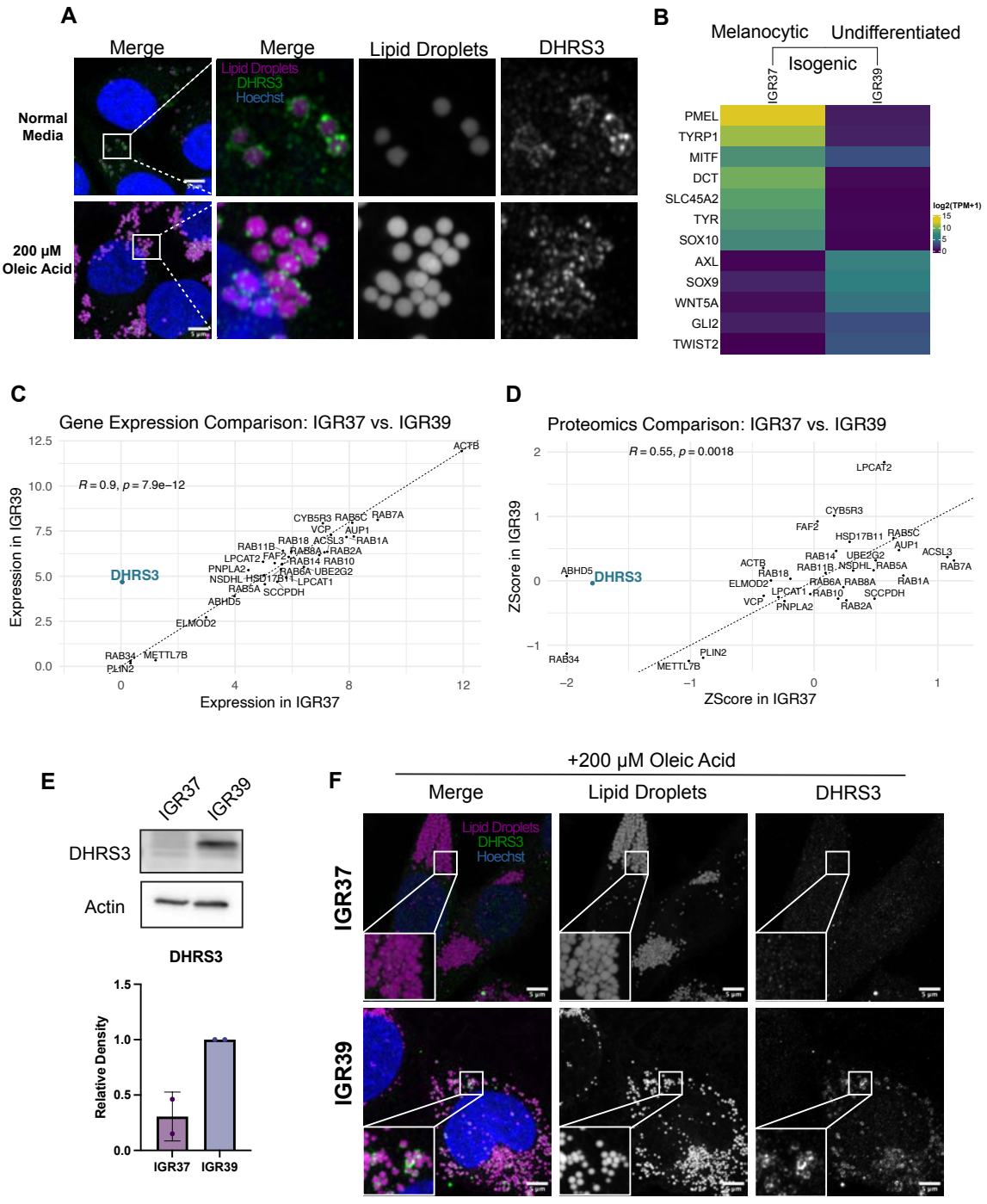

Figure 32. DHRS3 is enriched in undifferentiated/neural crest-like melanoma cells

A. Representative images of staining for endogenous DHRS3 and lipid droplets (BODIPY) in A375 cells. Where indicated cells were treated with oleic acid for 24 hours. Images are representative of 2 independent experiments and shown as max intensity projections. Scale bars are 5 µm. B. Heatmap of log2 Normalized Counts (from the

CCLE) of some representative genes known to differentiate undifferentiated vs. melanocytic cells. C. Scatter plot comparing the expression level (log2 Normalized Counts) of the top 30 lipid droplet genes in the melanoma lipid droplet proteome in IGR37 vs. IGR39 melanoma cells. DHRS3 is highlighted on the graph. Correlation calculated with Spearman Correlation Coefficient. D. Scatter plot comparing the protein level (ZScore) of the top 30 lipid droplet proteins in the melanoma lipid droplet proteome in IGR37 vs. IGR39 cells. DHRS3 is highlighted in the graph. Correlation calculated with Spearman Correlation Coefficient. E. Western blot with quantification of DHRS3 protein levels. Representative of 2 independent experiments. Data are presented as mean +/- SD. F. Representative images of IGR37 and IGR39 cells treated with oleic acid for 24 hours. Cells were fixed & stained with LipidTOX and an antibody against endogenous DHRS3. Data from 3 independent experiments. Shown as max intensity projections. Scale bars are 5 μm.

Figure 33—Related to Figure 31 & 32

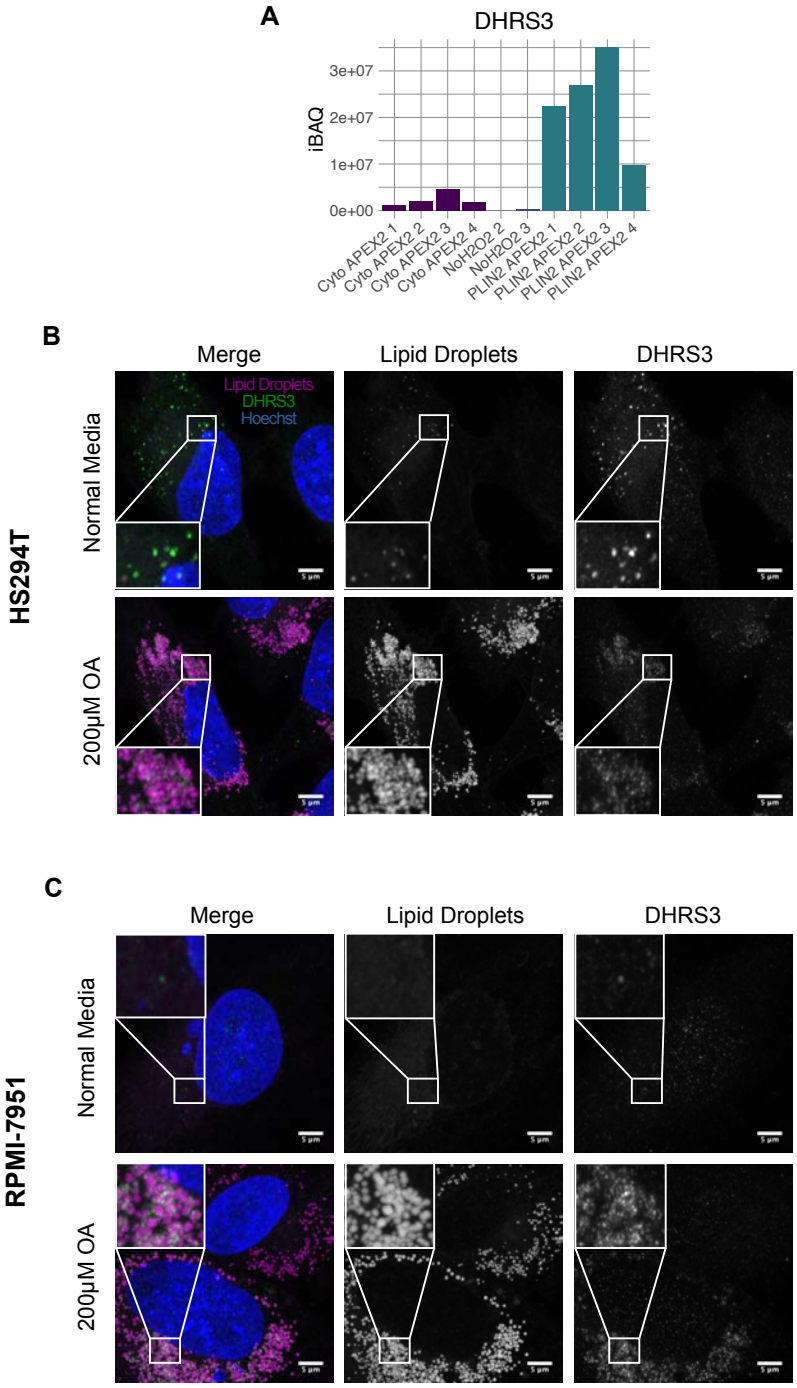

Figure 33—Related to figure 31 and 32. Localization of DHRS3 to the lipid droplet in undifferentiated melanoma cells.

A. iBAQ values from the lipid droplet proteomics dataset for DHRS3. B-C Representative images of HS294T (B) and RPMI-7951 (C) stained for lipid droplets (LipidTOX) and endogenous DHRS3 in normal media and media with 200 µM Oleic Acid for 24 hours. Scale bars are 5 µm.

To test the role of DHRS3 in melanoma cell state, we overexpressed DHRS3 in the IGR37 (melanocytic) cells, which normally have very low levels of the protein (Figure 34A-B). Consistent with the hypothesis that DHRS3 promotes de-differentiation of melanoma cells, overexpression of DHRS3 in IGR37 cells resulted in a visible decrease in pigmentation (Figure 34C). To define the downstream targets of DHRS3 in melanoma, we performed bulk RNA-sequencing on IGR37 DHRS3 overexpressing versus control cells. This revealed a total of 297 differentially expressed genes (Figure 35A). To determine whether overexpression of DHRS3 induced transcriptional changes in IGR37 cells representative of de-differentiation, we used Gene Set Enrichment Analysis (GSEA) to calculate an enrichment score for each of the previously published gene sets corresponding to melanoma cell state.[57] Cells overexpressing DHRS3 highly upregulated genes corresponding to the undifferentiated/neural crest-like states (Figure 34D, Figure 35B-C). GSEA also revealed that pathways related to tumor invasion and epithelial-to-mesenchymal transition were highly enriched in DHRS3^{OE} cells (Figure 34E), consistent with a less differentiated cell state.[54,57,71]

Figure 34

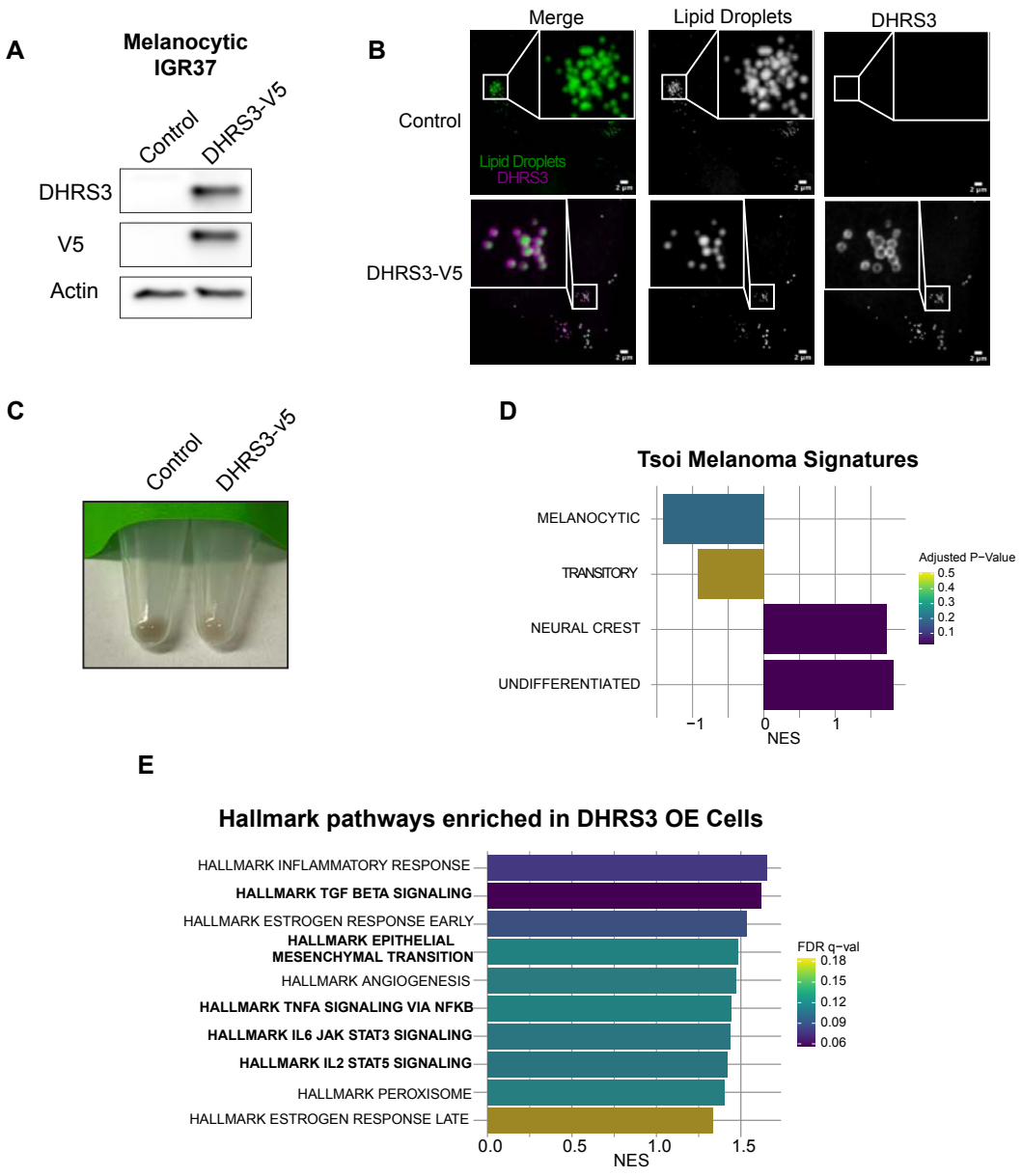

Figure 34. DHRS3 is an effector of melanoma cell state

A. Representative western blot of DHRS3 overexpression. Data from 3 independent experiments. B. Representative images of DHRS3 overexpressing and control IGR37 cells. Data from n = 2 independent experiments. Shown as max intensity projections. Scale bars are 2 µm. C. Representative image of pellet color in Control and DHRS3 overexpressing cells. Cells were counted prior to spinning down to ensure equal numbers. Data representative of at least 3 independent experiments. D. GSEA results using log2FC generated by DESeq2 using custom pathways generated from the Tsoi classifications.[57] E. GSEA results using normalized counts from bulk RNA-seq. Hallmark pathways related to invasion and EMT are shown in bold. RNA-seq data was collected in triplicate.

DHRS3 regulates differentiation through retinoid signaling

We next performed a broader pathway analysis using the Curated Gene Sets from MSigDB. Amongst the enriched pathways were those related to retinoid metabolism, which is in line with the known function of DHRS3[230] (Figure 36A). In further support of a relationship between DHRS3 overexpression and retinoid metabolism, when we performed motif analysis to identify conserved transcription factor binding motifs within the promoter regions of genes upregulated upon $DHRS3^{OE}$, we found significant enrichment of a HOX motif (Figure 35D). HOX genes are well established downstream targets of RXR/RAR signaling.[237,238] Enrichment of the HOX motif further suggested to us that RXR/RAR activity was impacted, which in turn caused changes in HOX gene activity and regulation of downstream genes.

Figure 35—Related to Figure 34 & 36

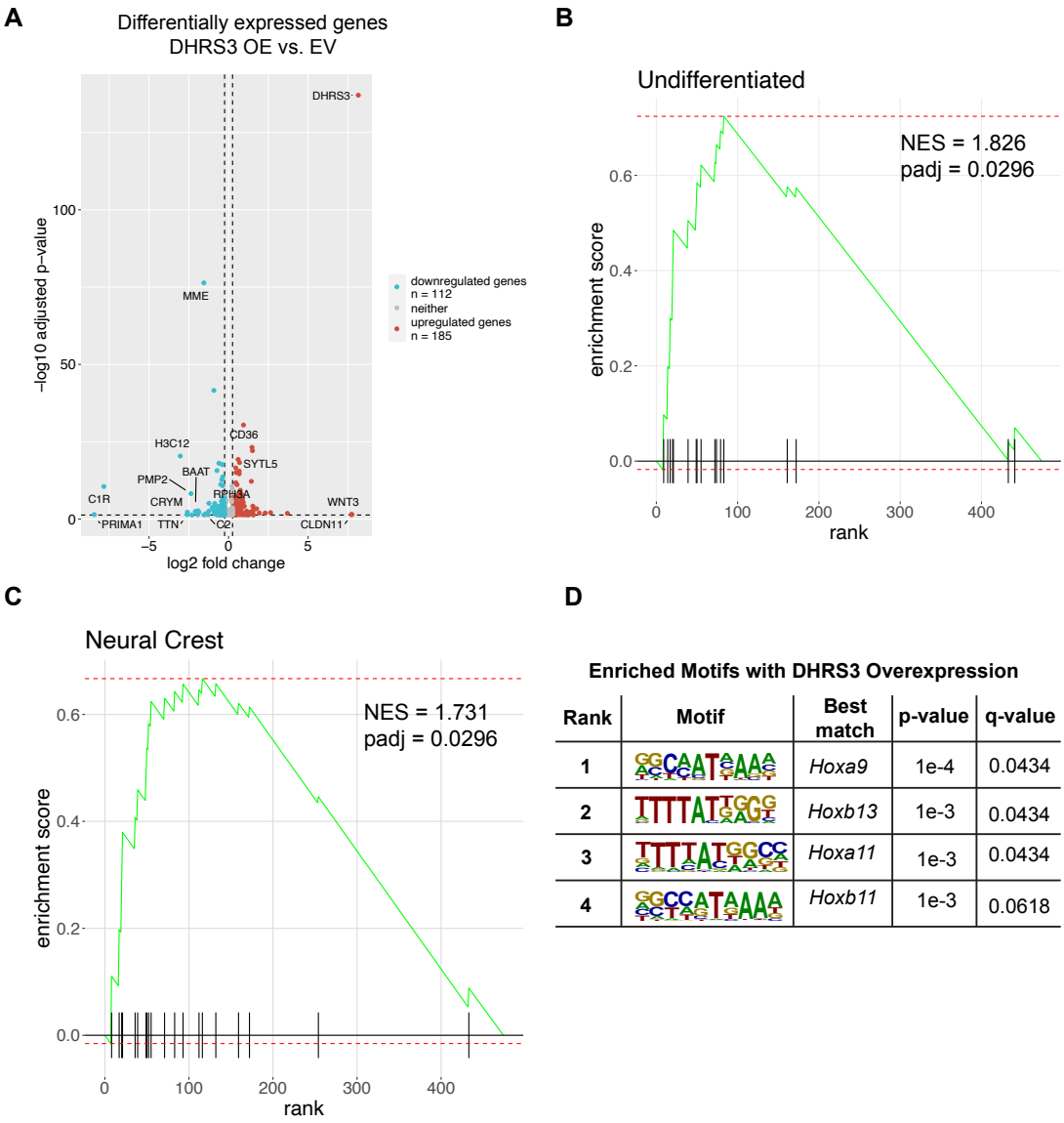

Rank	Motif	Best match	p-value	q-value
1		*Hoxa9*	1e-4	0.0434
2		*Hoxb13*	1e-3	0.0434
3		*Hoxa11*	1e-3	0.0434
4		*Hoxb11*	1e-3	0.0618

Figure 35—Related to Figure 34 & 36. Differential gene expression & pathway analysis of DHRS3 RNA-seq.

A. Volcano plot showing differentially expressed genes in DHRS3 OE vs. Control cells. B-C. Enrichment plots of Tsoi undifferentiated (B) and neural crest-like (C) pathways in DHRS3 OE cells. D. Top known motifs from HOMER motif enrichment analysis of the upregulated genes in DHRS3 OE cells (with $p<0.05$).

DHRS3 functions in an intermediate step of retinoic acid metabolism. It acts in opposition to RDH10, converting all-trans-retinal (which is converted to active retinoic

acid) to all-trans-retinol, which can be esterified and stored in lipid droplets (Figure 31B).[230] Retinoic acid metabolism has long been known to influence melanocyte differentiation and retinoids have been explored as treatment options in melanoma.[232,233,239] We hypothesized that higher DHRS3 levels would decrease the level of retinoic acid in the cell. This decrease would in turn downregulate RAR/RXR transcriptional activity and in part explain the change in cell state we observe in DHRS3 overexpressing IGR37 cells. To explore the link between DHRS3 levels, retinoic acid metabolism, and cell state we treated IGR37 cells with 9-cis-Retinoic Acid (9-cis-RA), a well-known agonist of retinoid X receptors (Figure 36B).[240] In line with previous data,[241] 9-cis-RA treatment causes a significant increase in pigmentation in control cells (Figure 36C). However, consistent with our hypothesis, DHRS3^{OE} cells treated with an equivalent dose of 9-cis-RA were significantly less pigmented than control cells (Figure 36C). This suggests that DHRS3 is acting antagonistically to retinoic acid mediated activation of RXRs. Echoing the effect on pigmentation, when we performed qPCR analysis of Tyrosinase (*TYR*), a key enzyme required for melanin synthesis and pigmentation, we observed a significant decrease in *TYR* expression in DHRS3^{OE} cells. Treatment with 9-cis-RA could rescue this defect, but *TYR* expression remained somewhat lower than in control cells also treated with 9-cis-RA (Figure 36D). This would suggest that DHRS3 antagonizes the effects of RXR activation, potentially by shuttling retinoic acid intermediates towards retinyl ester formation and sequestration in the lipid droplet (Figure 37H).

Figure 36

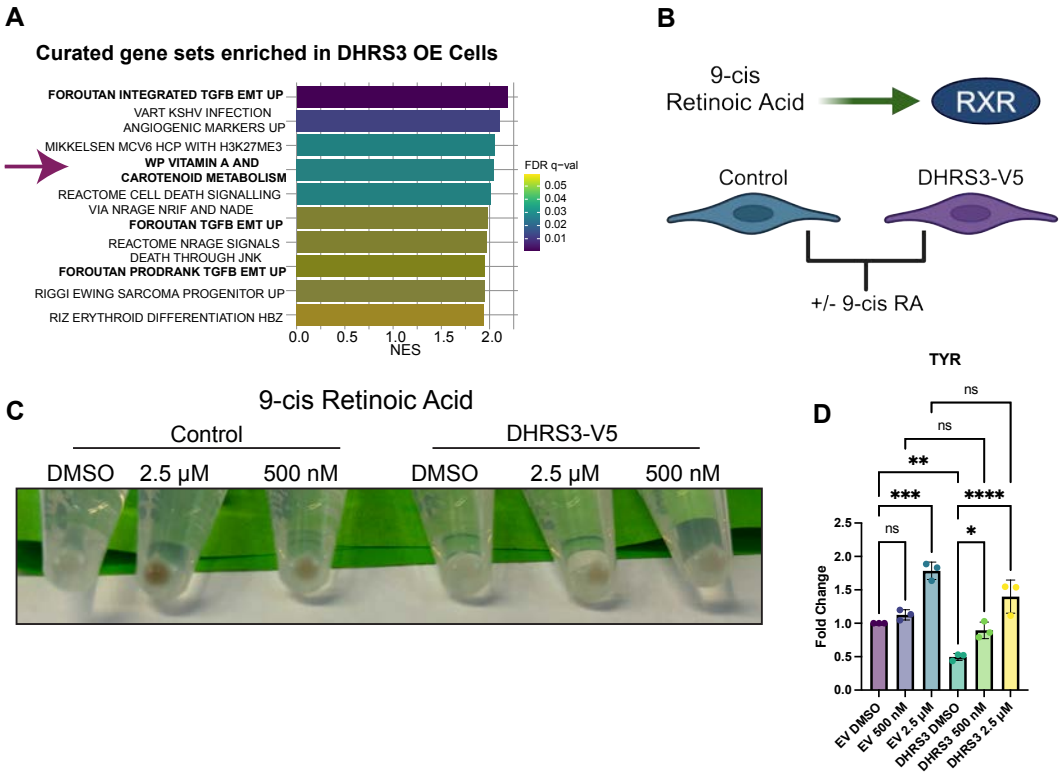

Figure 36. DHRS3 regulates differentiation through retinoid signaling

A. GSEA results using normalized counts from bulk RNA-seq and the Curated Gene Sets list from MSigDB. Retinoic acid related pathway is highlighted by the arrow. B. Schematic of the 9-cis-RA experiment that is shown in C. C. Cells were treated with indicated doses of 9-cis-RA for 3 days and then collected. 250,000 cells per condition were collected, washed in PBS, and imaged to assess pellet color. Image is representative of n = 3 independent experiments. D. qPCR of TYR from cells treated as in C. Data were collected in triplicate for n = 3 independent experiments. Graphs are shown with mean +/- SEM and statistics via One-way ANOVA with Holm-Sidak's multiple comparison correction. * $p < 0.05$, ** $p < 0.01$, *** $p < 0.001$, **** $p < 0.0001$. Diagrams made with Biorender.com.

DHRS3 is regulated by MITF, the key regulator of melanoma cell plasticity

It has long been observed that melanoma cell state is regulated by MITF, a transcription factor that acts as the master regulator of melanocyte development.[242] In normal melanocyte development, undifferentiated/neural crest cells express low levels of *MITF* and are unpigmented. As these cells differentiate, MITF activity increases and directly

activates expression of pigmentation genes such as Tyrosinase (*TYR*) and *PMEL*.[243] In melanoma, a similar cascade is maintained, with the $MITF^{LO}$ cells representing the undifferentiated/neural crest-like state, and the $MITF^{HI}$ cells representing the melanocytic state.[56] Given that we found high levels of DHRS3 mRNA and protein only in the undifferentiated/neural crest-like cells, this raised the question of whether DHRS3 expression is regulated by MITF.

To test this, we interrogated a previously published MITF ChIP-seq data set.[244] This analysis revealed an 8 bp MITF consensus sequence[245] within the first DHRS3 exon (Figure 37A). As DNA binding is not necessarily indicative of regulation, we next determined whether DHRS3 could be regulated by β-catenin, a known regulator of *MITF* expression[246-248] and a MITF co-factor.[249] We used IGR37 human melanoma cells engineered to express doxycycline-inducible β-catenin[250] followed by RNA-seq of cells treated with doxycycline compared to untreated cells (Figure 37B).[250] In IGR37 cells overexpressing β-catenin, we quantified a marked 18-fold up(+4.2log2) up-regulation of *MITF* expression and a dramatic reduction (128-fold, -7log2) in *DHRS3* mRNA expression (Figure 37C). This result suggests that DHRS3 is repressed either by β-catenin complexed with other DNA binding factors such as LEF/TCF, or by MITF itself. To test for regulation by MITF, we used two human melanoma cell lines, MeWo and SKmel28, engineered to express doxycycline inducible shRNA for MITF (Figure 37D-E). Eight days after induction of MITF-targeting shRNA or a control non-targeting, we performed bulk RNA-seq (Figure 37D, F). The results were consistent with MITF repressing *DHRS3* expression, with a 12-fold (+3.2 log) increase in *DHRS3* expression in MITF

depleted MeWo cells, and a 6.6-fold (+2.72 log2) increase in *DHRS3* expression in MITF depleted SKmel28 cells (Figure 37F-G). Together with the ChIP-seq result showing binding of MITF with the first intron of *DHRS3*, these data strongly suggest that DHRS3 is directly repressed by MITF. This is consistent with previous observations[251] that revealed repression of genes by MITF is rarely via promoter binding. Collectively, this data demonstrates that expression of DHRS3 is directly controlled by MITF, and that in turn high levels of DHRS3 support the undifferentiated/neural crest-like cell state by affecting expression of genes linked to de-differentiation and retinoic acid metabolism (Figure 37H).

Figure 37

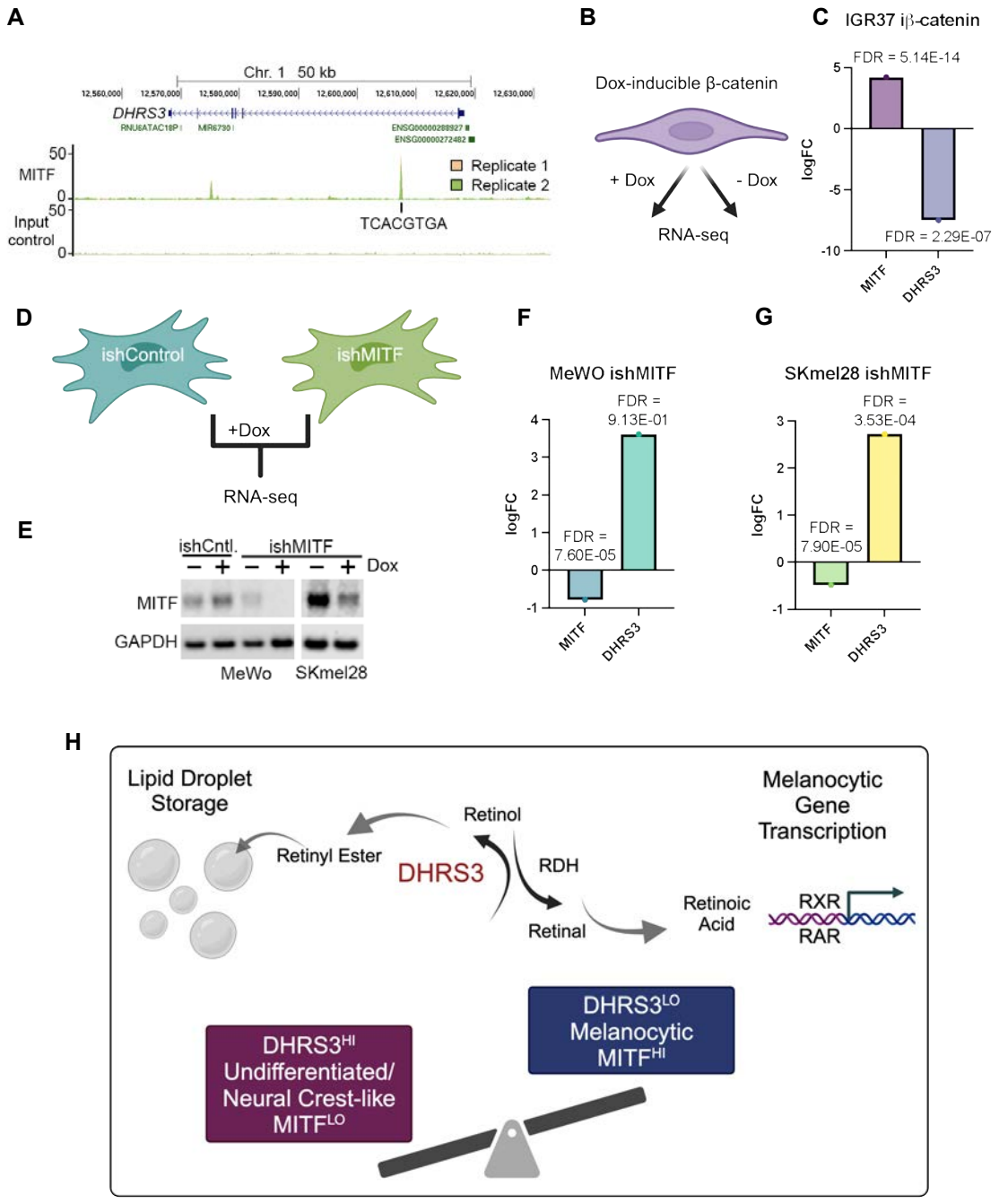

Figure 37. DHRS3 is regulated by MITF, the key regulator of melanoma cell plasticity

A. ChIP-seq data for MITF. The DHRS3 locus is shown and the 8 bp binding site of MITF to Exon 1 of DHRS3 is highlighted.[244] B-C. Schematic and results of RNA-seq from iβ-catenin cell lines. RNA-seq performed in triplicate. Graph shows the fold change as calculated with EdgeR (see methods). D. Schematic of set up for RNA-seq of MeWO and SKmel28 MITF KD. E. Western blot validating MITF expression levels in the

indicated cell lines and conditions. F-G. Graphs showing RNA-seq results for MITF and DHRS3 in the indicated cell lines and conditions. H. Model for DHRS3 role in melanoma cell state. High levels of DHRS3 promote conversion of retinal to retinol. This increases the shuttling of retinoid intermediates away from retinoic acid formation and towards storage as retinyl esters in the droplet. As a consequence, RAR/RXR transcriptional activity is decreased, and cells acquire a more undifferentiated cell state. Diagrams made with Biorender.com.

Discussion

It is now well recognized that tumors exist in a large number of distinct transcriptional states.[48] While such heterogeneity has been observed for decades, the advent of single-cell RNA seq has provided further nuance to defining these states.[55,226] In melanoma, these different transcriptional states have important practical consequences in that each state corresponds to a distinct cellular phenotype. For example, cells with a low level of MITF are more invasive and drug resistant, whereas cells with high levels of MITF are more pigmented but also more proliferative.[3,52,54,56-59] Dynamic switching between these states is known to occur, but both the upstream triggers as well as the downstream effectors of switching remain intense areas of investigation.

Lipids are increasingly being investigated as mediators of cell state plasticity in cancer. Because lipids are strikingly diverse in structure and function, each species can act at multiple levels to mediate changes in cellular physiology. Increased fatty acid uptake, mediated by molecules such as CD36 or the SLC27A/FATP family of proteins, can render the cancer cell more invasive and drug resistant across multiple tumor types.[85,86,88,90,92] These fatty acids can be used for diverse processes including incorporation into membranes, β-oxidation, or conversion into acetyl-CoA and subsequent protein acetylation.[82,93,229,252-254] Lipids can also play a key role in ferroptosis, a central mediator

of cancer cell survival. Dependent on fatty acid saturation, excess lipids can promote ferroptosis through lipid peroxidation while uptake of monounsaturated fatty acids can protect cancer cells from ferroptosis.[227,255-257]

Less well studied is the role of the lipid droplet itself. In both de novo lipid synthesis as well as after uptake from extrinsic sources, lipids such as fatty acids are stored in these specialized organelles. But this organelle is not simply an inert storage container. The droplet itself plays a role in the physiology of both normal and cancer cells.[143,258] In part, this is because the lipid droplet makes close contact with many other organelles within the cell, including the ER, mitochondria, peroxisomes, and lysosomes.[259] The specific role of lipid droplets in cancer is less well understood, but they likely play diverse roles in processes such as preventing lipotoxicity, buffering nutrient deprivation, metabolic flux, signaling, and stemness.[260-268]

While many of the above studies have focused on the lipid content within the droplet, an increasing number of studies have begun to characterize the diverse array of proteins found on the surface of the lipid droplet membrane. In the past few years, there have been meaningful advances in generating high confidence lipid droplet proteomes. For example, a recently developed proximity labeling approach in U2OS osteosarcoma and Huh7 hepatocellular carcinoma cells generated a high confidence list of LD proteins.[135] revealing both expected but also unexpected components of the membrane. At a functional level, genetic perturbation of lipid droplet proteins such as DGAT1[93,151,269,270]

or PLIN2[271-273] can affect many canonical hallmarks of cancer such as proliferation, invasion, metastasis and drug resistance.

A major unanswered question is whether these lipid droplet proteins are simply a reflection of cell state, or whether they can act as drivers of cell state. In our study, we find that DHRS3 itself can enact a change in melanoma cells towards a more undifferentiated state. However, this effect is tightly linked to the way that DHRS3 interacts with the lipid content of the droplet. DHRS3 and RDH10 act in opposition to each other,[230] and overall regulate the relative levels of retinal versus retinol. In the presence of high levels of DHRS3, there is less active retinoic acid in the cell, which therefore makes the cell less differentiated and pigmented. Rescuing this deficiency via exogenous retinoic acid restores pigmentation and promotes differentiation. Our data are consistent with a model in which DHRS3 levels are linked to melanoma cell state through the balance of retinoic acid within the lipid droplet (Figure 7H). However, one unresolved question in our work is the observation that drug resistant, neural crest-like cells have previously been shown to have high levels of RXRG signaling, and that treatment with RXR antagonists can delay such resistance.[3] It is probable that RXR signaling can play different roles in homeostatic conditions (as in our study) versus after the pressure of drug therapy. We do not fully understand how retinoic acid levels would differ in these unique conditions, but one possibility is that the binding partners of RXR could differ. Delineating these discrepancies should be a major focus of future studies.

A key finding of our study is the observation that DHRS3 is repressed by MITF, the master regulator of melanoma cell plasticity. While it is clear that MITF can shift the balance between the undifferentiated vs. differentiated state, what is less clear is the way in which it regulates other aspects of cell state. Aside from differentiation and pigmentation MITF also regulates cell cycle progression through an interaction with Rb and p21.[274] Our data suggests a new role for MITF in cellular plasticity, which is repression of DHRS3, which in turn regulates lipid droplet composition. It further demonstrates the complexity of the ways in which MITF can act as both a transcriptional activator and repressor, which in part is determined by its interaction with β-catenin.[249]

While our study initially characterized the lipid droplet proteome in A375 cells, a limitation of our study is that there could be significant variation in the lipid droplet proteome in distinct melanoma cell states. DHRS3 is one such example, since it is highly enriched in the undifferentiated/neural crest-like cell state, and not very well expressed in more differentiated cells. Given this diversity, future studies should aim to characterize the proteome more broadly across a range of cell states. In addition, our study is limited by the fact that we were only able to characterize the proteome in cell lines, as opposed to *in vivo* tumors. Repeating these studies *in vivo* would be a major challenge, as the number of cells required to isolate the droplets and then perform mass spectrometry is large. However, with the advent of increasingly sensitive mass spectrometry methods, this may be overcome in the near future. Finally, an unanswered question in our study is the function of the other lipid droplet proteins (aside from DHRS3) that we have identified. Some of these proteins are shared with other compendium lipid droplet proteomes from

different cell types, but others appear to be somewhat unique to melanoma. Future studies should aim to systematically investigate the function of these other proteins in different melanoma cell contexts to understand whether they directly affect melanoma cell state or play other roles in the disease.

3.3 Author Contributions

EJ and RMW developed the experiments and interpreted the results. EJ performed all experiments and analysis unless otherwise noted. YM performed RNA-sequencing analysis of IGR37 DHRS3 cells. MVH and JR assisted with computational analyses. CP and HM helped with experimental design and execution of LC-MS/MS and performed the respective data analysis. PL and CRG performed ChIP-seq analysis and RNA-seq experiments of iβ-Catenin and ishMITF cells. EJ and RMW wrote the manuscript. RMW acquired funding for the project. All authors read and edited the manuscript.

3.4 Methods

Cell Culture

A375, HS294T, and RPMI-7951 cells were obtained from ATCC and routinely tested for Mycoplasma. IGR37 and IGR39 cells were a gift from the Colin Goding lab. Upon receipt cell line identity was confirmed by STR profiling and cells were tested for Mycoplasma (09/2023). All cells were maintained in a 37°C and 5% CO_2 humidified incubator. A375, HS294T, and RPMI-7951 cells were maintained in DMEM (Gibco, 11965) supplemented with 10% FBS (Gemini Bio, 100-500). IGR37 and IGR39 cells were maintained in RPMI (Gibco, 11875119) supplemented with 10% FBS. Where

indicated cells were treated with pre-conjugated Oleic Acid (Sigma Aldrich #O3008) or Oleic Acid:BSA as described below.

APEX2 expressing A375 cells were generated as follows. A375 cells were infected with pLenti CMV-TetR Blast virus (Addgene #17492) with 4 µg/ml polybrene followed by selection with 10 µg/ml Blasticidin. A375 TetR expressing cells were subsequently infected with PLIN2-v5-APEX2 (Addgene #170573) or Cyto-v5-APEX2 (Addgene #170572) with 4 µg/ml polybrene followed by selection with 1 µg/ml Puromycin.

IGR37 DHRS3 overexpression cells were generated as follows. IGR37 cells were infected with either pLX304 empty vector virus (Addgene #25890) or CCSB-Broad LentiORF-DHRS3 Clone (Clone ID: ccsbBroad304_07379) virus with 4 µg/ml polybrene followed by selection with 10 µg/ml Blasticidin.

MeWo Cells were maintained in EMEM (ATCC) with 10% FBS while SKmel28 cells were maintained in RPMI-1640 (GIBCO) with 10% FBS (Biosera) Both were grown in a humidified incubator at 37°C and 10% CO_2.

Western Blotting

For APEX2 expressing cells, cells were lysed in HLM buffer (20mM Tris-HCl, pH 7.4 and 1 mM EDTA, 1x Halt protease inhibitor cocktail) supplemented with 1% SDS and sonicated at 10% power with 10 1 second pulses. Following sonication, lysates were boiled for 5 min at 65°C and spun down for 10 mins at 13,000 RPM at RT. Protein concentration was measured with the Pierce BCA Assay and equal amounts of protein (in µg) were mixed with 1X Laemmli Sample Buffer (#BP-111R) and boiled at 95°C for 5 mins. For DHRS3 westerns, cells were lysed in 1% SDS (50mM Tris-HCl, 150mM NaCl, 2.5mM EDTA, 1x Halt protease inhibitor cocktail). Lysates were boiled for 5 minutes and

then spun down for 10 mins at 13,000 RPM at RT. Protein concentration was measured as above.

Equal amounts of protein (10-40 ug) were loaded onto 4-15% Mini-PROTEAN TGX Precast Protein Gels for electrophoresis at 120 volts followed by semi-dry electrophoretic transfer to nitrocellulose membranes via the Bio-Rad Trans-Blot Turbo transfer system. Membranes were blocked in 5% nonfat milk/TBS-T (0.1% Tween-20) at RT for 1 hour. Membranes were then incubated in primary antibody overnight at 4 °C in either 5% BSA or 5% Milk in TBST followed by 3x 5 min washes at RT. Secondary antibodies were added (1:10,000) in 5% milk in TBST for incubation at RT for 1 hour follow by 3x 5 min washes. ECL substrate (Cat #32106 or #WBKLS0500). Visualization was carried out on an Amersham Imager 600. Antibody dilutions: PLIN2 (Abgent AP5118c-ev) 1:1000, Calnexin (Proteintech 10427-2-AP) 1:20,000, Tubulin (EMD Millipore CP06) 1:1000, ATGL (CST 2138) 1:1000, GM130 (CST 12480) 1:1000, GAPDH (CST 5174) 1:5000, VDAC1 (CST 4866) 1:1000, Actin (Sigma A2228) 1:10,000, V5 (Thermo Fisher R960-25) #1:5000, Streptavidin HRP (CST 3999) 1:2000, DHRS3 (Proteintech 15294-1-AP) 1:500.

For Figure 5H Treated cells were lysed directly in 4x LDS (Invitrogen, # NP0008) supplemented with 10% v/v β-mercaptoethanol, heated at 95 °C for 10 min before SDS-PAGE using Bis-Tris gels (Invitrogen, #WG1403) Gels were transferred onto PVDF Membrane (Amersham) at 100 V for 60 min for Western-blotting, blocked 1 h, room temperature in 5% non-fat milk in TBS containing 0.25% TWEEN-20 (TBST). Primary antibody incubations were done in 5% BSA-TBST overnight and 1 h RT for secondary antibodies. Visualization was carried out on X-ray film (Fujifilm) using ECL

(Amersham). Antibodies used were MITF (RRID:AB_1079381) and GAPDH (RRID: AB_627679).

Immunofluorescence Staining

Cells were seeded in either a Millicell EZ 4-well chamber slide (#PEZGS0416) or #1.5 coverslips (EMS #50-192-9522) coated with Poly-L-lysine (Millipore Sigma #P4707). After washing with PBS, cells were fixed for 15 minutes in 4% Formaldehyde (Fisher Scientific #FB002) at room temp. Cells were permeabilized with either 1% Triton or 0.01% Digitonin (for DHRS3) for 30 min at RT. For antibody staining, cells were washed 3x in PBS and then blocked in 10% normal goat serum (Thermo Fisher #50-062Z) for 1 hr at RT. Primary antibodies were added at the indicated concentrations in 10% goat serum and incubated overnight at 4°C. Samples were washed 3x in PBS and then incubated with the appropriate secondary antibodies at 1:500 in 10% goat serum for 1 hr at RT. If using, BODIPY 493/503 (Thermo Fisher D3922) was added to the secondary antibody solution at 1:100. Where indicated, LipidTOX Deep Red 1:1000 (Invitrogen #H34477) in PBS was added to samples to stain LDs for 30 mins at RT. After staining with secondaries/LD dyes, samples were washed 3x in PBS and incubated with Hoechst 1:2000 (Thermo Fisher #H3570) for 5 mins at RT. Samples were then washed an additional 3x times in PBS before mounting on slides in Vectashield (Vector Laboratories #H-1900-10). If no antibody staining was required, cells were permeabilized, washed 3x in PBS and then incubated with PBS containing 1% BSA, BODIPY 493/503 1:100, and Phalloidin 647 1:200 (Thermo Fisher A22287) for 1 hour at RT. This was followed by staining with Hoechst and mounting as above. Antibody concentrations: V5 (Thermo Fisher R960-25) 1:500, Streptavidin-594 (Thermo Fisher S32356) 1:500, DHRS3

(Proteintech 15294-1-AP) 1:200, Tubulin (EMD Millipore CP06) 1:1000. Samples were imaged with the Zeiss LSM880 inverted microscope with 63x oil immersion objective. Where needed, Airyscan was used to increase resolution. Confocal z-stacks were visualized in Fiji.

APEX2 Labeling & Lipid Droplet Isolation

LD labeling & isolation was performed as previously described with some modifications.[135,136] For LD isolation 4 million cells were seeded in each 245 mm square plate with 4 plates per condition. 24 hours after seeding, cells were treated with Dox at 5 ng/ml. 24 hours before collecting, Oleic Acid (200 μM) + Dox 5 ng/ml was added to the media. For APEX2 labeling, 500 μM Biotin Phenol was added to cells and incubated at 37°C for 30 mins. Then, 1 mM H_2O_2 was added to the media and incubated for 1 min at RT. The reaction was quenched with 3x washes in Quenching Buffer (5mM Trolox, 10mM Sodium Ascorbate in DPBS) followed by a final wash in PBS. Cells were scraped in PBS on ice and transferred to a 50 ml conical tube followed by a spin at 500g, 4°C for 10 mins. Cells were resuspended in 3ml HLM buffer (20mM Tris-HCl, pH 7.4 and 1 mM EDTA, 1x Roche cOmplete Protease inhibitor cocktail), incubated for 10 mins on ice, and then transferred to a Dounce Homogenizer. Cells were homogenized with 80x strokes of the tight fitting Dounce Homogenizer, followed by a spin at 1000xg for 10 mins at 4°C. Between 2-3 ml of Post Nuclear Supernatant (PNS) was transferred to a Beckman Open-Top Thinwall Ultra-Clear Tube (#344059). The PNS was diluted to a final concentration of 20% sucrose, then 5 ml of 5% sucrose was layered on top, followed by 3.5-4.5 ml HLM (0% sucrose). Tubes were spun at 28,000g for 30 mins at 4°C in a TH-641 swinging bucket rotor. After centrifugation, lipid droplet fraction (~1 mL) was sliced off

the top of the tube using a tube slicer. The remaining volume was collected in 1 mL fractions to assess the quality of the fractionation.

To analyze fractionation by western blot, equal percent by volume of each fraction was mixed with 10% SDS to a final concentration of 1% SDS. For the lipid droplet fraction, samples were incubated at 37°C and sonicated 3x 10 seconds at 10% amplitude every 20 minutes for a total of 1 hour. This was followed by a final incubation for 10 mins at 65°C, a spin for 10 mins at 14,000 RPM. The soluble layer was removed and transferred to a new tube. All other fractions were sonicated 3x 10 seconds at 10% amplitude followed by a final incubation for 10 mins at 65°C.

For streptavidin IP and mass spectrometry: Lipid droplet fractions were collected sequentially and stored at -80°C until use. LD proteins were precipitated with 6x volume ice cold acetone at -20°C overnight. Samples were spun down at 14,000 x g at 4°C for 10 mins. Acetone was removed and pellet was allowed to dry (under foil) for 5-10 mins. Pellet was resuspended in RIPA + protease inhibitors + 2% SDS and boiled at 95°C for 10 mins and then spun down to ensure no visible pellet for 10 mins at 14,000 RPM. Equal amounts of protein per sample were then diluted in SDS free RIPA to a final 0.1% SDS concentration and then incubated with 25 µl solubilized, samples were diluted in SDS free RIPA buffer (0.1% final SDS) and then incubated with Pierce Streptavidin Magnetic Beads (cat #88817) overnight at 4°C in an end over end rotator. The next day, beads were washed for 2 min at RT (unless otherwise indicated) with the following: 2x RIPA buffer (SDS free) buffer, 2x NP-40 buffer (1% NP-40), 1x 1M KCl, 1x 0.1 M Sodium Carbonate (10 seconds), 1x 2 M Urea, (10 seconds), 3x 10mM Tris-HCl, pH8.0

(changing tubes each time). At the final wash 100 µl of buffer/beads was removed (10% of sample) for WB analysis of IP while the rest was used for mass spectrometry.

Lipid Droplet Proteomics by Mass Spectrometry

Dried magnetic streptavidin beads were suspended in a solution 25 µL of 50 mM Ammonium Bicarbonate/10 mM DTT for reduction of proteins and incubated for one hour at room temperature. Reduction was followed by alkylation with the addition 7.5µL of 100mM Iodoacetamide/50 mM Ammonium Bicarbonate and incubated for one hour at room temperature in the dark. Beads then underwent partial on-bead digestion with 250 ng of Porcine Trypsin (Promega) in 50 mM Ammonium Bicarbonate for three hours at room temperature. Supernatant was then extracted to undergo digestion with 500 ng of Porcine Trypsin (Promega) and 500 ng of Endopeptidase Lys-C (Wako) in 50 mM Ammonium Bicarbonate overnight at room temperature. Digestion was halted by addition of neat trifluoroacetic acid. Peptides underwent reversed phase based micro solid phase extraction.[275] 3 of 10µL were injected and analyzed by nano LC-MS/MS (Fusion LUMOS coupled to an Easy-nLC 1200, Thermo Scientific). Mass spectrometer were mass calibrated weekly and operated with lock mass.[276] MS and MS/MS were recorded at a resolution (@ 200 Th) of 120,000 and 30,000, respectively. Automatic Gain Control (AGC) was set to 4e5 and 5e4 for MS and MS/MS. Samples were analyzed using a gradient increasing from 2% B/98% A to 35% B/65% A in 70 min (A: 0.1% formic acid, B: 80% Acetonitrile/0.1% formic acid). Peptides were separated using a 12cm/100um packed in column emitter (NIKKYO TECHNOS CO., LTD.).

Analysis of Mass Spectrometry Data

Data were queried against the database: Uniprot_human_June_2022 concatenated with common contaminants[277] using MaxQuant[278,279] v 2.0.3.0. In short: 20 ppm mass accuracy was used for precursor mass accuracy and 20 mDa for fragment ions. Carbamidomethylation of cysteines was set as a fixed modification and oxidation of methionine and protein N-termini acetylation were set as variable modifications. Search results were filtered using false discovery rates of 2% or better for peptides and 1% or better for proteins. Intensity-Based Absolute Quantitation (iBAQ) values[280] were used to relative quantify matched proteins. Utilizing Perseus[281] software platform (v 1.6.15.0), iBAQ values were log2 transformed, filtered for common contaminants and proteins found via reverse search. The data was further filtered by requiring signals in at least 75% of replicates for at least one of the conditions, resulting in 407 proteins being quantitated. Missing values were imputed. In addition, to generate normalized values, the average (non-log2 transformed) Cyto-APEX2 iBAQ value for each protein was subtracted from the average PLIN2-APEX2 iBAQ values as previously described.[136] Proteins were then ranked from highest to lowest normalized iBAQ value. To generate a high confidence list of lipid droplet proteins, we set a manual cutoff such that approximately 60% of previously validated lipid droplet proteins were identified. This yielded a list of 96 LD proteins total. To generate the heatmap, Log_2 normalized iBAQ values with imputation are shown across all 10 conditions.

To test for enrichment of lipid droplet proteins, we ran g:Profiler[282] with GO:Cellular Components and Biological Processes using the high confidence lipid droplet protein list. This revealed significant enrichment of lipid droplet and related pathways.

Oleic Acid:BSA Preparation

For proteomics experiments, Oleic Acid:BSA was prepared as follows. Stock solutions of Oleic Acid (Sigma #O1383) were resuspended in ethanol and aliquoted. To complex; 9 mM Oleic Acid was mixed with 3 mM BSA (Sigma #A8806) in PBS (3:1 ratio) and incubated at 37°C in a shaker for 2 hours until the solution cleared. OA:BSA was then sterile filtered, aliquoted, and stored at -20°C until use.

Re-analysis of publicly available melanoma -omics data

CCLE and TCGA RNA-seq data was downloaded and analyzed as previously described.[93] CCLE Proteomics data was downloaded from https://depmap.org/portal/download/custom/ and z-scores were used to compare protein levels across different cell states as above.

Single-cell RNA-seq data from human melanoma patients[59] was downloaded from GEO (GSE134432). All analysis was done in R (v. 4.3.1) using the Seurat[283] package (version 5.0.2). The counts matrices for each cell line were imported into R and converted into Seurat objects using the function CreateSeuratObject with default parameters. The Seurat objects were then merged into one combined object containing data for all cell lines. Using the merged object, counts were normalized with SCTransform.[284] UMAP was calculated using the Seurat function RunUMAP with 15 principal components.

Bulk RNA-sequencing and analysis

For RNA-seq of IGR37 DHRS3 OE cells, 3 replicates of 1 million cells each were seeded in 10 cm dishes. Cells were allowed to grow for 2 days and then collected for RNA-seq and snap frozen. Library preparation and sequencing was done by Azenta Life Sciences. FASTQ reads were trimmed with Trimmomatic[285] v.0.39.1, then mapped and quantified with Salmon[286] v1.10.2 using selective alignment with the GRCh38 reference genome2.

Downstream analysis was done in R v4.2 or v4.3.2. Differential gene expression analysis was performed using DESeq2 (v1.36)[287] with default parameters. Gene set enrichment analysis was done using GSEA[288] with Hallmark and Curated Gene Set pathways from MSigDB or fgsea.[289] To run GSEA, we pre-filtered the normalized counts matrix to remove genes with counts <10 and genes with no official gene name. For fgsea, we ran this using the log2FC output from DESeq2 against the custom gene pathways for melanoma cell state.[57]

Known motif analysis was performed with HOMER function findmotifs.pl and searching for motifs 8, 10, and 16 bp in length within +/- 500 bp of the TSS.

For RNA-seq of iβ-Catenin and ishMITF cells: iβ-Catenin cell line was generated, validated and treated as previously described[250] for total RNA extraction and sequencing as ishMITF cells**.** ishMITF cell lines and lentiviral vectors were a kind gift from Jiri Vachtenheim.[290] Cells were seeded on 6 cm dish overnight, the next day, fresh media with 1 µg/ml Doxycycline was added. Media with or without Doxycycline was changed every other day. After 8 days, the media was aspirated, and the plates snap frozen at -80 °C before total RNA extraction using RNeasy Mini Kit (QIAGEN #74106) as per manufacturer protocol. RNA quality was assessed on Bioanalyzer 2100 (Agilent) using Agilent RNA 6000 Nano Kit (#5067-1511). Only samples with RIN values of over 9.5 were subjected to library prep and sequencing using the Wellcome Trust genomic service, Oxford. QuantSeq Forward kit (LEXOGEN #0.15.96) was used for library prep, using 500 ng starting material to minimize the PCR amplification step. Samples were sequenced on HiSeq 4000 (Illumina).

Base calling, demultiplexing were carried out by the Wellcome Trust Genomic Service, Oxford. Quality of the raw sequencing fastq files were evaluated using FastQC (v.0.11.7). Adapter contamination removed and poly-A trimmed using CutAdapt[291] (v.2.8) before mapping to the human reference genome (hg38) with STAR[292] (version 2.5.1b). Gene expression normalization and differential gene expression analyses were performed as previously described[71,72,250] using edgeR glmQLFTest.

qRT-PCR

Cells were treated with the indicated RXR agonists and inhibitors for 3 days. After collecting the cell pellet, total RNA was isolated using the Quick-RNA Miniprep Kit (Zymo R1055) according to manufacturer's instructions. cDNA was synthesized using SuperScript IV First-Strand Synthesis System (Thermo Fisher, 18091200) and qPCR was performed using Applied Biosystems PowerUp SYBR Green Master Mix (Thermo Fisher, A25742). Results were normalized to the *beta-actin* housekeeping gene.

Statistics and Reproducibility

Statistical analysis and figures were produced using GraphPad Prism, R/RStudio and Biorender.com. Image processing and analysis was performed using Fiji. The statistical analysis and p-values are presented in each respective figure legend. Unless otherwise noted in the legend, data are representative of at least 3 independent experiments.

Data and Code Availability

Raw and processed RNA-seq and Proteomics data generated in this study have been deposited in Gene Expression Omnibus (GEO) under GSE262095 and PRIDE under PXD050693. Previously generated RNA-seq of iβ-Catenin and ishMITF cells are available under accession code GSE136803 and GSE255256 respectively. Re-analyzed

scRNAseq data are available under GSE134432. ChIP-seq data is available on GEO under GSE132624. All other relevant data supporting key findings in this study are available within the article or from the corresponding authors upon request. Original code used in this study will be deposited on Github.

Declaration of Interests

RMW is a paid consultant to N-of-One Therapeutics, a subsidiary of Qiagen. RMW is on the scientific advisory board of Consano but receives no income for this. RMW receives royalty payments for the use of the casper zebrafish line from Carolina Biologicals. EJ, YM, MVH, JHR, PL, CRG, HM and CP declare no competing interests.

Acknowledgements

We thank the Rockefeller Proteomics Resource Center for their technical support for LC-MS/MS experiments. The Molecular Cytology Core Facility provided confocal imaging support. We also thank all members of the White lab for helpful discussions. EJ was supported by a F31 Ruth L. Kirschstein Predoctoral Individual National Research Service Award (F31AR079215) from the National Institute of Arthritis and Musculoskeletal and Skin Diseases. MVH was funded by a K99/R00 Pathway to Independence Award from the National Cancer Institute (K99CA266931). CRG was funded by the Ludwig Institute for Cancer Research and CRG and PL by NIH R01 CA268597-01. YM was supported by a Medical Scientist Training Program grant from the NIH under award number T32GM007739 to the Weill Cornell/Rockefeller/Sloan Kettering Tri-Institutional MD-PhD Program and Kirschstein-National Research Service Award (NRSA) predoctoral fellowship under award number F30CA265124. R.M.W. was funded through the NIH/NCI Cancer Center Support Grant P30 CA008748, the Melanoma Research

Alliance, The Debra and Leon Black Family Foundation, NIH Research Program Grants R01CA229215 and R01CA238317, NIH Director's New Innovator Award DP2CA186572, The Pershing Square Sohn Foundation, The Mark Foundation for Cancer Research, The American Cancer Society, The Alan and Sandra Gerry Metastasis Research Initiative at the Memorial Sloan Kettering Cancer Center, The Harry J. Lloyd Foundation, Consano and the Starr Cancer Consortium (all to R.M.W.).

CHAPTER 4: CONCLUSIONS

4.1 General Conclusions and Summary

Although metabolic reprogramming during cancer has been known for many years,[293,294] recent findings in cancer cell metabolism have led to several therapeutic advances.[295-297] This has widened the scope of our understanding of the role of metabolism in various types of cancer. In multiple tumor types, lipid droplets have been identified to play a role and represent a relatively unexplored therapeutic opportunity.[93,151,270,298] Inhibiting lipid droplet biogenesis, by targeting the enzymes DGAT1 and DGAT2, has been explored in other diseases such as Nonalcoholic Fatty Liver Disease (NAFLD) as well as obesity and diabetes,[109,299-301] raising the question of whether these inhibitors could also be utilized to treat certain cancers. However, our understanding of lipid droplet dynamics, how they are regulated and the variety of roles they play in the cell remains an active area of investigation. In particular, less is known about the role of lipid droplets in specific cell lineages and how this may be co-opted in cancers such as melanoma.

To explore these questions in melanoma we took multiple approaches. First, we developed an in vivo and in vitro zebrafish reporter for lipid droplets *-3.5ubb:plin2-tdTomato* to facilitate high resolution imaging in melanoma tumors and the tumor microenvironment. We used the zebrafish reporter to monitor pharmacologic and diet induced perturbations to adipocyte tissue in the developing fish larvae. Biologically, we found regulation of LDs by the nitric oxide pathway, which is interesting in that our proteomic analysis of the LD proteome also found an enrichment for thioredoxin (TXN), a known regulator of this pathway. In addition, we showed that the in vitro reporter in

zebrafish melanoma cells is more sensitive than classic lipid droplet dyes in monitoring changes in lipid droplet quantity. This data suggests several uses for both model systems.

In addition to imaging lipid droplets, we were interested in understanding the specific regulation of lipid droplets in melanoma. In particular, an unexplored question in the field is the role of cell type or lineage specific protein localization to the lipid droplet. By adapting a previously developed APEX2 proximity labeling approach[135,136] to isolate lipid droplet proteins, we could characterize a high confidence lipid droplet proteome in human melanoma cell lines. As we expected, the majority of lipid droplet proteins are shared across cell lines and tissue types. However, we were able to identify several proteins which have not been previously validated to localize to lipid droplets (Table 1), suggesting that they could be enriched in the melanocytic lineage/melanoma. Interestingly, we also observed an enrichment for proteins involved in retinoic acid metabolism in undifferentiated/neural crest-like melanoma cells. Upregulation of these proteins suggested a role for retinoic acid regulation at the lipid droplet in maintaining specific melanoma cell states. We identified DHRS3 as a clear outlier, as it consistently showed higher expression in undifferentiated vs. melanocytic melanoma cells. We found that high levels of DHRS3 push cells to a more undifferentiated cell state. In addition, our data suggests that DHRS3, through its role in converting all-trans-retinal to all-trans-retinol, controls the levels of active retinoic acid in the cell. This in turn affects activation of RXRs, which can affect the differentiation state of melanoma cells.

4.2 Future Directions

4.2.A Imaging lipid droplet dynamics

A chemical screen for novel lipid droplet regulators in melanoma

The *-3.5ubb:plin2-tdTomato* reporter opens up many avenues of investigation in melanoma. In particular, one clear area of interest would be to explore regulators of lipid droplet levels in the ZMEL-LD cell line. Given that we have demonstrated the sensitivity of the PLIN2-tdTOMATO signal in reading out changes in lipid droplet levels by flow cytometry, we could adapt this approach for a high throughput chemical or genetic screen (Figure 38A). Hits from this screen would likely include known regulators of processes like lipolysis or TAG synthesis, however, it would be intriguing to see if there are more unique hits for pathways which could be upregulated in melanoma. Furthermore, we could target specific aspects of lipid droplet biology in the design parameters of the screen. For example, we could use treatment of cells with oleic acid to screen for regulators of LD formation (Figure 38B). Conversely, we could enrich for regulators of turnover of LDs by pulsing in oleic acid followed by a chase in full or starvation media with the chemical library (Figure 38C). These more targeted approaches could aid in further uncovering unexplored aspects of LD dynamics in melanoma. In addition, given the fact that the ZMEL-LD cells can be transplanted into zebrafish,[161] this presents the opportunity to follow up on hits of interest in vivo with ease.

Figure 38

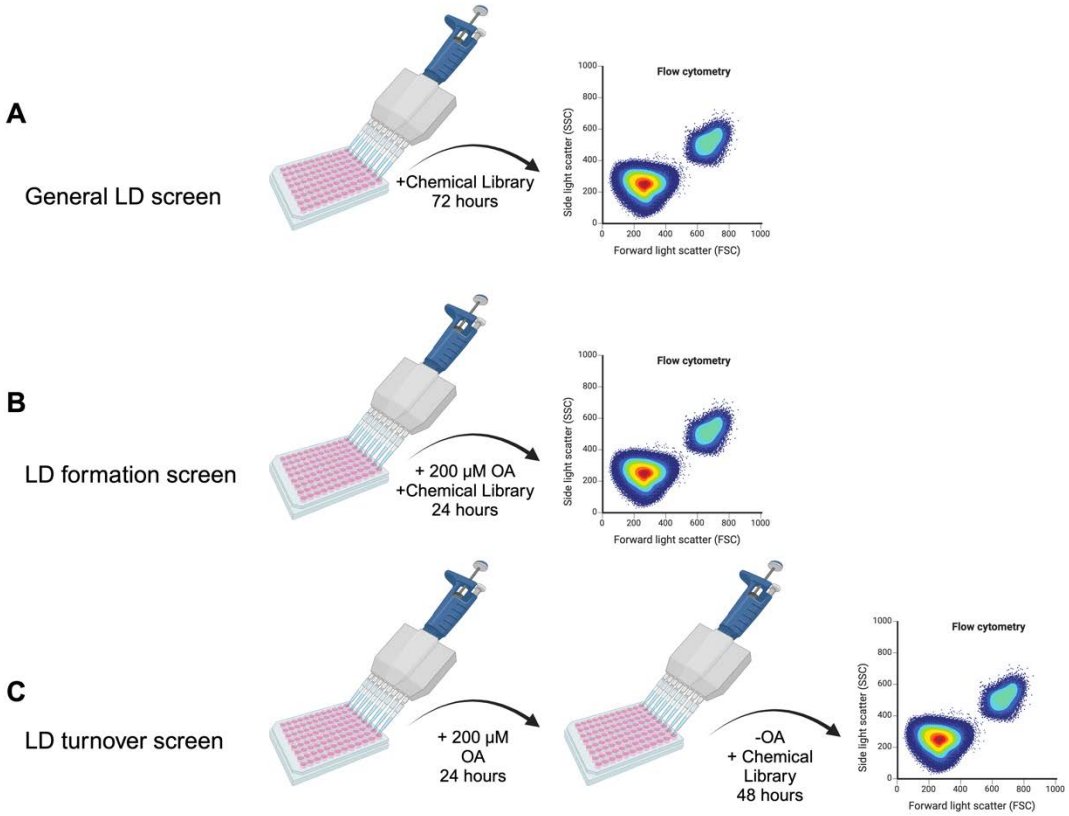

Figure 38. ZMEL-LD Chemical Screens.

The ZMEL-LD cell line can be used to conduct high throughput screens to identify regulators of LD dynamics in melanoma. A. Proposes a general screen of ZMEL-LD cells in full media. This would primarily identify chemicals which increase LD quantity, as ZMELs have low LD levels in full media. B. LD formation screen. By treating cells with Oleic Acid to induce formation simultaneous to treatment with the chemical library we can identify compounds which block or increase LD formation. C. LD turnover screen. Treating cells with Oleic Acid to induce LD formation, and then chasing the cells in normal media while treating with the chemical library will identify compounds that block or increase LD turnover. The proposed readout for these screens is flow cytometry, as we have established that this system is sensitive enough to detect changes in LD protein levels. However, another approach would be to do endpoint fluorescence imaging. Images created with Biorender.com

4.2.B DHRS3 and the role of retinoic acid metabolism at the lipid droplet in melanoma

The role of DHRS3 in melanoma tumors in vivo

Our findings implicate that cells within a tumor with high levels of DHRS3 will be more undifferentiated and invasive. However, we have not characterized this phenotype in vivo. Based on the in vitro data, we would hypothesize that knock-out of *dhrs3* in tumors would push cells towards a more melanocytic and proliferative state, which could lead to larger primary tumors with decreased metastasis. We have already begun to study this with a pilot experiment. In this model we inject zebrafish which are *mitfa*$^{-/-}$*; mpv17*$^{-/-}$*; p53*$^{-/-}$*;* Tg(*mitfa:*BRAF^{V600E}) with a plasmid mix to induce focal melanoma growth (Figure 39A).[162,163] The plasmid mix includes a *mitfa:cas9* plasmid as well as guides against *dhrs3a/b* versus a non-targeting guide (Figure 39A). This system enables us to monitor tumor initiation, growth and metastasis in an immunologically competent animal.

Figure 39

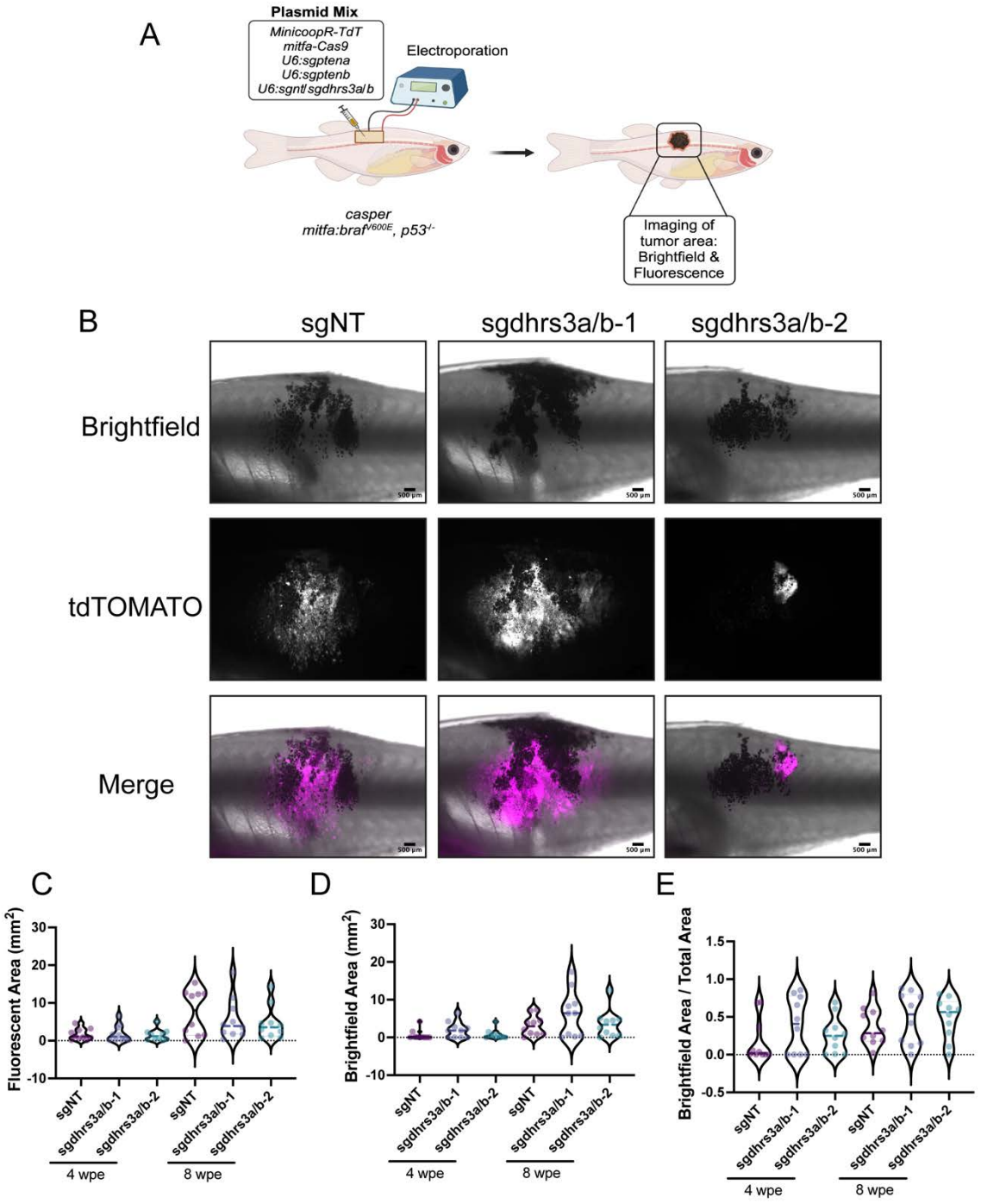

Figure 39. Pilot TEAZ experiment of dhrs3a/b knockout.

A. Schematic of TEAZ experiment. Zebrafish of the indicated background are injected with a plasmid mix containing guides against *dhrs3a/b*. Injection of the plasmid mix induces tumor formation which can be monitored with fluorescent and brightfield imaging to track tumor growth over time. B. Representative images from each condition.

C. Quantification of representative images in B. Quantifying tumor area based on the total tdTOMATO+ signal. D. Quantification of pigmented tumor area with brightfield imaging. E. Quantification of the percent pigmented tumor area / total area (quantified as: Brightfield / (Fluorescent area + Brightfield Area). Data are from 1 independent experiment: sgNT N = 10, sgdhrs3a/b-1 N = 10, sgdhrs3a/b-2 N = 10. Diagrams created with Biorender.com.

Preliminary data from the pilot experiment indicates that, contrary to our initial hypothesis, *dhrs3a/b* KO does not increase fluorescent tumor area. TEAZ tumors are typically quantified based on the total fluorescent area (tdTOMATO+) (Figure 39B-C), however, quantification of tumors is complicated by the fact that pigmented tumors quench the fluorescent signal. To account for this, we also quantified total pigmented area with brightfield imaging. Interestingly, we saw a modest increase in tumor area when only considering pigmented tumor area (Figure 39B,D). Furthermore, when we took a ratio of the pigmented area over the total tumor area (Brightfield + Fluorescence), we observed a more substantial increase in conditions with *dhrs3a/b* KO relative to nontargeting (Figure 39E). These data suggest that knockout of *dhrs3a/b* could lead to an increase in tumor pigmentation, but not necessarily in total tumor area. Given that the number of animals used for these experiments was limited, it is not possible to assess statistical significance of these results. Future work will need to be done to conduct these experiments with the typical number of animals (usually between 30-50 per condition). This will further elucidate the role of *dhrs3* in vivo. In addition, we have not yet explored whether there are differences in invasion or metastasis in this model. It would also be interesting to look at overexpression of DHRS3 in the tumor, which we would predict to cause increased metastasis. These data would further aid in our understanding of how DHRS3 functions in melanoma.

RXR regulation of melanocytic genes

A major mechanistic finding in our studies is the role of DHRS3 in antagonizing activation of RXR transcription factors. We show that high levels of DHRS3 decreases 9-cis-retinoic acid mediated activation of RXRs, which decreases expression of tyrosinase and cell pigmentation. One mechanism through which this could occur is by regulation of MITF through RXR. Inconsistent with this hypothesis, in our DHRS3 RNA-seq data we did not observe any decrease in MITF levels (Figure 40A), although we have not quantified MITF protein level or localization. Interestingly, we did observe a marginal decrease in MITF expression in DHRS3 OE cells by qPCR (Figure 40B). However, interpretation of these results is complicated by the fact that treatment of control cells with 9-cis-RA, which we found increases pigmentation, also modestly decreases MITF levels (Figure 40C). Interestingly, 9-cis-RA treatment of DHRS3 OE cells was unable to further decrease MITF levels, suggesting that there may be overlap between the effects of 9-cis-RA treatment and high levels of DHRS3.

Figure 40

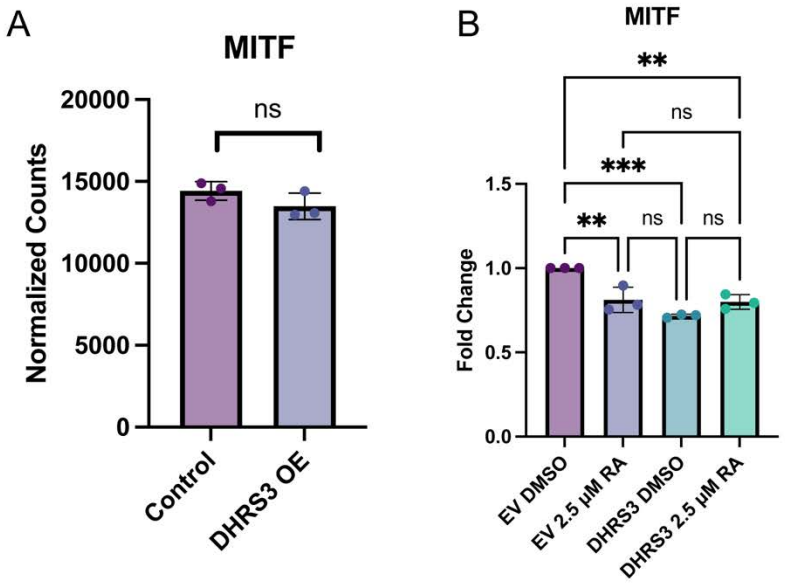

Figure 40. MITF expression does not explain downstream phenotypes of DHRS3 OE.

A. Normalized counts of bulk RNA-seq data from control and DHRS3-V5 OE IGR37 cells. Calculation of log2FC between conditions by DESeq2 was not significant for MITF. B. qPCR of MITF in Control or DHRS3 OE cells treated with either 2.5 µM 9-cis-RA or DMSO. Statistics via One-way Anova with Tukey's multiple hypothesis correction. Data are from 3 independent experiments. * $p<0.05$, ** $p<0.01$, *** $p<0.001$

While these data are intriguing, they do not clearly implicate MITF as the downstream regulator of DHRS3 overexpression. In particular, the modest changes in expression suggest that there could be additional mechanisms by which DHRS3 OE can push cells to an undifferentiated cell state, independent of MITF. One explanation for this could be that RXRs are able to bind to and activate genes involved in cell state and pigmentation without MITF. Previous work has shown that transcription factors in the TFAP2 family can likely perform this role.[302] To address this, we could perform ChIP-seq experiments to look at binding of RXRs in Control vs. DHRS3 OE or DHRS3 KO cells. Data from

this experiment would help us to understand more of the mechanistic action of DHRS3 and how it can affect expression of genes involved in melanoma cell state.

Lipid droplet localization of DHRS3 & its activity

We found that DHRS3 localizes to lipid droplets in melanoma, and that this localization is increased in undifferentiated/neural crest-like cells. In addition, we also showed that higher levels of DHRS3 in cells decreases retinoic acid mediated transcriptional activity. However, an open question is whether DHRS3 localization to the lipid droplet is required for its activity. Interestingly, RDH10, which is the known binding partner of DHRS3, can also be localized to the lipid droplet[230,303] (Figure 41A-B). It has been shown in other systems that binding of DHRS3 to RDH10 is required for the activity of both enzymes, where the two enzymes act antagonistically to each other to regulate the levels of all-trans-retinal vs. all-trans-retinol in the cell.[230,303] Collectively this would suggest that localization of both enzymes to the lipid droplet could facilitate their interaction. In addition to this, in vivo data from our lab suggests that there is a relationship between lipid droplet formation and *dhrs3* expression. In a zebrafish model of melanoma (Figure 41C), knockout of *dgat1a*, which reduces lipid droplet levels,[93] leads to a strong reduction in the expression of both copies of *dhrs3* (Figure 41D). This suggests that there is a link between *dhrs3* expression and the ability to form lipid droplets. This is consistent with the idea that localization of DHRS3 to the lipid droplet is required for its activity, where decreased lipid droplet levels could lead to a reciprocal downregulation of *dhrs3.*

To test whether localization of DHRS3 to lipid droplets is required, we could express truncated versions of DHRS3 that cannot localize to the lipid droplet and look for changes in cell pigmentation or gene expression compared to the full length DHRS3. Truncated versions of DHRS3 have been previously published[236] which would facilitate this work. These experiments would further our understanding of the role of the lipid droplet as a signaling hub in melanoma. It would also raise questions of how fluctuating lipid droplet levels inside the cell could affect retinoic acid production if interaction of DHRS3 with the lipid droplet is required for its activity.

Figure 41

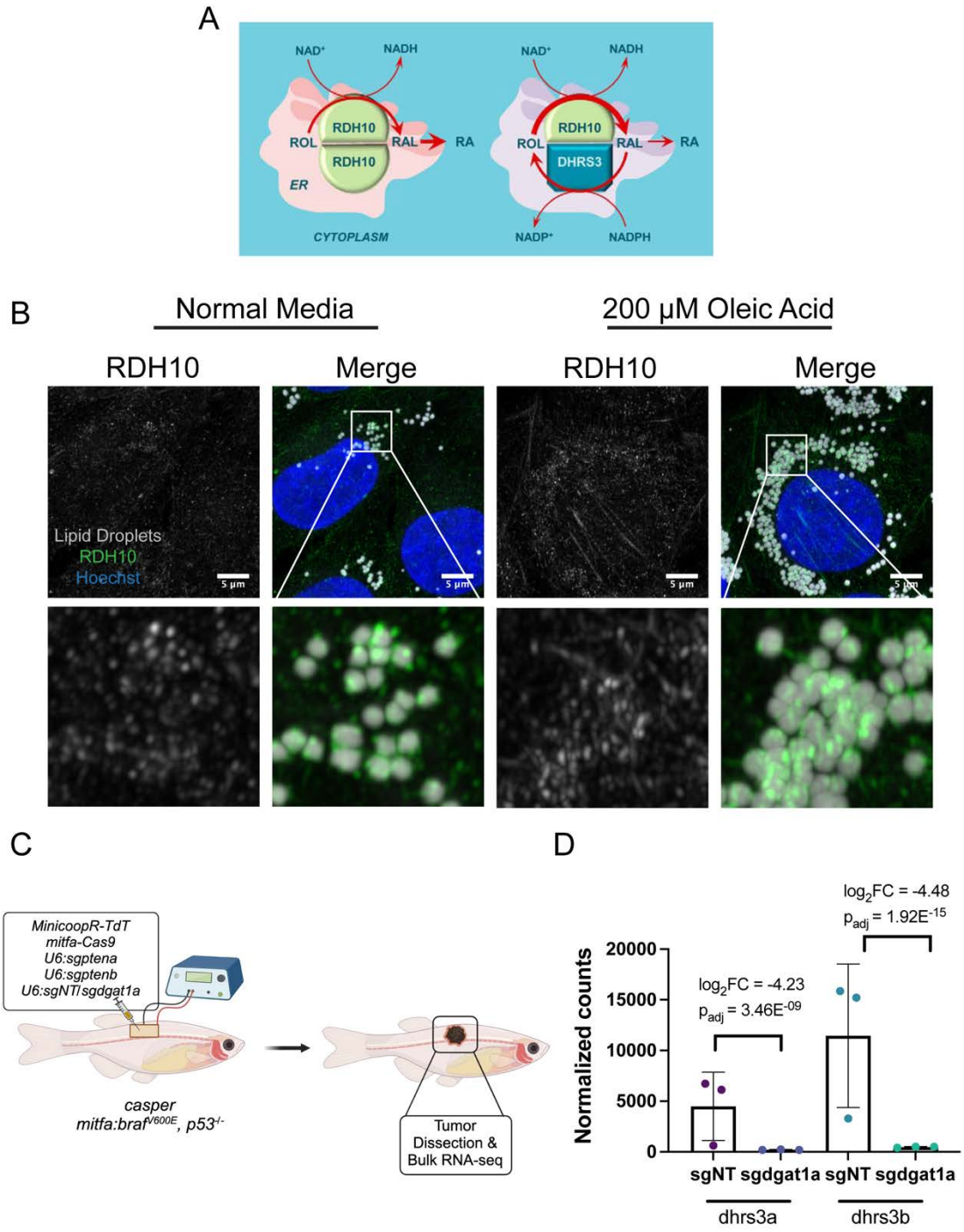

Figure 41. DHRS3 localization and activity at the lipid droplet.

A. Model of RDH10 and DHRS3 interaction. It is thought that DHRS3 binding to RDH10 enhances its activity. However, binding to RDH10 also activates DHRS3, which helps to maintain a balance of all-trans-retinal vs. retinol in the cell. Reproduced from[230]

under the Creative Commons CC BY 4.0 License
https://creativecommons.org/licenses/by/4.0/. B. Immunofluorescence staining of RDH10 localization in A375 cells. RDH10 appears localized in multiple locations throughout the cell. However, signal does appear enriched at the lipid droplet in cells treated with or without oleic acid for 24 hours. C. Schematic of the zebrafish TEAZ experiment to knockout dgat1a followed by tumor dissection and RNA-seq analysis as in (Lumaquin-Yin et al., 2023). Created in Biorender.com D. RNA-seq of sgNT vs. *sgdgat1a* tumors reveals a significant decrease in dhrs3a/b expression as measured by normalized counts and log2FC.

A requirement for DHRS3 in melanoma cell state

In our studies we show that high DHRS3 is sufficient to push cells to a more undifferentiated/NC-like cell state. However, we have not yet been able to address whether DHRS3 is required for the undifferentiated/NC-like cell state. We have attempted to make DHRS3 knockdown or knockout cell lines with CRISPR-Cas9 or siRNA transfection in undifferentiated IGR39 melanoma cells. Neither of these methods were successful in generating observable decreases in DHRS3 by western blot. To account for this, we have generated stable cell lines of doxycycline inducible shRNA against DHRS3. The inducible system alleviates difficulties which could be caused by decreased cell survival following knockdown of the gene. Validation of this system is ongoing. In a parallel approach, we have also generated stable CRISPR knockout lines of DHRS3 in A375 melanoma cells (which are neural crest-like). Both systems together should allow future work to demonstrate the effect of lack of DHRS3 on melanoma cell state.

4.2.C The melanoma lipid droplet proteome

Novel lipid droplet proteins in melanoma

Exploration of the melanoma lipid droplet proteomics dataset led us to investigate DHRS3. However, there were also several proteins that we identified which have not been well characterized, either in melanoma or in lipid droplets generally. For example, Thioredoxin (TXN) is intriguing given that we found the nitric oxide pathway to be a regulator of LDs in melanoma lipid droplets with our PLIN2 reporter. It would be interesting in future studies to characterize this and the other proteins from our proteomic analysis. To do this, it is likely necessary to first generate GFP fusion proteins to confirm their localization to the LD. Preliminary work with available antibodies for several of the proteins was unsuccessful. Once localization has been established, functional genetic experiments to look at altered lipid droplet behavior and morphology would be informative.

Table 1

Gene Name	**Full Name**	**NCBI gene summary**
TXN	Thioredoxin	Part of the nitric oxide response. It is involved in the reversible s-nitrosylation of proteins [Refseq, 2024]
TMEM263	Transmembrane Protein 263	Predicted to be an integral component of the membrane [Refseq, 2024]
GNB2	G protein subunit beta 2	Beta subunit of G proteins which are involved in cell signaling [Refseq, 2024]

GNAI2	G protein subunit alpha i2	Alpha subunit of G proteins. Involved in the hormonal regulation of adenylate cyclase [Refseq 2024]
TACC1	Transforming acidic coiled-coil containing protein 1	Candidate breast cancer gene. Located close to FGF2 on chromosomes. FGF2 is frequently amplified in breast cancer. [Refseq, 2024]
MAGEA4	Melanoma Associated Antigen family member A4	Part of the MAGE protein family. Members of this family have been implicated in some hereditary disorders [Refseq, 2024]

Proteomic characterization of lipid droplets from different cell states

In our work, we focused on performing proteomic analysis of lipid droplet proteins in human A375 melanoma cells. This dataset provides a baseline list for lipid droplet proteins in melanoma, however it does not explore lipid droplet proteome remodeling in different cellular phenotypes. One area of investigation that is highlighted by our work with DHRS3 is the potential for there to be changes in the lipid droplet proteome across melanoma cell states. In further support of this, imaging of lipid droplets in melanocytic IGR37 and undifferentiated IGR39 cells reveals dramatic differences in lipid droplet

localization and size between the two cell states (Figure 32F). Because these two cell lines are isogenic, they are an ideal model system to study this question. In addition, the APEX2 LD proximity labeling method could be substantially helpful here, as it is well known that lipid droplets of different sizes will separate differently via gradient ultracentrifugation.[127] Therefore, an approach which isolates APEX2 labeling from gradient ultracentrifugation could allow a more reliable comparison between lipid droplets of different sizes. Finally, this work could be applied more broadly. Because melanoma cell states are thought to approximate a differentiation trajectory[56] comparing melanocytic vs. undifferentiated cells could generate insight into how the lipid droplet proteome is modified during cellular differentiation.

APPENDICES

Table 2

Uniprot ID	Symbol	LD localization reference	PMID
O60664	PLIN3	Wolins et al. JBC 2001	12840023
Q99541	PLIN2	Brasaemle et al. JLR 1997	9392423
Q9NP72	RAB18	Martin et al. JBC 2005, Ozeki et al. JCS 2005, Liu et al. BBA 2007	Martin et al. JBC 2005, Ozeki et al. JCS 2005, Liu et al. BBA 2007
Q8NBQ5	HSD17B11	Horiguchi et al. ABB 2008	18804447
Q96AD5	PNPLA2	Smirnova et al. EMBO Rep 2006	16239926
P00387	CYB5R3	Zehmer et al. JCS 2008	18477614
P62820	RAB1A	Nevo-Yassaf et al. JV 2012	22491470
O95573	ACSL3	Poppelreuther et al. JLR 2012, Kassan et al. JCB 2013	22357706, 24368806
P60604	UBE2G2	Spandl et al. JBC 2011, Klemm et al. JBC 2011	21127063, 21857022
Q15738	NSDHL	Caldas et al. HMG 2003, Ohashi et al. JBC 2003	14506130, 12837764
Q96CS3	FAF2	Olzmann et al. PNAS 2013, Zehmer et al. JCS 2009, Suzuki et al. MBoC 2012	23297223, 19773358, 22238364
P61026	RAB10	Li et al. Science Advances 2016	28028537
Q9Y679	AUP1	Spandl et al. JBC 2011, Klemm et al. JBC 2011	21127063, 21857022
Q15907	RAB11B	Liu et al. BBA 2007	17395284
Q92575	UBXN4	Suzuki et al. MBoC 2012	22238364
Q6UXV4	APOOL	Lamant et al. JBC 2006	16956892
Q6UX53	METTL7B	Zehmer et al. JCS 2008, Zehmer et al. JCS 2009	18477614, 19773358
Q8NF37	LPCAT1	Moessinger et al. JBC 2011	21498505
Q8N6T3	ARFGAP1	Gannon et al. PLOS One 2014	25397679
P48449	LSS	Milla et al. JBC 2002	11706015
Q03135	CAV1	Pol et al. MBoC 2004, Le Lay et al. Traffic 2006	14528016, 16643278
P61020	RAB5B	Liu et al. BBA 2007	17395284
Q8WTS1	ABHD5	Subramanian et al. JBC 2004, Yamaguchi et al. JBC 2004	15292255, 15136565
Q709C8	VPS13C	Ramseyer and Granneman, Endocrine Society Abstract	
Q14534	SQLE	Wang et al. JCS 2012; Minh et al. FEBS J 2012; Leber et al. MBoC 1998	22454508, 23013491, 9450962
Q8IZ81	ELMOD2	East et al. JBC 2012, Suzuki et al. MBoC 2015	23014990, 25904333
Q86UL3	GPAT4	Wilfling et al. Dev Cell 2013	23415954

P61006	RAB8A	Wu et al. Dev Cell 2014	25158853
Q2TAZ0	ATG2A	Velikkakath et al. MBoC 2012, Pfisterer et al. JLR 2014	22219374, 24776541
O60313	OPA1	Pidoux et al. EMBO J 2011	21983901
P55072	VCP	Olzmann et al. PNAS 2013	23297223
Q9Y4P8	WIPI2	Dupont et al. Curr Biol 2014	24613307
Q8N0X7	SPG20	Eastman et al. JCB 2009	19307600
Q53EU6	GPAT3	Pagac et al. Cell Rep 2016	27806294
Q15042	RAB3GAP1	Spang et al. Autophagy 2014	25495476
Q9NST1	PNPLA3	He et al. JBC 2010	20034933
Q9Y5L2	HILPDA	Gimm et al. FASEB J 2010	20624928
Q99878	HIST1H2AJ	Cermelli et al. Curr Biol 2006	16979555
Q05469	LIPE	Sztalryd et al. JCB 2003	12810697
P51636	CAV2	Ingelmo-Torres et al. Traffic 2009	19874557
Q8IZV5	RDH10	Jiang et al. JBC 2012	23155051
Q9H2M9	RAB3GAP2	Spang et al. Autophagy 2014	25495476
Q96Q06	PLIN4	Hsieh et al. JCS 2012	22685330
Q9H6V9	LDAH	Goo et al. ATVB 2014	24357060
P62491	RAB11A	Liu et al. BBA 2007	17395284
Q9UHD4	CIDEB	Liu et al. AJPEM 2009	19843876
Q99685	MGLL	Sun et al. Oncogene 2013	22349814
Q8IUS5	EPHX4	Dahlhoff et al. Exp Cell Res 2015	25523620
P56937	HSD17B7	Bersuker, et. al., 2018	
Q8TC12	RDH11	Bersuker, et. al., 2018	
P48739	PITPNB	Bersuker, et. al., 2018	
Q9BRQ8	AIFM2	Bersuker, et. al., 2018	
Q8NBX0	SCCPDH	Bersuker, et. al., 2018	
Q9HBF4	ZFYVE1	Bersuker, et. al., 2018	
Q9H0U4	RAB1B	Bersuker, et. al., 2018	
P20339	RAB5A	Bersuker, et. al., 2018	
Q8TCD1	c18orf32	Bersuker, et. al., 2018	
Q99640	PKMYT1	Bersuker, et. al., 2018	

Table 2

Previously validated lipid droplet proteins

Table 3

Gene Name
PLIN2
RAB7A
RAB5C

ACSL3
HSD17B11
CYB5R3
FAF2
AUP1
RAB10
RAB8A
UBE2G2
RAB11B;RAB11A
SCCPDH
RAB14
PNPLA2
RAB18
RAB1A
LPCAT1
NSDHL
RAB2A
ACTB;ACTG1
LPCAT2
METTL7B
RAB6A
ABHD5
RAB5A
ELMOD2
VCP
RAB34
DHRS3
AGPAT9
DHRS1
PLIN3
LSS
HSPA8
CAV1
PRDX1
ARL1
UBC;UBB;RPS27A;UBA52
HSD17B7
RAP1B;RAP1A
TXN
RDH10
TMEM159
LDAH;C2orf43
AIFM2
ACSL4
TUBA1C;TUBA1A;TUBA1B;TUBA3E;TUBA4A

KATNAL2
TUBB
RAB1B
ANO1
RAB43
C18orf32
CFL1
LPCAT4
RHOA;RHOC
UBXN4
RAB21
TMEM263
VIM
CRACR2A
METTL7A
GAPDH
EEF1A1;EEF1A1P5;EEF1A2
HSP90AB1
DCD
RAB5B
RAB35
TAGLN2
HAP1
RAB13
TACC1
MAGEA4
RAB32
PCBP1
KIF16B
MYO1D
YWHAZ;YWHAQ
ALG5
DHDDS
TFG
RPS14
EPHX4
ARF4
HILPDA
KIAA0101
A0A1B0GVS8
GNAI2;GNAI1
RPS6
GNB2;GNB4
SAR1B;SAR1A
RAB3D

RPS25
PFN1
PKMYT1

Table 3

List of 96 high confidence lipid droplet proteins in melanoma

REFERENCES

1. About Melanoma Skin Cancer. (2024). https://www.cancer.org/cancer/types/melanoma-skin-cancer/about/key-statistics.html.
2. Long, G.V., Swetter, S.M., Menzies, A.M., Gershenwald, J.E., and Scolyer, R.A. (2023). Cutaneous melanoma. The Lancet *402*, 485-502. https://doi.org/10.1016/S0140-6736(23)00821-8.
3. Rambow, F., Rogiers, A., Marin-Bejar, O., Aibar, S., Femel, J., Dewaele, M., Karras, P., Brown, D., Chang, Y.H., Debiec-Rychter, M., et al. (2018). Toward Minimal Residual Disease-Directed Therapy in Melanoma. Cell *174*, 843-855.e819. 10.1016/j.cell.2018.06.025.
4. Burrell, R.A., McGranahan, N., Bartek, J., and Swanton, C. (2013). The causes and consequences of genetic heterogeneity in cancer evolution. Nature *501*, 338-345. 10.1038/nature12625.
5. Vogelstein, B., Papadopoulos, N., Velculescu, V.E., Zhou, S., Diaz, L.A., and Kinzler, K.W. (2013). Cancer Genome Landscapes. Science *339*, 1546-1558. 10.1126/science.1235122.
6. Chang, K., Creighton, C.J., Davis, C., Donehower, L., Drummond, J., Wheeler, D., Ally, A., Balasundaram, M., Birol, I., Butterfield, Y.S.N., et al. (2013). The Cancer Genome Atlas Pan-Cancer analysis project. Nature Genetics *45*, 1113-1120. 10.1038/ng.2764.
7. Bailey, M.H., Tokheim, C., Porta-Pardo, E., Sengupta, S., Bertrand, D., Weerasinghe, A., Colaprico, A., Wendl, M.C., Kim, J., Reardon, B., et al. (2018). Comprehensive Characterization of Cancer Driver Genes and Mutations. Cell *173*, 371-385.e318. https://doi.org/10.1016/j.cell.2018.02.060.
8. Gillies, R.J., Verduzco, D., and Gatenby, R.A. (2012). Evolutionary dynamics of carcinogenesis and why targeted therapy does not work. Nature Reviews Cancer *12*, 487-493. 10.1038/nrc3298.
9. McGranahan, N., and Swanton, C. (2015). Biological and Therapeutic Impact of Intratumor Heterogeneity in Cancer Evolution. Cancer Cell *27*, 15-26. https://doi.org/10.1016/j.ccell.2014.12.001.
10. Black, J.R.M., and McGranahan, N. (2021). Genetic and non-genetic clonal diversity in cancer evolution. Nature Reviews Cancer *21*, 379-392. 10.1038/s41568-021-00336-2.
11. Lawrence, M.S., Stojanov, P., Polak, P., Kryukov, G.V., Cibulskis, K., Sivachenko, A., Carter, S.L., Stewart, C., Mermel, C.H., Roberts, S.A., et al. (2013). Mutational heterogeneity in cancer and the search for new cancer-associated genes. Nature *499*, 214-218. 10.1038/nature12213.
12. Hanahan, D., and Weinberg, Robert A. (2011). Hallmarks of Cancer: The Next Generation. Cell *144*, 646-674. 10.1016/j.cell.2011.02.013.
13. Hachey, S.J., and Boiko, A.D. (2016). Therapeutic implications of melanoma heterogeneity. Experimental Dermatology *25*, 497-500. https://doi.org/10.1111/exd.13002.

14. Govindarajan, B., Bai, X., Cohen, C., Zhong, H., Kilroy, S., Louis, G., Moses, M., and Arbiser, J.L. (2003). Malignant Transformation of Melanocytes to Melanoma by Constitutive Activation of Mitogen-activated Protein Kinase Kinase (MAPKK) Signaling*. Journal of Biological Chemistry *278*, 9790-9795. https://doi.org/10.1074/jbc.M212929200.
15. Sullivan, R.J., and Flaherty, K.T. (2013). Resistance to BRAF-targeted therapy in melanoma. European Journal of Cancer *49*, 1297-1304. 10.1016/j.ejca.2012.11.019.
16. Davies, H., Bignell, G.R., Cox, C., Stephens, P., Edkins, S., Clegg, S., Teague, J., Woffendin, H., Garnett, M.J., Bottomley, W., et al. (2002). Mutations of the BRAF gene in human cancer. Nature *417*, 949-954. 10.1038/nature00766.
17. Brose, M.S., Volpe, P., Feldman, M., Kumar, M., Rishi, I., Gerrero, R., Einhorn, E., Herlyn, M., Minna, J., Nicholson, A., et al. (2002). BRAF and RAS Mutations in Human Lung Cancer and Melanoma1. Cancer Research *62*, 6997-7000.
18. Grzywa, T.M., Paskal, W., and Włodarski, P.K. (2017). Intratumor and Intertumor Heterogeneity in Melanoma. Translational Oncology *10*, 956-975. https://doi.org/10.1016/j.tranon.2017.09.007.
19. Colombino, M., Capone, M., Lissia, A., Cossu, A., Rubino, C., De Giorgi, V., Massi, D., Fonsatti, E., Staibano, S., Nappi, O., et al. (2012). BRAF/NRAS mutation frequencies among primary tumors and metastases in patients with melanoma. J Clin Oncol *30*, 2522-2529. 10.1200/jco.2011.41.2452.
20. Lee, J.H., Choi, J.W., and Kim, Y.S. (2011). Frequencies of BRAF and NRAS mutations are different in histological types and sites of origin of cutaneous melanoma: a meta-analysis. British Journal of Dermatology *164*, 776-784. 10.1111/j.1365-2133.2010.10185.x.
21. Dhomen, N., Reis-Filho, J.S., da Rocha Dias, S., Hayward, R., Savage, K., Delmas, V., Larue, L., Pritchard, C., and Marais, R. (2009). Oncogenic Braf Induces Melanocyte Senescence and Melanoma in Mice. Cancer Cell *15*, 294-303. 10.1016/j.ccr.2009.02.022.
22. Dankort, D., Curley, D.P., Cartlidge, R.A., Nelson, B., Karnezis, A.N., Damsky Jr, W.E., You, M.J., DePinho, R.A., McMahon, M., and Bosenberg, M. (2009). BrafV600E cooperates with Pten loss to induce metastatic melanoma. Nature Genetics *41*, 544-552. 10.1038/ng.356.
23. Falchook, G.S., Long, G.V., Kurzrock, R., Kim, K.B., Arkenau, T.H., Brown, M.P., Hamid, O., Infante, J.R., Millward, M., Pavlick, A.C., et al. (2012). Dabrafenib in patients with melanoma, untreated brain metastases, and other solid tumours: a phase 1 dose-escalation trial. The Lancet *379*, 1893-1901. 10.1016/S0140-6736(12)60398-5.
24. Chapman, P.B., Hauschild, A., Robert, C., Haanen, J.B., Ascierto, P., Larkin, J., Dummer, R., Garbe, C., Testori, A., Maio, M., et al. (2011). Improved Survival with Vemurafenib in Melanoma with BRAF V600E Mutation. New England Journal of Medicine *364*, 2507-2516. doi:10.1056/NEJMoa1103782.
25. Sosman, J.A., Kim, K.B., Schuchter, L., Gonzalez, R., Pavlick, A.C., Weber, J.S., McArthur, G.A., Hutson, T.E., Moschos, S.J., Flaherty, K.T., et al. (2012). Survival in BRAF V600–Mutant Advanced Melanoma Treated with

Vemurafenib. New England Journal of Medicine *366*, 707-714. doi:10.1056/NEJMoa1112302.
26. Flaherty, K.T., Robert, C., Hersey, P., Nathan, P., Garbe, C., Milhem, M., Demidov, L.V., Hassel, J.C., Rutkowski, P., Mohr, P., et al. (2012). Improved Survival with MEK Inhibition in BRAF-Mutated Melanoma. New England Journal of Medicine *367*, 107-114. doi:10.1056/NEJMoa1203421.
27. Flaherty, K.T., Infante, J.R., Daud, A., Gonzalez, R., Kefford, R.F., Sosman, J., Hamid, O., Schuchter, L., Cebon, J., Ibrahim, N., et al. (2012). Combined BRAF and MEK Inhibition in Melanoma with BRAF V600 Mutations. New England Journal of Medicine *367*, 1694-1703. doi:10.1056/NEJMoa1210093.
28. Sanchez-Laorden, B., Viros, A., Girotti, M.R., Pedersen, M., Saturno, G., Zambon, A., Niculescu-Duvaz, D., Turajlic, S., Hayes, A., Gore, M., et al. (2014). BRAF Inhibitors Induce Metastasis in RAS Mutant or Inhibitor-Resistant Melanoma Cells by Reactivating MEK and ERK Signaling. Science Signaling *7*, ra30-ra30. 10.1126/scisignal.2004815.
29. Subbiah, V., Baik, C., and Kirkwood, J.M. (2020). Clinical Development of BRAF plus MEK Inhibitor Combinations. Trends in Cancer *6*, 797-810. 10.1016/j.trecan.2020.05.009.
30. Shi, H., Hugo, W., Kong, X., Hong, A., Koya, R.C., Moriceau, G., Chodon, T., Guo, R., Johnson, D.B., Dahlman, K.B., et al. (2014). Acquired Resistance and Clonal Evolution in Melanoma during BRAF Inhibitor Therapy. Cancer Discovery *4*, 80-93. 10.1158/2159-8290.CD-13-0642.
31. Ascierto, P.A., McArthur, G.A., Dréno, B., Atkinson, V., Liszkay, G., Di Giacomo, A.M., Mandalà, M., Demidov, L., Stroyakovskiy, D., Thomas, L., et al. (2016). Cobimetinib combined with vemurafenib in advanced BRAF^{V600}-mutant melanoma (coBRIM): updated efficacy results from a randomised, double-blind, phase 3 trial. The Lancet Oncology *17*, 1248-1260. 10.1016/S1470-2045(16)30122-X.
32. Hauschild, A., Grob, J.-J., Demidov, L.V., Jouary, T., Gutzmer, R., Millward, M., Rutkowski, P., Blank, C.U., Miller, W.H., Jr., Kaempgen, E., et al. (2012). Dabrafenib in BRAF-mutated metastatic melanoma: a multicentre, open-label, phase 3 randomised controlled trial. The Lancet *380*, 358-365. 10.1016/S0140-6736(12)60868-X.
33. Trunzer, K., Pavlick, A.C., Schuchter, L., Gonzalez, R., McArthur, G.A., Hutson, T.E., Moschos, S.J., Flaherty, K.T., Kim, K.B., Weber, J.S., et al. (2013). Pharmacodynamic Effects and Mechanisms of Resistance to Vemurafenib in Patients With Metastatic Melanoma. Journal of Clinical Oncology *31*, 1767-1774. 10.1200/JCO.2012.44.7888.
34. Robert, C., Grob Jean, J., Stroyakovskiy, D., Karaszewska, B., Hauschild, A., Levchenko, E., Chiarion Sileni, V., Schachter, J., Garbe, C., Bondarenko, I., et al. (2019). Five-Year Outcomes with Dabrafenib plus Trametinib in Metastatic Melanoma. New England Journal of Medicine *381*, 626-636. 10.1056/NEJMoa1904059.
35. Sharma, P., and Allison, James P. (2015). Immune Checkpoint Targeting in Cancer Therapy: Toward Combination Strategies with Curative Potential. Cell *161*, 205-214. 10.1016/j.cell.2015.03.030.

36. Ribas, A., and Wolchok, J.D. (2018). Cancer immunotherapy using checkpoint blockade. Science *359*, 1350-1355. 10.1126/science.aar4060.
37. Yang, J.C., Hughes, M., Kammula, U., Royal, R., Sherry, R.M., Topalian, S.L., Suri, K.B., Levy, C., Allen, T., Mavroukakis, S., et al. (2007). Ipilimumab (Anti-CTLA4 Antibody) Causes Regression of Metastatic Renal Cell Cancer Associated With Enteritis and Hypophysitis. Journal of Immunotherapy *30*.
38. Hodi, F.S., Butler, M., Oble, D.A., Seiden, M.V., Haluska, F.G., Kruse, A., MacRae, S., Nelson, M., Canning, C., Lowy, I., et al. (2008). Immunologic and clinical effects of antibody blockade of cytotoxic T lymphocyte-associated antigen 4 in previously vaccinated cancer patients. Proceedings of the National Academy of Sciences *105*, 3005-3010. 10.1073/pnas.0712237105.
39. Brahmer, J.R., Tykodi, S.S., Chow, L.Q.M., Hwu, W.-J., Topalian, S.L., Hwu, P., Drake, C.G., Camacho, L.H., Kauh, J., Odunsi, K., et al. (2012). Safety and Activity of Anti–PD-L1 Antibody in Patients with Advanced Cancer. New England Journal of Medicine *366*, 2455-2465. doi:10.1056/NEJMoa1200694.
40. Topalian, S.L., Hodi, F.S., Brahmer, J.R., Gettinger, S.N., Smith, D.C., McDermott, D.F., Powderly, J.D., Carvajal, R.D., Sosman, J.A., Atkins, M.B., et al. (2012). Safety, Activity, and Immune Correlates of Anti–PD-1 Antibody in Cancer. New England Journal of Medicine *366*, 2443-2454. doi:10.1056/NEJMoa1200690.
41. Cancer Facts and Figures 2024. (2024). https://www.cancer.org/research/cancer-facts-statistics/all-cancer-facts-figures/2024-cancer-facts-figures.html.
42. Wolchok, J.D., Chiarion-Sileni, V., Gonzalez, R., Rutkowski, P., Grob, J.-J., Cowey, C.L., Lao, C.D., Wagstaff, J., Schadendorf, D., Ferrucci, P.F., et al. (2017). Overall Survival with Combined Nivolumab and Ipilimumab in Advanced Melanoma. New England Journal of Medicine *377*, 1345-1356. doi:10.1056/NEJMoa1709684.
43. Hodi, F.S., O'Day, S.J., McDermott, D.F., Weber, R.W., Sosman, J.A., Haanen, J.B., Gonzalez, R., Robert, C., Schadendorf, D., Hassel, J.C., et al. (2010). Improved Survival with Ipilimumab in Patients with Metastatic Melanoma. New England Journal of Medicine *363*, 711-723. doi:10.1056/NEJMoa1003466.
44. Robert, C., Thomas, L., Bondarenko, I., O'Day, S., Weber, J., Garbe, C., Lebbe, C., Baurain, J.-F., Testori, A., Grob, J.-J., et al. (2011). Ipilimumab plus Dacarbazine for Previously Untreated Metastatic Melanoma. New England Journal of Medicine *364*, 2517-2526. doi:10.1056/NEJMoa1104621.
45. Robert, C., Long, G.V., Brady, B., Dutriaux, C., Maio, M., Mortier, L., Hassel, J.C., Rutkowski, P., McNeil, C., Kalinka-Warzocha, E., et al. (2015). Nivolumab in Previously Untreated Melanoma without BRAF Mutation. New England Journal of Medicine *372*, 320-330. doi:10.1056/NEJMoa1412082.
46. Larkin, J., Chiarion-Sileni, V., Gonzalez, R., Grob, J.J., Cowey, C.L., Lao, C.D., Schadendorf, D., Dummer, R., Smylie, M., Rutkowski, P., et al. (2015). Combined Nivolumab and Ipilimumab or Monotherapy in Untreated Melanoma. New England Journal of Medicine *373*, 23-34. doi:10.1056/NEJMoa1504030.
47. Robert, C., Ribas, A., Hamid, O., Daud, A., Wolchok, J.D., Joshua, A.M., Hwu, W.-J., Weber, J.S., Gangadhar, T.C., Joseph, R.W., et al. (2017). Durable Complete Response After Discontinuation of Pembrolizumab in Patients With

Metastatic Melanoma. Journal of Clinical Oncology *36*, 1668-1674. 10.1200/JCO.2017.75.6270.
48. Marusyk, A., Almendro, V., and Polyak, K. (2012). Intra-tumour heterogeneity: a looking glass for cancer? Nature Reviews Cancer *12*, 323-334. 10.1038/nrc3261.
49. Shackleton, M., Quintana, E., Fearon, E.R., and Morrison, S.J. (2009). Heterogeneity in Cancer: Cancer Stem Cells versus Clonal Evolution. Cell *138*, 822-829. 10.1016/j.cell.2009.08.017.
50. Quintana, E., Shackleton, M., Sabel, M.S., Fullen, D.R., Johnson, T.M., and Morrison, S.J. (2008). Efficient tumour formation by single human melanoma cells. Nature *456*, 593-598. 10.1038/nature07567.
51. Batlle, E., and Clevers, H. (2017). Cancer stem cells revisited. Nature Medicine *23*, 1124-1134. 10.1038/nm.4409.
52. Hoek, K.S., and Goding, C.R. (2010). Cancer stem cells versus phenotype-switching in melanoma. Pigment Cell & Melanoma Research *23*, 746-759. https://doi.org/10.1111/j.1755-148X.2010.00757.x.
53. Hoek, K.S., Schlegel, N.C., Brafford, P., Sucker, A., Ugurel, S., Kumar, R., Weber, B.L., Nathanson, K.L., Phillips, D.J., Herlyn, M., Schadendorf, D., and Dummer, R. (2006). Metastatic potential of melanomas defined by specific gene expression profiles with no BRAF signature. Pigment Cell Research *19*, 290-302. https://doi.org/10.1111/j.1600-0749.2006.00322.x.
54. Hoek, K.S., Eichhoff, O.M., Schlegel, N.C., Döbbeling, U., Kobert, N., Schaerer, L., Hemmi, S., and Dummer, R. (2008). In vivo Switching of Human Melanoma Cells between Proliferative and Invasive States. Cancer Research *68*, 650-656. 10.1158/0008-5472.CAN-07-2491.
55. Gavish, A., Tyler, M., Greenwald, A.C., Hoefflin, R., Simkin, D., Tschernichovsky, R., Galili Darnell, N., Somech, E., Barbolin, C., Antman, T., et al. (2023). Hallmarks of transcriptional intratumour heterogeneity across a thousand tumours. Nature *618*, 598-606. 10.1038/s41586-023-06130-4.
56. Rambow, F., Marine, J.-C., and Goding, C.R. (2019). Melanoma plasticity and phenotypic diversity: therapeutic barriers and opportunities. Genes & Development *33*, 1295-1318. 10.1101/gad.329771.119.
57. Tsoi, J., Robert, L., Paraiso, K., Galvan, C., Sheu, K.M., Lay, J., Wong, D.J.L., Atefi, M., Shirazi, R., Wang, X., et al. (2018). Multi-stage Differentiation Defines Melanoma Subtypes with Differential Vulnerability to Drug-Induced Iron-Dependent Oxidative Stress. Cancer Cell *33*, 890-904.e895. 10.1016/j.ccell.2018.03.017.
58. Widmer, D.S., Cheng, P.F., Eichhoff, O.M., Belloni, B.C., Zipser, M.C., Schlegel, N.C., Javelaud, D., Mauviel, A., Dummer, R., and Hoek, K.S. (2012). Systematic classification of melanoma cells by phenotype-specific gene expression mapping. Pigment Cell & Melanoma Research *25*, 343-353. https://doi.org/10.1111/j.1755-148X.2012.00986.x.
59. Wouters, J., Kalender-Atak, Z., Minnoye, L., Spanier, K.I., De Waegeneer, M., Bravo González-Blas, C., Mauduit, D., Davie, K., Hulselmans, G., Najem, A., et al. (2020). Robust gene expression programs underlie recurrent cell states and phenotype switching in melanoma. Nature Cell Biology *22*, 986-998. 10.1038/s41556-020-0547-3.

60. Carreira, S., Goodall, J., Denat, L., Rodriguez, M., Nuciforo, P., Hoek, K.S., Testori, A., Larue, L., and Goding, C.R. (2006). Mitf regulation of Dia1 controls melanoma proliferation and invasiveness. Genes & Development *20*, 3426-3439. 10.1101/gad.406406.
61. Hemesath, T.J., Steingrímsson, E., McGill, G., Hansen, M.J., Vaught, J., Hodgkinson, C.A., Arnheiter, H., Copeland, N.G., Jenkins, N.A., and Fisher, D.E. (1994). microphthalmia, a critical factor in melanocyte development, defines a discrete transcription factor family. Genes & Development *8*, 2770-2780. 10.1101/gad.8.22.2770.
62. Hertwig, P. (1942). Neue Mutationen und Koppelungsgruppen bei der Hausmaus. Zeitschrift für Induktive Abstammungs- und Vererbungslehre *80*, 220-246. 10.1007/BF01741984.
63. Hodgkinson, C.A., Moore, K.J., Nakayama, A., Steingrímsson, E., Copeland, N.G., Jenkins, N.A., and Arnheiter, H. (1993). Mutations at the mouse microphthalmia locus are associated with defects in a gene encoding a novel basic-helix-loop-helix-zipper protein. Cell *74*, 395-404. https://doi.org/10.1016/0092-8674(93)90429-T.
64. Krakowsky, J.M., Boissy, R.E., Neumann, J.C., and Lingrel, J.B. (1993). A DNA insertional mutation results in microphthalmia in transgenic mice. Transgenic Res *2*, 14-20. 10.1007/bf01977676.
65. George, A., Zand, Dina J., Hufnagel, Robert B., Sharma, R., Sergeev, Yuri V., Legare, Janet M., Rice, Gregory M., Scott Schwoerer, J.A., Rius, M., Tetri, L., et al. (2016). Biallelic Mutations in MITF Cause Coloboma, Osteopetrosis, Microphthalmia, Macrocephaly, Albinism, and Deafness. The American Journal of Human Genetics *99*, 1388-1394. https://doi.org/10.1016/j.ajhg.2016.11.004.
66. Lister, J.A., Robertson, C.P., Lepage, T., Johnson, S.L., and Raible, D.W. (1999). nacre encodes a zebrafish microphthalmia-related protein that regulates neural-crest-derived pigment cell fate. Development *126*, 3757-3767. 10.1242/dev.126.17.3757.
67. Goding, C.R., and Arnheiter, H. (2019). MITF—the first 25 years. Genes & Development *33*, 983-1007. 10.1101/gad.324657.119.
68. Cheli, Y., Ohanna, M., Ballotti, R., and Bertolotto, C. (2010). Fifteen-year quest for microphthalmia-associated transcription factor target genes. Pigment Cell & Melanoma Research *23*, 27-40. https://doi.org/10.1111/j.1755-148X.2009.00653.x.
69. Hunter, M.V., Montal, E., Ma, Y., Moncada, R., Yanai, I., Koche, R.P., and White, R.M. (2024). Mechanical confinement governs phenotypic plasticity in melanoma. bioRxiv, 2024.2001.2030.577120. 10.1101/2024.01.30.577120.
70. Falletta, P., Sanchez-del-Campo, L., Chauhan, J., Effern, M., Kenyon, A., Kershaw, C.J., Siddaway, R., Lisle, R., Freter, R., Daniels, M.J., et al. (2017). Translation reprogramming is an evolutionarily conserved driver of phenotypic plasticity and therapeutic resistance in melanoma. Genes & Development *31*, 18-33. 10.1101/gad.290940.116.
71. Vivas-García, Y., Falletta, P., Liebing, J., Louphrasitthiphol, P., Feng, Y., Chauhan, J., Scott, D.A., Glodde, N., Chocarro-Calvo, A., Bonham, S., et al. (2020). Lineage-Restricted Regulation of SCD and Fatty Acid Saturation by

MITF Controls Melanoma Phenotypic Plasticity. Molecular Cell *77*, 120-137.e129. 10.1016/j.molcel.2019.10.014.
72. Louphrasitthiphol, P., Ledaki, I., Chauhan, J., Falletta, P., Siddaway, R., Buffa, F.M., Mole, D.R., Soga, T., and Goding, C.R. (2019). MITF controls the TCA cycle to modulate the melanoma hypoxia response. Pigment Cell & Melanoma Research *32*, 792-808. https://doi.org/10.1111/pcmr.12802.
73. Feige, E., Yokoyama, S., Levy, C., Khaled, M., Igras, V., Lin, R.J., Lee, S., Widlund, H.R., Granter, S.R., Kung, A.L., and Fisher, D.E. (2011). Hypoxia-induced transcriptional repression of the melanoma-associated oncogene MITF. Proceedings of the National Academy of Sciences *108*, E924-E933. 10.1073/pnas.1106351108.
74. Pavlova, Natalya N., and Thompson, Craig B. (2016). The Emerging Hallmarks of Cancer Metabolism. Cell Metabolism *23*, 27-47. https://doi.org/10.1016/j.cmet.2015.12.006.
75. García-Jiménez, C., and Goding, C.R. (2019). Starvation and Pseudo-Starvation as Drivers of Cancer Metastasis through Translation Reprogramming. Cell Metabolism *29*, 254-267. https://doi.org/10.1016/j.cmet.2018.11.018.
76. Marchiq, I., and Pouysségur, J. (2016). Hypoxia, cancer metabolism and the therapeutic benefit of targeting lactate/H+ symporters. Journal of Molecular Medicine *94*, 155-171. 10.1007/s00109-015-1307-x.
77. Semenza, G.L. (2013). HIF-1 mediates metabolic responses to intratumoral hypoxia and oncogenic mutations. The Journal of Clinical Investigation *123*, 3664-3671. 10.1172/JCI67230.
78. Shweiki, D., Neeman, M., Itin, A., and Keshet, E. (1995). Induction of vascular endothelial growth factor expression by hypoxia and by glucose deficiency in multicell spheroids: implications for tumor angiogenesis. Proceedings of the National Academy of Sciences *92*, 768-772. 10.1073/pnas.92.3.768.
79. Senger, D.R., Van De Water, L., Brown, L.F., Nagy, J.A., Yeo, K.-T., Yeo, T.-K., Berse, B., Jackman, R.W., Dvorak, A.M., and Dvorak, H.F. (1993). Vascular permeability factor (VPF, VEGF) in tumor biology. Cancer and Metastasis Reviews *12*, 303-324. 10.1007/BF00665960.
80. Stein, I., Itin, A., Einat, P., Skaliter, R., Grossman, Z., and Keshet, E. (1998). Translation of Vascular Endothelial Growth Factor mRNA by Internal Ribosome Entry: Implications for Translation under Hypoxia. Molecular and Cellular Biology *18*, 3112-3119. 10.1128/MCB.18.6.3112.
81. Shalapour, S., and Karin, M. (2015). Immunity, inflammation, and cancer: an eternal fight between good and evil. The Journal of Clinical Investigation *125*, 3347-3355. 10.1172/JCI80007.
82. Koundouros, N., and Poulogiannis, G. (2020). Reprogramming of fatty acid metabolism in cancer. British Journal of Cancer *122*, 4-22. 10.1038/s41416-019-0650-z.
83. Huang, T.-H., Ma, Y., Montal, E., Suresh, S., Tagore, M.M., Corbin, A., Lumaquin, D., Campbell, N.R., Baggiolini, A., Koche, R.P., and White, R.M. (2022). Epigenetic reprogramming of melanoma cell state through fatty acid β-oxidation and Toll-like receptor 4 signaling. bioRxiv, 2022.2006.2016.496450. 10.1101/2022.06.16.496450.

84. Pascual, G., Avgustinova, A., Mejetta, S., Martín, M., Castellanos, A., Attolini, C.S.-O., Berenguer, A., Prats, N., Toll, A., Hueto, J.A., et al. (2017). Targeting metastasis-initiating cells through the fatty acid receptor CD36. Nature *541*, 41-45. 10.1038/nature20791.
85. Nieman, K.M., Kenny, H.A., Penicka, C.V., Ladanyi, A., Buell-Gutbrod, R., Zillhardt, M.R., Romero, I.L., Carey, M.S., Mills, G.B., Hotamisligil, G.S., et al. (2011). Adipocytes promote ovarian cancer metastasis and provide energy for rapid tumor growth. Nature Medicine *17*, 1498-1503. 10.1038/nm.2492.
86. Watt, M.J., Clark, A.K., Selth, L.A., Haynes, V.R., Lister, N., Rebello, R., Porter, L.H., Niranjan, B., Whitby, S.T., Lo, J., et al. (2019). Suppressing fatty acid uptake has therapeutic effects in preclinical models of prostate cancer. Science Translational Medicine *11*, eaau5758. 10.1126/scitranslmed.aau5758.
87. Casciano, J.C., Perry, C., Cohen-Nowak, A.J., Miller, K.D., Vande Voorde, J., Zhang, Q., Chalmers, S., Sandison, M.E., Liu, Q., Hedley, A., et al. (2020). MYC regulates fatty acid metabolism through a multigenic program in claudin-low triple negative breast cancer. British Journal of Cancer *122*, 868-884. 10.1038/s41416-019-0711-3.
88. Zhang, M., Di Martino, J.S., Bowman, R.L., Campbell, N.R., Baksh, S.C., Simon-Vermot, T., Kim, I.S., Haldeman, P., Mondal, C., Yong-Gonzales, V., et al. (2018). Adipocyte-Derived Lipids Mediate Melanoma Progression via FATP Proteins. Cancer Discovery *8*, 1006-1025. 10.1158/2159-8290.CD-17-1371.
89. Alicea, G.M., Rebecca, V.W., Goldman, A.R., Fane, M.E., Douglass, S.M., Behera, R., Webster, M.R., Kugel, C.H., III, Ecker, B.L., Caino, M.C., et al. (2020). Changes in Aged Fibroblast Lipid Metabolism Induce Age-Dependent Melanoma Cell Resistance to Targeted Therapy via the Fatty Acid Transporter FATP2. Cancer Discovery *10*, 1282-1295. 10.1158/2159-8290.CD-20-0329.
90. Henderson, F., Johnston, H.R., Badrock, A.P., Jones, E.A., Forster, D., Nagaraju, R.T., Evangelou, C., Kamarashev, J., Green, M., Fairclough, M., et al. (2019). Enhanced Fatty Acid Scavenging and Glycerophospholipid Metabolism Accompany Melanocyte Neoplasia Progression in Zebrafish. Cancer Research *79*, 2136-2151. 10.1158/0008-5472.CAN-18-2409.
91. Lazar, I., Clement, E., Dauvillier, S., Milhas, D., Ducoux-Petit, M., LeGonidec, S., Moro, C., Soldan, V., Dalle, S., Balor, S., et al. (2016). Adipocyte Exosomes Promote Melanoma Aggressiveness through Fatty Acid Oxidation: A Novel Mechanism Linking Obesity and Cancer. Cancer Research *76*, 4051-4057. 10.1158/0008-5472.CAN-16-0651.
92. Clement, E., Lazar, I., Attané, C., Carrié, L., Dauvillier, S., Ducoux-Petit, M., Esteve, D., Menneteau, T., Moutahir, M., Le Gonidec, S., et al. (2020). Adipocyte extracellular vesicles carry enzymes and fatty acids that stimulate mitochondrial metabolism and remodeling in tumor cells. The EMBO Journal *39*, e102525. https://doi.org/10.15252/embj.2019102525.
93. Lumaquin-Yin, D., Montal, E., Johns, E., Baggiolini, A., Huang, T.-H., Ma, Y., LaPlante, C., Suresh, S., Studer, L., and White, R.M. (2023). Lipid droplets are a metabolic vulnerability in melanoma. Nature Communications *14*, 3192. 10.1038/s41467-023-38831-9.

94. Broadfield, L.A., Pane, A.A., Talebi, A., Swinnen, J.V., and Fendt, S.-M. (2021). Lipid metabolism in cancer: New perspectives and emerging mechanisms. Developmental Cell *56*, 1363-1393. https://doi.org/10.1016/j.devcel.2021.04.013.
95. Kuhajda, F.P., Jenner, K., Wood, F.D., Hennigar, R.A., Jacobs, L.B., Dick, J.D., and Pasternack, G.R. (1994). Fatty acid synthesis: a potential selective target for antineoplastic therapy. Proceedings of the National Academy of Sciences *91*, 6379-6383. 10.1073/pnas.91.14.6379.
96. Tao, B.-B., He, H., Shi, X.-h., Wang, C.-l., Li, W.-q., Li, B., Dong, Y., Hu, G.-H., Hou, L.-J., Luo, C., et al. (2013). Up-regulation of USP2a and FASN in gliomas correlates strongly with glioma grade. Journal of Clinical Neuroscience *20*, 717-720. https://doi.org/10.1016/j.jocn.2012.03.050.
97. Calvisi, D.F., Wang, C., Ho, C., Ladu, S., Lee, S.A., Mattu, S., Destefanis, G., Delogu, S., Zimmermann, A., Ericsson, J., et al. (2011). Increased Lipogenesis, Induced by AKT-mTORC1-RPS6 Signaling, Promotes Development of Human Hepatocellular Carcinoma. Gastroenterology *140*, 1071-1083.e1075. https://doi.org/10.1053/j.gastro.2010.12.006.
98. Zaidi, N., Swinnen, J.V., and Smans, K. (2012). ATP-Citrate Lyase: A Key Player in Cancer Metabolism. Cancer Research *72*, 3709-3714. 10.1158/0008-5472.CAN-11-4112.
99. Schug, Zachary T., Peck, B., Jones, Dylan T., Zhang, Q., Grosskurth, S., Alam, Israt S., Goodwin, Louise M., Smethurst, E., Mason, S., Blyth, K., et al. (2015). Acetyl-CoA Synthetase 2 Promotes Acetate Utilization and Maintains Cancer Cell Growth under Metabolic Stress. Cancer Cell *27*, 57-71. https://doi.org/10.1016/j.ccell.2014.12.002.
100. Wu, S., and Näär, A.M. (2019). SREBP1-dependent de novo fatty acid synthesis gene expression is elevated in malignant melanoma and represents a cellular survival trait. Scientific Reports *9*, 10369. 10.1038/s41598-019-46594-x.
101. Olzmann, J.A., and Carvalho, P. (2019). Dynamics and functions of lipid droplets. Nature Reviews Molecular Cell Biology *20*, 137-155. 10.1038/s41580-018-0085-z.
102. Tauchi-Sato, K., Ozeki, S., Houjou, T., Taguchi, R., and Fujimoto, T. (2002). The surface of lipid droplets is a phospholipid monolayer with a unique Fatty Acid composition. J Biol Chem *277*, 44507-44512. 10.1074/jbc.M207712200.
103. Czabany, T., Wagner, A., Zweytick, D., Lohner, K., Leitner, E., Ingolic, E., and Daum, G. (2008). Structural and Biochemical Properties of Lipid Particles from the Yeast Saccharomyces cerevisiae*. Journal of Biological Chemistry *283*, 17065-17074. https://doi.org/10.1074/jbc.M800401200.
104. Molenaar, M.R., Yadav, K.K., Toulmay, A., Wassenaar, T.A., Mari, M.C., Caillon, L., Chorlay, A., Lukmantara, I.E., Haaker, M.W., Wubbolts, R.W., et al. (2021). Retinyl esters form lipid droplets independently of triacylglycerol and seipin. Journal of Cell Biology *220*, e202011071. 10.1083/jcb.202011071.
105. Bartz, R., Li, W.-H., Venables, B., Zehmer, J.K., Roth, M.R., Welti, R., Anderson, R.G.W., Liu, P., and Chapman, K.D. (2007). Lipidomics reveals that adiposomes store ether lipids and mediate phospholipid traffic1,s. Journal of Lipid Research *48*, 837-847. https://doi.org/10.1194/jlr.M600413-JLR200.

106. Blaner, W.S., O'Byrne, S.M., Wongsiriroj, N., Kluwe, J., D'Ambrosio, D.M., Jiang, H., Schwabe, R.F., Hillman, E.M.C., Piantedosi, R., and Libien, J. (2009). Hepatic stellate cell lipid droplets: A specialized lipid droplet for retinoid storage. Biochimica et Biophysica Acta (BBA) - Molecular and Cell Biology of Lipids *1791*, 467-473. https://doi.org/10.1016/j.bbalip.2008.11.001.
107. Walther, T.C., and Farese, R.V. (2012). Lipid Droplets and Cellular Lipid Metabolism. Annual Review of Biochemistry *81*, 687-714. https://doi.org/10.1146/annurev-biochem-061009-102430.
108. Cases, S., Smith, S.J., Zheng, Y.-W., Myers, H.M., Lear, S.R., Sande, E., Novak, S., Collins, C., Welch, C.B., Lusis, A.J., Erickson, S.K., and Farese, R.V. (1998). Identification of a gene encoding an acyl CoA:diacylglycerol acyltransferase, a key enzyme in triacylglycerol synthesis. Proceedings of the National Academy of Sciences *95*, 13018-13023. 10.1073/pnas.95.22.13018.
109. Sui, X., Wang, K., Gluchowski, N.L., Elliott, S.D., Liao, M., Walther, T.C., and Farese, R.V. (2020). Structure and catalytic mechanism of a human triacylglycerol-synthesis enzyme. Nature *581*, 323-328. 10.1038/s41586-020-2289-6.
110. Sandager, L., Gustavsson, M.H., Ståhl, U., Dahlqvist, A., Wiberg, E., Banas, A., Lenman, M., Ronne, H., and Stymne, S. (2002). Storage Lipid Synthesis Is Non-essential in Yeast*. Journal of Biological Chemistry *277*, 6478-6482. https://doi.org/10.1074/jbc.M109109200.
111. Hamilton, J.A., and Small, D.M. (1981). Solubilization and localization of triolein in phosphatidylcholine bilayers: a 13C NMR study. Proceedings of the National Academy of Sciences *78*, 6878-6882. 10.1073/pnas.78.11.6878.
112. Walther, T.C., Kim, S., Arlt, H., Voth, G.A., and Farese, R.V. (2023). Structure and function of lipid droplet assembly complexes. Current Opinion in Structural Biology *80*, 102606. https://doi.org/10.1016/j.sbi.2023.102606.
113. Chung, J., Wu, X., Lambert, T.J., Lai, Z.W., Walther, T.C., and Farese, R.V. (2019). LDAF1 and Seipin Form a Lipid Droplet Assembly Complex. Developmental Cell *51*, 551-563.e557. https://doi.org/10.1016/j.devcel.2019.10.006.
114. Wang, H., Becuwe, M., Housden, B.E., Chitraju, C., Porras, A.J., Graham, M.M., Liu, X.N., Thiam, A.R., Savage, D.B., Agarwal, A.K., et al. (2016). Seipin is required for converting nascent to mature lipid droplets. eLife *5*, e16582. 10.7554/eLife.16582.
115. Arlt, H., Sui, X., Folger, B., Adams, C., Chen, X., Remme, R., Hamprecht, F.A., DiMaio, F., Liao, M., Goodman, J.M., Farese, R.V., and Walther, T.C. (2022). Seipin forms a flexible cage at lipid droplet formation sites. Nature Structural & Molecular Biology *29*, 194-202. 10.1038/s41594-021-00718-y.
116. Roberts, M.A., and Olzmann, J.A. (2020). Protein Quality Control and Lipid Droplet Metabolism. Annual Review of Cell and Developmental Biology *36*, 115-139. 10.1146/annurev-cellbio-031320-101827.
117. Olarte, M.-J., Swanson, J.M.J., Walther, T.C., and Farese, R.V., Jr. (2022). The CYTOLD and ERTOLD pathways for lipid droplet–protein targeting. Trends in Biochemical Sciences *47*, 39-51. 10.1016/j.tibs.2021.08.007.

118. Bersuker, K., and Olzmann, J.A. (2017). Establishing the lipid droplet proteome: Mechanisms of lipid droplet protein targeting and degradation. Biochimica et Biophysica Acta (BBA) - Molecular and Cell Biology of Lipids *1862*, 1166-1177. https://doi.org/10.1016/j.bbalip.2017.06.006.
119. Wilfling, F., Wang, H., Haas, Joel T., Krahmer, N., Gould, Travis J., Uchida, A., Cheng, J.-X., Graham, M., Christiano, R., Fröhlich, F., et al. (2013). Triacylglycerol Synthesis Enzymes Mediate Lipid Droplet Growth by Relocalizing from the ER to Lipid Droplets. Developmental Cell *24*, 384-399. 10.1016/j.devcel.2013.01.013.
120. Krahmer, N., Guo, Y., Wilfling, F., Hilger, M., Lingrell, S., Heger, K., Newman, Heather W., Schmidt-Supprian, M., Vance, Dennis E., Mann, M., Farese, Robert V., and Walther, Tobias C. (2011). Phosphatidylcholine Synthesis for Lipid Droplet Expansion Is Mediated by Localized Activation of CTP:Phosphocholine Cytidylyltransferase. Cell Metabolism *14*, 504-515. https://doi.org/10.1016/j.cmet.2011.07.013.
121. Grabner, G.F., Xie, H., Schweiger, M., and Zechner, R. (2021). Lipolysis: cellular mechanisms for lipid mobilization from fat stores. Nature Metabolism *3*, 1445-1465. 10.1038/s42255-021-00493-6.
122. Krahmer, N., Najafi, B., Schueder, F., Quagliarini, F., Steger, M., Seitz, S., Kasper, R., Salinas, F., Cox, J., Uhlenhaut, N.H., et al. (2018). Organellar Proteomics and Phospho-Proteomics Reveal Subcellular Reorganization in Diet-Induced Hepatic Steatosis. Developmental Cell *47*, 205-221.e207. https://doi.org/10.1016/j.devcel.2018.09.017.
123. Herms, A., Bosch, M., Reddy, B.J.N., Schieber, N.L., Fajardo, A., Rupérez, C., Fernández-Vidal, A., Ferguson, C., Rentero, C., Tebar, F., et al. (2015). AMPK activation promotes lipid droplet dispersion on detyrosinated microtubules to increase mitochondrial fatty acid oxidation. Nature Communications *6*, 7176. 10.1038/ncomms8176.
124. Mejhert, N., Kuruvilla, L., Gabriel, K.R., Elliott, S.D., Guie, M.-A., Wang, H., Lai, Z.W., Lane, E.A., Christiano, R., Danial, N.N., Farese, R.V., Jr., and Walther, T.C. (2020). Partitioning of MLX-Family Transcription Factors to Lipid Droplets Regulates Metabolic Gene Expression. Molecular Cell *77*, 1251-1264.e1259. 10.1016/j.molcel.2020.01.014.
125. Stephenson, R.A., Thomalla, J.M., Chen, L., Kolkhof, P., White, R.P., Beller, M., and Welte, M.A. (2021). Sequestration to lipid droplets promotes histone availability by preventing turnover of excess histones. Development *148*, dev199381. 10.1242/dev.199381.
126. Brasaemle, D.L., and Wolins, N.E. (2016). Isolation of Lipid Droplets from Cells by Density Gradient Centrifugation. Current Protocols in Cell Biology *72*, 3.15.11-13.15.13. https://doi.org/10.1002/cpcb.10.
127. Ding, Y., Zhang, S., Yang, L., Na, H., Zhang, P., Zhang, H., Wang, Y., Chen, Y., Yu, J., Huo, C., et al. (2013). Isolating lipid droplets from multiple species. Nature Protocols *8*, 43-51. 10.1038/nprot.2012.142.
128. Brasaemle, D.L., Dolios, G., Shapiro, L., and Wang, R. (2004). Proteomic Analysis of Proteins Associated with Lipid Droplets of Basal and Lipolytically

Stimulated 3T3-L1 Adipocytes*. Journal of Biological Chemistry *279*, 46835-46842. https://doi.org/10.1074/jbc.M409340200.
129. Pu, J., Ha, C.W., Zhang, S., Jung, J.P., Huh, W.-K., and Liu, P. (2011). Interactomic study on interaction between lipid droplets and mitochondria. Protein & Cell *2*, 487-496. 10.1007/s13238-011-1061-y.
130. Zhang, H., Wang, Y., Li, J., Yu, J., Pu, J., Li, L., Zhang, H., Zhang, S., Peng, G., Yang, F., and Liu, P. (2011). Proteome of Skeletal Muscle Lipid Droplet Reveals Association with Mitochondria and Apolipoprotein A-I. Journal of Proteome Research *10*, 4757-4768. 10.1021/pr200553c.
131. Blouin, C.M., Le Lay, S., Eberl, A., Köfeler, H.C., Guerrera, I.C., Klein, C., Le Liepvre, X., Lasnier, F., Bourron, O., Gautier, J.-F., et al. (2010). Lipid droplet analysis in caveolin-deficient adipocytes: alterations in surface phospholipid composition and maturation defects[S]. Journal of Lipid Research *51*, 945-956. https://doi.org/10.1194/jlr.M001016.
132. Cermelli, S., Guo, Y., Gross, S.P., and Welte, M.A. (2006). The Lipid-Droplet Proteome Reveals that Droplets Are a Protein-Storage Depot. Current Biology *16*, 1783-1795. https://doi.org/10.1016/j.cub.2006.07.062.
133. Krahmer, N., Hilger, M., Kory, N., Wilfling, F., Stoehr, G., Mann, M., Farese, R.V., and Walther, T.C. (2013). Protein Correlation Profiles Identify Lipid Droplet Proteins with High Confidence*. Molecular & Cellular Proteomics *12*, 1115-1126. https://doi.org/10.1074/mcp.M112.020230.
134. Andersen, J.S., and Mann, M. (2006). Organellar proteomics: turning inventories into insights. EMBO reports *7*, 874-879-879. https://doi.org/10.1038/sj.embor.7400780.
135. Bersuker, K., Peterson, C.W.H., To, M., Sahl, S.J., Savikhin, V., Grossman, E.A., Nomura, D.K., and Olzmann, J.A. (2018). A Proximity Labeling Strategy Provides Insights into the Composition and Dynamics of Lipid Droplet Proteomes. Developmental Cell *44*, 97-112.e117. https://doi.org/10.1016/j.devcel.2017.11.020.
136. Peterson, C.W.H., Deol, K.K., To, M., and Olzmann, J.A. (2021). Optimized protocol for the identification of lipid droplet proteomes using proximity labeling proteomics in cultured human cells. STAR Protocols *2*, 100579. https://doi.org/10.1016/j.xpro.2021.100579.
137. Mejhert, N., Gabriel, K.R., Frendo-Cumbo, S., Krahmer, N., Song, J., Kuruvilla, L., Chitraju, C., Boland, S., Jang, D.-K., von Grotthuss, M., et al. (2022). The Lipid Droplet Knowledge Portal: A resource for systematic analyses of lipid droplet biology. Developmental Cell *57*, 387-397.e384. https://doi.org/10.1016/j.devcel.2022.01.003.
138. Listenberger, L.L., Han, X., Lewis, S.E., Cases, S., Farese, R.V., Ory, D.S., and Schaffer, J.E. (2003). Triglyceride accumulation protects against fatty acid-induced lipotoxicity. Proceedings of the National Academy of Sciences *100*, 3077-3082.
139. Chitraju, C., Mejhert, N., Haas, J.T., Diaz-Ramirez, L.G., Grueter, C.A., Imbriglio, J.E., Pinto, S., Koliwad, S.K., Walther, T.C., and Farese, R.V., Jr. (2017). Triglyceride Synthesis by DGAT1 Protects Adipocytes from Lipid-

Induced ER Stress during Lipolysis. Cell metabolism *26*, 407-418.e403. 10.1016/j.cmet.2017.07.012.

140. Bailey, Andrew P., Koster, G., Guillermier, C., Hirst, Elizabeth M.A., MacRae, James I., Lechene, Claude P., Postle, Anthony D., and Gould, Alex P. (2015). Antioxidant Role for Lipid Droplets in a Stem Cell Niche of Drosophila. Cell *163*, 340-353. https://doi.org/10.1016/j.cell.2015.09.020.
141. Nguyen, T.B., Louie, S.M., Daniele, J.R., Tran, Q., Dillin, A., Zoncu, R., Nomura, D.K., and Olzmann, J.A. (2017). DGAT1-Dependent Lipid Droplet Biogenesis Protects Mitochondrial Function during Starvation-Induced Autophagy. Developmental cell *42*, 9-21.e25. 10.1016/j.devcel.2017.06.003.
142. Wang, H., Sreenivasan, U., Hu, H., Saladino, A., Polster, B.M., Lund, L.M., Gong, D.-w., Stanley, W.C., and Sztalryd, C. (2011). Perilipin 5, a lipid droplet-associated protein, provides physical and metabolic linkage to mitochondria. Journal of Lipid Research *52*, 2159-2168. https://doi.org/10.1194/jlr.M017939.
143. Mathiowetz, A.J., and Olzmann, J.A. (2024). Lipid droplets and cellular lipid flux. Nature Cell Biology. 10.1038/s41556-024-01364-4.
144. Petan, T. (2023). Lipid Droplets in Cancer. In Organelles in Disease, S.H.F. Pedersen, and D.L. Barber, eds. (Springer International Publishing), pp. 53-86. 10.1007/112_2020_51.
145. Jarc, E., and Petan, T. (2019). Lipid Droplets and the Management of Cellular Stress. Yale J Biol Med *92*, 435-452.
146. Dixon, Scott J., Lemberg, Kathryn M., Lamprecht, Michael R., Skouta, R., Zaitsev, Eleina M., Gleason, Caroline E., Patel, Darpan N., Bauer, Andras J., Cantley, Alexandra M., Yang, Wan S., Morrison, B., and Stockwell, Brent R. (2012). Ferroptosis: An Iron-Dependent Form of Nonapoptotic Cell Death. Cell *149*, 1060-1072. https://doi.org/10.1016/j.cell.2012.03.042.
147. Qiu, B., Ackerman, D., Sanchez, D.J., Li, B., Ochocki, J.D., Grazioli, A., Bobrovnikova-Marjon, E., Diehl, J.A., Keith, B., and Simon, M.C. (2015). HIF2α-Dependent Lipid Storage Promotes Endoplasmic Reticulum Homeostasis in Clear-Cell Renal Cell Carcinoma. Cancer Discovery *5*, 652-667. 10.1158/2159-8290.CD-14-1507.
148. Przybytkowski, E., Joly, É., Nolan, C.J., Hardy, S., Francoeur, A.-M., Langelier, Y., and Prentki, M. (2007). Upregulation of cellular triacylglycerol – free fatty acid cycling by oleate is associated with long-term serum-free survival of human breast cancer cells. Biochemistry and Cell Biology *85*, 301-310. 10.1139/O07-001.
149. Pucer, A., Brglez, V., Payré, C., Pungerčar, J., Lambeau, G., and Petan, T. (2013). Group X secreted phospholipase A2 induces lipid droplet formation and prolongs breast cancer cell survival. Molecular Cancer *12*, 111. 10.1186/1476-4598-12-111.
150. Petan, T., Jarc, E., and Jusović, M. (2018). Lipid Droplets in Cancer: Guardians of Fat in a Stressful World. Molecules *23*, 1941. 10.3390/molecules23081941.
151. Wilcock, D.J., Badrock, A.P., Wong, C.W., Owen, R., Guerin, M., Southam, A.D., Johnston, H., Telfer, B.A., Fullwood, P., Watson, J., et al. (2022). Oxidative stress from DGAT1 oncoprotein inhibition in melanoma suppresses tumor growth

when ROS defenses are also breached. Cell Reports *39*, 110995. https://doi.org/10.1016/j.celrep.2022.110995.
152. Berry, R., Church, C.D., Gericke, M.T., Jeffery, E., Colman, L., and Rodeheffer, M.S. (2014). Chapter Four - Imaging of Adipose Tissue. In Methods in Enzymology, O.A. Macdougald, ed. (Academic Press), pp. 47-73. https://doi.org/10.1016/B978-0-12-411619-1.00004-5.
153. Chi, J., Crane, A., Wu, Z., and Cohen, P. (2018). Adipo-Clear: A Tissue Clearing Method for Three-Dimensional Imaging of Adipose Tissue. Journal of visualized experiments : JoVE, 58271. 10.3791/58271.
154. Targett-Adams, P., Chambers, D., Gledhill, S., Hope, R.G., Coy, J.F., Girod, A., and McLauchlan, J. (2003). Live Cell Analysis and Targeting of the Lipid Droplet-binding Adipocyte Differentiation-related Protein * 210. Journal of Biological Chemistry *278*, 15998-16007. 10.1074/jbc.M211289200.
155. Beller, M., Bulankina, A.V., Hsiao, H.-H., Urlaub, H., Jäckle, H., and Kühnlein, R.P. (2010). PERILIPIN-Dependent Control of Lipid Droplet Structure and Fat Storage in Drosophila. Cell Metabolism *12*, 521-532. 10.1016/j.cmet.2010.10.001.
156. Liu, Z., Li, X., Ge, Q., Ding, M., and Huang, X. (2014). A Lipid Droplet-Associated GFP Reporter-Based Screen Identifies New Fat Storage Regulators in C. elegans. Journal of Genetics and Genomics *41*, 305-313. https://doi.org/10.1016/j.jgg.2014.03.002.
157. Liu, L., Zhang, K., Sandoval, H., Yamamoto, S., Jaiswal, M., Sanz, E., Li, Z., Hui, J., Graham, B.H., Quintana, A., and Bellen, H.J. (2015). Glial lipid droplets and ROS induced by mitochondrial defects promote neurodegeneration. Cell *160*, 177-190. 10.1016/j.cell.2014.12.019.
158. White, R.M., Sessa, A., Burke, C., Bowman, T., LeBlanc, J., Ceol, C., Bourque, C., Dovey, M., Goessling, W., Burns, C.E., and Zon, L.I. (2008). Transparent adult zebrafish as a tool for in vivo transplantation analysis. Cell stem cell *2*, 183-189. 10.1016/j.stem.2007.11.002.
159. Cagan, R.L., Zon, L.I., and White, R.M. (2019). Modeling Cancer with Flies and Fish. Developmental Cell *49*, 317-324. https://doi.org/10.1016/j.devcel.2019.04.013.
160. Parichy, D.M., and Spiewak, J.E. (2015). Origins of adult pigmentation: diversity in pigment stem cell lineages and implications for pattern evolution. Pigment Cell & Melanoma Research *28*, 31-50. https://doi.org/10.1111/pcmr.12332.
161. Heilmann, S., Ratnakumar, K., Langdon, E.M., Kansler, E.R., Kim, I.S., Campbell, N.R., Perry, E.B., McMahon, A.J., Kaufman, C.K., van Rooijen, E., et al. (2015). A Quantitative System for Studying Metastasis Using Transparent Zebrafish. Cancer Research *75*, 4272-4282. 10.1158/0008-5472.CAN-14-3319.
162. Callahan, S.J., Tepan, S., Zhang, Y.M., Lindsay, H., Burger, A., Campbell, N.R., Kim, I.S., Hollmann, T.J., Studer, L., Mosimann, C., and White, R.M. (2018). Cancer modeling by Transgene Electroporation in Adult Zebrafish (TEAZ). Disease Models & Mechanisms *11*, dmm034561. 10.1242/dmm.034561.
163. Montal, E., Suresh, S., Ma, Y., Tagore, M.M., and White, R.M. (2024). Cancer Modeling by Transgene Electroporation in Adult Zebrafish (TEAZ). In Zebrafish:

Methods and Protocols, J.F. Amatruda, C. Houart, K. Kawakami, and K.D. Poss, eds. (Springer US), pp. 83-97. 10.1007/978-1-0716-3401-1_5.
164. Kurat, C.F., Wolinski, H., Petschnigg, J., Kaluarachchi, S., Andrews, B., Natter, K., and Kohlwein, S.D. (2009). Cdk1/Cdc28-Dependent Activation of the Major Triacylglycerol Lipase Tgl4 in Yeast Links Lipolysis to Cell-Cycle Progression. Molecular Cell *33*, 53-63. 10.1016/j.molcel.2008.12.019.
165. Kuerschner, L., Moessinger, C., and Thiele, C. (2008). Imaging of Lipid Biosynthesis: How a Neutral Lipid Enters Lipid Droplets. Traffic *9*, 338-352. https://doi.org/10.1111/j.1600-0854.2007.00689.x.
166. Fujimoto, Y., Itabe, H., Kinoshita, T., Homma, K.J., Onoduka, J., Mori, M., Yamaguchi, S., Makita, M., Higashi, Y., Yamashita, A., and Takano, T. (2007). Involvement of ACSL in local synthesis of neutral lipids in cytoplasmic lipid droplets in human hepatocyte HuH7. Journal of Lipid Research *48*, 1280-1292. https://doi.org/10.1194/jlr.M700050-JLR200.
167. Zimmermann, R., Strauss, J.G., Haemmerle, G., Schoiswohl, G., Birner-Gruenberger, R., Riederer, M., Lass, A., Neuberger, G., Eisenhaber, F., Hermetter, A., and Zechner, R. (2004). Fat Mobilization in Adipose Tissue Is Promoted by Adipose Triglyceride Lipase. Science *306*, 1383-1386.
168. Vevea, Jason D., Garcia, Enrique J., Chan, Robin B., Zhou, B., Schultz, M., Di Paolo, G., McCaffery, J.M., and Pon, Liza A. (2015). Role for Lipid Droplet Biogenesis and Microlipophagy in Adaptation to Lipid Imbalance in Yeast. Developmental Cell *35*, 584-599. https://doi.org/10.1016/j.devcel.2015.11.010.
169. Fei, W., Wang, H., Fu, X., Bielby, C., and Yang, H. (2009). Conditions of endoplasmic reticulum stress stimulate lipid droplet formation in Saccharomyces cerevisiae. Biochem J *424*, 61-67. 10.1042/bj20090785.
170. Liu, L., MacKenzie, K.R., Putluri, N., Maletić-Savatić, M., and Bellen, H.J. (2017). The Glia-Neuron Lactate Shuttle and Elevated ROS Promote Lipid Synthesis in Neurons and Lipid Droplet Accumulation in Glia via APOE/D. Cell Metab *26*, 719-737.e716. 10.1016/j.cmet.2017.08.024.
171. Rambold, Angelika S., Cohen, S., and Lippincott-Schwartz, J. (2015). Fatty Acid Trafficking in Starved Cells: Regulation by Lipid Droplet Lipolysis, Autophagy, and Mitochondrial Fusion Dynamics. Developmental Cell *32*, 678-692. 10.1016/j.devcel.2015.01.029.
172. Bosma, M., Dapito, D.H., Drosatos-Tampakaki, Z., Huiping-Son, N., Huang, L.-S., Kersten, S., Drosatos, K., and Goldberg, I.J. (2014). Sequestration of fatty acids in triglycerides prevents endoplasmic reticulum stress in an in vitro model of cardiomyocyte lipotoxicity. Biochimica et Biophysica Acta (BBA) - Molecular and Cell Biology of Lipids *1841*, 1648-1655. https://doi.org/10.1016/j.bbalip.2014.09.012.
173. Velázquez, A.P., Tatsuta, T., Ghillebert, R., Drescher, I., and Graef, M. (2016). Lipid droplet-mediated ER homeostasis regulates autophagy and cell survival during starvation. J Cell Biol *212*, 621-631. 10.1083/jcb.201508102.
174. Bosch, M., Sánchez-Álvarez, M., Fajardo, A., Kapetanovic, R., Steiner, B., Dutra, F., Moreira, L., López, J.A., Campo, R., Marí, M., et al. (2020). Mammalian lipid droplets are innate immune hubs integrating cell metabolism and host defense. Science *370*, eaay8085. 10.1126/science.aay8085.

175. Barba, G., Harper, F., Harada, T., Kohara, M., Goulinet, S., Matsuura, Y., Eder, G., Schaff, Z., Chapman, M.J., Miyamura, T., and Bréchot, C. (1997). Hepatitis C virus core protein shows a cytoplasmic localization and associates to cellular lipid storage droplets. Proceedings of the National Academy of Sciences *94*, 1200. 10.1073/pnas.94.4.1200.
176. Miyanari, Y., Atsuzawa, K., Usuda, N., Watashi, K., Hishiki, T., Zayas, M., Bartenschlager, R., Wakita, T., Hijikata, M., and Shimotohno, K. (2007). The lipid droplet is an important organelle for hepatitis C virus production. Nature Cell Biology *9*, 1089-1097. 10.1038/ncb1631.
177. Vieyres, G., Reichert, I., Carpentier, A., Vondran, F.W.R., and Pietschmann, T. (2020). The ATGL lipase cooperates with ABHD5 to mobilize lipids for hepatitis C virus assembly. PLOS Pathogens *16*, e1008554. 10.1371/journal.ppat.1008554.
178. Kuniyoshi, S., Miki, Y., Sasaki, A., Iwabuchi, E., Ono, K., Onodera, Y., Hirakawa, H., Ishida, T., Yoshimi, N., and Sasano, H. (2019). The significance of lipid accumulation in breast carcinoma cells through perilipin 2 and its clinicopathological significance. Pathology International *69*, 463-471. 10.1111/pin.12831.
179. Bergman, R.N., Van Citters, G.W., Mittelman, S.D., Dea, M.K., Hamilton-Wessler, M., Kim, S.P., and Ellmerer, M. (2001). Central Role of the Adipocyte in the Metabolic Syndrome. Journal of Investigative Medicine *49*, 119. 10.2310/6650.2001.34108.
180. Minchin, J.E.N., and Rawls, J.F. (2017). A classification system for zebrafish adipose tissues. Disease Models & Mechanisms *10*, 797. 10.1242/dmm.025759.
181. Fam, T.K., Klymchenko, A.S., and Collot, M. (2018). Recent Advances in Fluorescent Probes for Lipid Droplets. Materials (Basel) *11*, 1768. 10.3390/ma11091768.
182. Xue, Y., Lim, S., Bråkenhielm, E., and Cao, Y. (2010). Adipose angiogenesis: quantitative methods to study microvessel growth, regression and remodeling in vivo. Nature Protocols *5*, 912-920. 10.1038/nprot.2010.46.
183. Berry, R., and Rodeheffer, M.S. (2013). Characterization of the adipocyte cellular lineage in vivo. Nature Cell Biology *15*, 302-308. 10.1038/ncb2696.
184. Minchin, J.N., Scahill, C.M., Staudt, N., Busch-Nentwich, E.M., and Rawls, J.F. (2018). Deep phenotyping in zebrafish reveals genetic and diet-induced adiposity changes that may inform disease risk. Journal of Lipid Research *59*, 1536-1545. 10.1194/jlr.D084525.
185. Minchin, J.E.N., and Rawls, J.F. (2017). Chapter 1 - In vivo imaging and quantification of regional adiposity in zebrafish. In Methods in Cell Biology, H.W. Detrich, M. Westerfield, and L.I. Zon, eds. (Academic Press), pp. 3-27. https://doi.org/10.1016/bs.mcb.2016.11.010.
186. Carten, J.D., Bradford, M.K., and Farber, S.A. (2011). Visualizing digestive organ morphology and function using differential fatty acid metabolism in live zebrafish. Developmental Biology *360*, 276-285. https://doi.org/10.1016/j.ydbio.2011.09.010.
187. Farber, S.A., Pack, M., Ho, S.-Y., Johnson, I.D., Wagner, D.S., Dosch, R., Mullins, M.C., Hendrickson, H.S., Hendrickson, E.K., and Halpern, M.E. (2001).

Genetic Analysis of Digestive Physiology Using Fluorescent Phospholipid Reporters. Science *292*, 1385. 10.1126/science.1060418.
188. Otis, J.P., and Farber, S.A. (2016). High-fat Feeding Paradigm for Larval Zebrafish: Feeding, Live Imaging, and Quantification of Food Intake. J Vis Exp. 10.3791/54735.
189. Daemen, S., van Zandvoort, M.A.M.J., Parekh, S.H., and Hesselink, M.K.C. (2016). Microscopy tools for the investigation of intracellular lipid storage and dynamics. Molecular Metabolism *5*, 153-163. https://doi.org/10.1016/j.molmet.2015.12.005.
190. Høgset, H., Horgan, C.C., Armstrong, J.P.K., Bergholt, M.S., Torraca, V., Chen, Q., Keane, T.J., Bugeon, L., Dallman, M.J., Mostowy, S., and Stevens, M.M. (2020). In vivo biomolecular imaging of zebrafish embryos using confocal Raman spectroscopy. Nature Communications *11*, 6172. 10.1038/s41467-020-19827-1.
191. Wilson, M.H., Ekker, S.C., and Farber, S.A. (2021). Imaging cytoplasmic lipid droplets in vivo with fluorescent perilipin 2 and perilipin 3 knockin zebrafish. bioRxiv, 2021.2001.2010.426109. 10.1101/2021.01.10.426109.
192. Fujimoto, T., and Parton, R.G. (2011). Not just fat: the structure and function of the lipid droplet. Cold Spring Harb Perspect Biol *3*, a004838. 10.1101/cshperspect.a004838.
193. Heid, H., Rickelt, S., Zimbelmann, R., Winter, S., Schumacher, H., Dörflinger, Y., Kuhn, C., and Franke, W.W. (2014). On the Formation of Lipid Droplets in Human Adipocytes: The Organization of the Perilipin–Vimentin Cortex. PLOS ONE *9*, e90386. 10.1371/journal.pone.0090386.
194. Fujimoto, M., Matsuzaki, I., Nishitsuji, K., Yamamoto, Y., Murakami, D., Yoshikawa, T., Fukui, A., Mori, Y., Nishino, M., Takahashi, Y., et al. (2020). Adipophilin expression in cutaneous malignant melanoma is associated with high proliferation and poor clinical prognosis. Laboratory Investigation *100*, 727-737. 10.1038/s41374-019-0358-y.
195. Tchernof, A., and Després, J.-P. (2013). Pathophysiology of Human Visceral Obesity: An Update. Physiological Reviews *93*, 359-404. 10.1152/physrev.00033.2011.
196. Sawada, T., Miyoshi, H., Shimada, K., Suzuki, A., Okamatsu-Ogura, Y., Perfield, J.W., II, Kondo, T., Nagai, S., Shimizu, C., Yoshioka, N., et al. (2010). Perilipin Overexpression in White Adipose Tissue Induces a Brown Fat-Like Phenotype. PLOS ONE *5*, e14006. 10.1371/journal.pone.0014006.
197. Parichy, D.M., Elizondo, M.R., Mills, M.G., Gordon, T.N., and Engeszer, R.E. (2009). Normal table of postembryonic zebrafish development: Staging by externally visible anatomy of the living fish. Developmental Dynamics *238*, 2975-3015. https://doi.org/10.1002/dvdy.22113.
198. Henne, W.M., Reese, M.L., and Goodman, J.M. (2018). The assembly of lipid droplets and their roles in challenged cells. The EMBO journal *37*, e98947. 10.15252/embj.201898947.
199. Longo, Valter D., and Mattson, Mark P. (2014). Fasting: Molecular Mechanisms and Clinical Applications. Cell Metabolism *19*, 181-192. https://doi.org/10.1016/j.cmet.2013.12.008.

200. Tang, H.-N., Tang, C.-Y., Man, X.-F., Tan, S.-W., Guo, Y., Tang, J., Zhou, C.-L., and Zhou, H.-D. (2017). Plasticity of adipose tissue in response to fasting and refeeding in male mice. Nutrition & Metabolism *14*, 3. 10.1186/s12986-016-0159-x.
201. Litosch, I., Hudson, T.H., Mills, I., Li, S.Y., and Fain, J.N. (1982). Forskolin as an activator of cyclic AMP accumulation and lipolysis in rat adipocytes. Molecular Pharmacology *22*, 109-115.
202. Chu, C.-Y., Chen, C.-F., Rajendran, R.S., Shen, C.-N., Chen, T.-H., Yen, C.-C., Chuang, C.-K., Lin, D.-S., and Hsiao, C.-D. (2012). Overexpression of Akt1 Enhances Adipogenesis and Leads to Lipoma Formation in Zebrafish. PLOS ONE *7*, e36474. 10.1371/journal.pone.0036474.
203. Landgraf, K., Schuster, S., Meusel, A., Garten, A., Riemer, T., Schleinitz, D., Kiess, W., and Körner, A. (2017). Short-term overfeeding of zebrafish with normal or high-fat diet as a model for the development of metabolically healthy versus unhealthy obesity. BMC physiology *17*, 4-4. 10.1186/s12899-017-0031-x.
204. Oka, T., Nishimura, Y., Zang, L., Hirano, M., Shimada, Y., Wang, Z., Umemoto, N., Kuroyanagi, J., Nishimura, N., and Tanaka, T. (2010). Diet-induced obesity in zebrafish shares common pathophysiological pathways with mammalian obesity. BMC Physiology *10*, 21. 10.1186/1472-6793-10-21.
205. Krahmer, N., Farese, R.V., Jr., and Walther, T.C. (2013). Balancing the fat: lipid droplets and human disease. EMBO Mol Med *5*, 973-983. 10.1002/emmm.201100671.
206. Paar, M., Jüngst, C., Steiner, N.A., Magnes, C., Sinner, F., Kolb, D., Lass, A., Zimmermann, R., Zumbusch, A., Kohlwein, S.D., and Wolinski, H. (2012). Remodeling of lipid droplets during lipolysis and growth in adipocytes. The Journal of biological chemistry *287*, 11164-11173. 10.1074/jbc.M111.316794.
207. Duncan, R.E., Ahmadian, M., Jaworski, K., Sarkadi-Nagy, E., and Sul, H.S. (2007). Regulation of lipolysis in adipocytes. Annu Rev Nutr *27*, 79-101. 10.1146/annurev.nutr.27.061406.093734.
208. Lengyel, E., Makowski, L., DiGiovanni, J., and Kolonin, M.G. (2018). Cancer as a Matter of Fat: The Crosstalk between Adipose Tissue and Tumors. Trends in Cancer *4*, 374-384. 10.1016/j.trecan.2018.03.004.
209. Balaban, S., Shearer, R.F., Lee, L.S., van Geldermalsen, M., Schreuder, M., Shtein, H.C., Cairns, R., Thomas, K.C., Fazakerley, D.J., Grewal, T., et al. (2017). Adipocyte lipolysis links obesity to breast cancer growth: adipocyte-derived fatty acids drive breast cancer cell proliferation and migration. Cancer & Metabolism *5*, 1. 10.1186/s40170-016-0163-7.
210. Zebisch, K., Voigt, V., Wabitsch, M., and Brandsch, M. (2012). Protocol for effective differentiation of 3T3-L1 cells to adipocytes. Analytical Biochemistry *425*, 88-90. https://doi.org/10.1016/j.ab.2012.03.005.
211. Hellmér, J., Arner, P., and Lundin, A. (1989). Automatic luminometric kinetic assay of glycerol for lipolysis studies. Analytical Biochemistry *177*, 132-137. https://doi.org/10.1016/0003-2697(89)90027-4.
212. Mayer, N., Schweiger, M., Romauch, M., Grabner, G.F., Eichmann, T.O., Fuchs, E., Ivkovic, J., Heier, C., Mrak, I., Lass, A., et al. (2013). Development of small-

molecule inhibitors targeting adipose triglyceride lipase. Nature Chemical Biology *9*, 785-787. 10.1038/nchembio.1359.
213. Schweiger, M., Romauch, M., Schreiber, R., Grabner, G.F., Hütter, S., Kotzbeck, P., Benedikt, P., Eichmann, T.O., Yamada, S., Knittelfelder, O., et al. (2017). Pharmacological inhibition of adipose triglyceride lipase corrects high-fat diet-induced insulin resistance and hepatosteatosis in mice. Nature Communications *8*, 14859. 10.1038/ncomms14859.
214. Stamler, J.S., Lamas, S., and Fang, F.C. (2001). Nitrosylation: The Prototypic Redox-Based Signaling Mechanism. Cell *106*, 675-683. https://doi.org/10.1016/S0092-8674(01)00495-0.
215. Yamada, Y., Eto, M., Ito, Y., Mochizuki, S., Son, B.-K., Ogawa, S., Iijima, K., Kaneki, M., Kozaki, K., Toba, K., Akishita, M., and Ouchi, Y. (2015). Suppressive Role of PPARγ-Regulated Endothelial Nitric Oxide Synthase in Adipocyte Lipolysis. PLOS ONE *10*, e0136597. 10.1371/journal.pone.0136597.
216. Nath, N., Chattopadhyay, M., Pospishil, L., Cieciura, L.Z., Goswami, S., Kodela, R., Saavedra, J.E., Keefer, L.K., and Kashfi, K. (2010). JS-K, a nitric oxide-releasing prodrug, modulates ß-catenin/TCF signaling in leukemic Jurkat cells: evidence of an S-nitrosylated mechanism. Biochem Pharmacol *80*, 1641-1649. 10.1016/j.bcp.2010.08.011.
217. Shami, P.J., Saavedra, J.E., Wang, L.Y., Bonifant, C.L., Diwan, B.A., Singh, S.V., Gu, Y., Fox, S.D., Buzard, G.S., Citro, M.L., et al. (2003). JS-K, a Glutathione/Glutathione S-Transferase-activated Nitric Oxide Donor of the Diazeniumdiolate Class with Potent Antineoplastic Activity. Molecular Cancer Therapeutics *2*, 409-417.
218. Bensaad, K., Favaro, E., Lewis, Caroline A., Peck, B., Lord, S., Collins, Jennifer M., Pinnick, Katherine E., Wigfield, S., Buffa, Francesca M., Li, J.-L., et al. (2014). Fatty Acid Uptake and Lipid Storage Induced by HIF-1α Contribute to Cell Growth and Survival after Hypoxia-Reoxygenation. Cell Reports *9*, 349-365. https://doi.org/10.1016/j.celrep.2014.08.056.
219. Cabodevilla, A.G., Sánchez-Caballero, L., Nintou, E., Boiadjieva, V.G., Picatoste, F., Gubern, A., and Claro, E. (2013). Cell survival during complete nutrient deprivation depends on lipid droplet-fueled β-oxidation of fatty acids. The Journal of biological chemistry *288*, 27777-27788. 10.1074/jbc.M113.466656.
220. Fox, C.S., Massaro, J.M., Hoffmann, U., Pou, K.M., Maurovich-Horvat, P., Liu, C.-Y., Vasan, R.S., Murabito, J.M., Meigs, J.B., Cupples, L.A., D'Agostino, R.B., and O'Donnell, C.J. (2007). Abdominal Visceral and Subcutaneous Adipose Tissue Compartments. Circulation *116*, 39-48. doi:10.1161/CIRCULATIONAHA.106.675355.
221. Le Jemtel, T.H., Samson, R., Milligan, G., Jaiswal, A., and Oparil, S. (2018). Visceral Adipose Tissue Accumulation and Residual Cardiovascular Risk. Current Hypertension Reports *20*, 77. 10.1007/s11906-018-0880-0.
222. Verboven, K., Wouters, K., Gaens, K., Hansen, D., Bijnen, M., Wetzels, S., Stehouwer, C.D., Goossens, G.H., Schalkwijk, C.G., Blaak, E.E., and Jocken, J.W. (2018). Abdominal subcutaneous and visceral adipocyte size, lipolysis and inflammation relate to insulin resistance in male obese humans. Scientific Reports *8*, 4677. 10.1038/s41598-018-22962-x.

223. Bosma, M. (2016). Lipid droplet dynamics in skeletal muscle. Experimental Cell Research *340*, 180-186. https://doi.org/10.1016/j.yexcr.2015.10.023.
224. Wang, H., Quiroga, A.D., and Lehner, R. (2013). Chapter 7 - Analysis of Lipid Droplets in Hepatocytes. In Methods in Cell Biology, H. Yang, and P. Li, eds. (Academic Press), pp. 107-127. https://doi.org/10.1016/B978-0-12-408051-5.00007-3.
225. Kwan, K.M., Fujimoto, E., Grabher, C., Mangum, B.D., Hardy, M.E., Campbell, D.S., Parant, J.M., Yost, H.J., Kanki, J.P., and Chien, C.-B. (2007). The Tol2kit: A multisite gateway-based construction kit for Tol2 transposon transgenesis constructs. Developmental Dynamics *236*, 3088-3099. 10.1002/dvdy.21343.
226. Karras, P., Bordeu, I., Pozniak, J., Nowosad, A., Pazzi, C., Van Raemdonck, N., Landeloos, E., Van Herck, Y., Pedri, D., Bervoets, G., et al. (2022). A cellular hierarchy in melanoma uncouples growth and metastasis. Nature *610*, 190-198. 10.1038/s41586-022-05242-7.
227. Ubellacker, J.M., Tasdogan, A., Ramesh, V., Shen, B., Mitchell, E.C., Martin-Sandoval, M.S., Gu, Z., McCormick, M.L., Durham, A.B., Spitz, D.R., et al. (2020). Lymph protects metastasizing melanoma cells from ferroptosis. Nature *585*, 113-118. 10.1038/s41586-020-2623-z.
228. Broadfield, L.A., Duarte, J.A.G., Schmieder, R., Broekaert, D., Veys, K., Planque, M., Vriens, K., Karasawa, Y., Napolitano, F., Fujita, S., et al. (2021). Fat Induces Glucose Metabolism in Nontransformed Liver Cells and Promotes Liver Tumorigenesis. Cancer Research *81*, 1988-2001. 10.1158/0008-5472.CAN-20-1954.
229. Ting-Hsiang, H., Yilun, M., Emily, M., Shruthy, S., Mohita, M.T., Alexandra, C., Dianne, L., Nathaniel, R.C., Arianna, B., Richard, P.K., and Richard, M.W. (2022). Epigenetic reprogramming of melanoma cell state through fatty acid β-oxidation and Toll-like receptor 4 signaling. bioRxiv, 2022.2006.2016.496450. 10.1101/2022.06.16.496450.
230. Adams, M.K., Belyaeva, O.V., Wu, L., and Kedishvili, N.Y. (2014). The Retinaldehyde Reductase Activity of DHRS3 Is Reciprocally Activated by Retinol Dehydrogenase 10 to Control Retinoid Homeostasis*. Journal of Biological Chemistry *289*, 14868-14880. https://doi.org/10.1074/jbc.M114.552257.
231. Fernandes-Silva, H., Araújo-Silva, H., Correia-Pinto, J., and Moura, R.S. (2020). Retinoic Acid: A Key Regulator of Lung Development. Biomolecules *10*. 10.3390/biom10010152.
232. Inoue, Y., Hasegawa, S., Yamada, T., Date, Y., Mizutani, H., Nakata, S., Matsunaga, K., and Akamatsu, H. (2012). Bimodal effect of retinoic acid on melanocyte differentiation identified by time-dependent analysis. Pigment Cell & Melanoma Research *25*, 299-311. https://doi.org/10.1111/j.1755-148X.2012.00988.x.
233. Roméro, C., Aberdam, E., Larnier, C., and Ortonne, J.-P. (1994). Retinoic acid as modulator of UVB-induced melanocyte differentiation: Involvement of the melanogenic enzymes expression. Journal of Cell Science *107*, 1095-1103. 10.1242/jcs.107.4.1095.

234. Nusinow, D.P., Szpyt, J., Ghandi, M., Rose, C.M., McDonald, E.R., III, Kalocsay, M., Jané-Valbuena, J., Gelfand, E., Schweppe, D.K., Jedrychowski, M., et al. (2020). Quantitative Proteomics of the Cancer Cell Line Encyclopedia. Cell *180*, 387-402.e316. 10.1016/j.cell.2019.12.023.
235. Deisenroth, C., Itahana, Y., Tollini, L., Jin, A., and Zhang, Y. (2011). p53-inducible DHRS3 Is an Endoplasmic Reticulum Protein Associated with Lipid Droplet Accumulation*. Journal of Biological Chemistry *286*, 28343-28356. https://doi.org/10.1074/jbc.M111.254227.
236. Pataki, C.I., Rodrigues, J., Zhang, L., Qian, J., Efron, B., Hastie, T., Elias, J.E., Levitt, M., and Kopito, R.R. (2018). Proteomic analysis of monolayer-integrated proteins on lipid droplets identifies amphipathic interfacial alpha-helical membrane anchors. Proc Natl Acad Sci U S A *115*, E8172-E8180. 10.1073/pnas.1807981115.
237. Boncinelli, E., Simeone, A., Acampora, D., and Mavilio, F. (1991). HOX gene activation by retinoic acid. Trends in Genetics *7*, 329-334. https://doi.org/10.1016/0168-9525(91)90423-N.
238. Breier, G., Bućan, M., Francke, U., Colberg-Poley, A.M., and Gruss, P. (1986). Sequential expression of murine homeo box genes during F9 EC cell differentiation. The EMBO Journal *5*, 2209-2215-2215. https://doi.org/10.1002/j.1460-2075.1986.tb04486.x.
239. Tobin, R.P., Cogswell, D.T., Cates, V.M., Davis, D.M., Borgers, J.S.W., Van Gulick, R.J., Katsnelson, E., Couts, K.L., Jordan, K.R., Gao, D., et al. (2023). Targeting MDSC Differentiation Using ATRA: A Phase I/II Clinical Trial Combining Pembrolizumab and All-Trans Retinoic Acid for Metastatic Melanoma. Clinical Cancer Research *29*, 1209-1219. 10.1158/1078-0432.CCR-22-2495.
240. Kane, M.A. (2012). Analysis, occurrence, and function of 9-cis-retinoic acid. Biochimica et Biophysica Acta (BBA) - Molecular and Cell Biology of Lipids *1821*, 10-20. https://doi.org/10.1016/j.bbalip.2011.09.012.
241. Paterson, E.K., Ho, H., Kapadia, R., and Ganesan, A.K. (2013). 9-cis retinoic acid is the ALDH1A1 product that stimulates melanogenesis. Experimental Dermatology *22*, 202-209. https://doi.org/10.1111/exd.12099.
242. Goding, C.R., and Arnheiter, H. (2019). MITF-the first 25 years. Genes Dev *33*, 983-1007. 10.1101/gad.324657.119.
243. Mort, R.L., Jackson, I.J., and Patton, E.E. (2015). The melanocyte lineage in development and disease. Development *142*, 620-632. 10.1242/dev.106567.
244. Louphrasitthiphol, P., Siddaway, R., Loffreda, A., Pogenberg, V., Friedrichsen, H., Schepsky, A., Zeng, Z., Lu, M., Strub, T., Freter, R., et al. (2020). Tuning Transcription Factor Availability through Acetylation-Mediated Genomic Redistribution. Molecular Cell *79*, 472-487.e410. https://doi.org/10.1016/j.molcel.2020.05.025.
245. Aksan, I., and Goding, C.R. (1998). Targeting the Microphthalmia Basic Helix-Loop-Helix–Leucine Zipper Transcription Factor to a Subset of E-Box Elements In Vitro and In Vivo. Molecular and Cellular Biology *18*, 6930-6938. 10.1128/MCB.18.12.6930.

246. Dorsky, R.I., Raible, D.W., and Moon, R.T. (2000). Direct regulation of nacre, a zebrafish MITF homolog required for pigment cell formation, by the Wnt pathway. Genes Dev *14*, 158-162.
247. Takeda, K., Yasumoto, K.-i., Takada, R., Takada, S., Watanabe, K.-i., Udono, T., Saito, H., Takahashi, K., and Shibahara, S. (2000). Induction of Melanocyte-specific Microphthalmia-associated Transcription Factor by Wnt-3a*. Journal of Biological Chemistry *275*, 14013-14016. https://doi.org/10.1074/jbc.C000113200.
248. Widlund, H.R., Horstmann, M.A., Price, E.R., Cui, J., Lessnick, S.L., Wu, M., He, X., and Fisher, D.E. (2002). β-Catenin–induced melanoma growth requires the downstream target Microphthalmia-associated transcription factor. Journal of Cell Biology *158*, 1079-1087. 10.1083/jcb.200202049.
249. Schepsky, A., Bruser, K., Gunnarsson, G.J., Goodall, J., Hallsson, J.H., Goding, C.R., Steingrimsson, E., and Hecht, A. (2006). The Microphthalmia-Associated Transcription Factor Mitf Interacts with β-Catenin To Determine Target Gene Expression. Molecular and Cellular Biology *26*, 8914-8927. 10.1128/MCB.02299-05.
250. Louphrasitthiphol, P., Chauhan, J., and Goding, C.R. (2020). ABCB5 is activated by MITF and β-catenin and is associated with melanoma differentiation. Pigment Cell & Melanoma Research *33*, 112-118. https://doi.org/10.1111/pcmr.12830.
251. Chauhan, J.S., Hölzel, M., Lambert, J.-P., Buffa, F.M., and Goding, C.R. (2022). The MITF regulatory network in melanoma. Pigment Cell & Melanoma Research *35*, 517-533. https://doi.org/10.1111/pcmr.13053.
252. Park, Jun H., Vithayathil, S., Kumar, S., Sung, P.-L., Dobrolecki, Lacey E., Putluri, V., Bhat, Vadiraja B., Bhowmik, Salil K., Gupta, V., Arora, K., et al. (2016). Fatty Acid Oxidation-Driven Src Links Mitochondrial Energy Reprogramming and Oncogenic Properties in Triple-Negative Breast Cancer. Cell Reports *14*, 2154-2165. https://doi.org/10.1016/j.celrep.2016.02.004.
253. Schlaepfer, I.R., Rider, L., Rodrigues, L.U., Gijón, M.A., Pac, C.T., Romero, L., Cimic, A., Sirintrapun, S.J., Glodé, L.M., Eckel, R.H., and Cramer, S.D. (2014). Lipid Catabolism via CPT1 as a Therapeutic Target for Prostate Cancer. Molecular Cancer Therapeutics *13*, 2361-2371. 10.1158/1535-7163.MCT-14-0183.
254. Wang, T., Fahrmann, J.F., Lee, H., Li, Y.-J., Tripathi, S.C., Yue, C., Zhang, C., Lifshitz, V., Song, J., Yuan, Y., et al. (2018). JAK/STAT3-Regulated Fatty Acid β-Oxidation Is Critical for Breast Cancer Stem Cell Self-Renewal and Chemoresistance. Cell Metabolism *27*, 136-150.e135. https://doi.org/10.1016/j.cmet.2017.11.001.
255. Doll, S., Proneth, B., Tyurina, Y.Y., Panzilius, E., Kobayashi, S., Ingold, I., Irmler, M., Beckers, J., Aichler, M., Walch, A., et al. (2017). ACSL4 dictates ferroptosis sensitivity by shaping cellular lipid composition. Nature Chemical Biology *13*, 91-98. 10.1038/nchembio.2239.
256. Magtanong, L., Ko, P.-J., To, M., Cao, J.Y., Forcina, G.C., Tarangelo, A., Ward, C.C., Cho, K., Patti, G.J., Nomura, D.K., Olzmann, J.A., and Dixon, S.J. (2019). Exogenous Monounsaturated Fatty Acids Promote a Ferroptosis-Resistant Cell State. Cell Chemical Biology *26*, 420-432.e429. https://doi.org/10.1016/j.chembiol.2018.11.016.

257. Dierge, E., Debock, E., Guilbaud, C., Corbet, C., Mignolet, E., Mignard, L., Bastien, E., Dessy, C., Larondelle, Y., and Feron, O. (2021). Peroxidation of n-3 and n-6 polyunsaturated fatty acids in the acidic tumor environment leads to ferroptosis-mediated anticancer effects. Cell Metabolism *33*, 1701-1715.e1705. https://doi.org/10.1016/j.cmet.2021.05.016.
258. Cruz, A.L.S., Barreto, E.d.A., Fazolini, N.P.B., Viola, J.P.B., and Bozza, P.T. (2020). Lipid droplets: platforms with multiple functions in cancer hallmarks. Cell Death & Disease *11*, 105. 10.1038/s41419-020-2297-3.
259. Herker, E., Vieyres, G., Beller, M., Krahmer, N., and Bohnert, M. (2021). Lipid Droplet Contact Sites in Health and Disease. Trends in Cell Biology *31*, 345-358. https://doi.org/10.1016/j.tcb.2021.01.004.
260. Perera, R.M., Stoykova, S., Nicolay, B.N., Ross, K.N., Fitamant, J., Boukhali, M., Lengrand, J., Deshpande, V., Selig, M.K., Ferrone, C.R., et al. (2015). Transcriptional control of autophagy–lysosome function drives pancreatic cancer metabolism. Nature *524*, 361-365. 10.1038/nature14587.
261. Yang, S., Wang, X., Contino, G., Liesa, M., Sahin, E., Ying, H., Bause, A., Li, Y., Stommel, J.M., Dell'Antonio, G., et al. (2011). Pancreatic cancers require autophagy for tumor growth. Genes & Development *25*, 717-729.
262. Audet-Walsh, É., Vernier, M., Yee, T., Laflamme, C., Li, S., Chen, Y., and Giguère, V. (2018). SREBF1 Activity Is Regulated by an AR/mTOR Nuclear Axis in Prostate Cancer. Molecular Cancer Research *16*, 1396-1405. 10.1158/1541-7786.MCR-17-0410.
263. Chauhan, S.S., Casillas, A.L., Vizzerra, A.D., Liou, H., Clements, A.N., Flores, C.E., Prevost, C.T., Kashatus, D.F., Snider, A.J., Snider, J.M., and Warfel, N.A. (2024). PIM1 drives lipid droplet accumulation to promote proliferation and survival in prostate cancer. Oncogene *43*, 406-419. 10.1038/s41388-023-02914-0.
264. Lee, G., Zheng, Y., Cho, S., Jang, C., England, C., Dempsey, J.M., Yu, Y., Liu, X., He, L., Cavaliere, P.M., et al. (2017). Post-transcriptional Regulation of De Novo Lipogenesis by mTORC1-S6K1-SRPK2 Signaling. Cell *171*, 1545-1558.e1518. https://doi.org/10.1016/j.cell.2017.10.037.
265. Guri, Y., Colombi, M., Dazert, E., Hindupur, S.K., Roszik, J., Moes, S., Jenoe, P., Heim, M.H., Riezman, I., Riezman, H., and Hall, M.N. (2017). mTORC2 Promotes Tumorigenesis via Lipid Synthesis. Cancer Cell *32*, 807-823.e812. https://doi.org/10.1016/j.ccell.2017.11.011.
266. Accioly, M.T., Pacheco, P., Maya-Monteiro, C.M., Carrossini, N., Robbs, B.K., Oliveira, S.S., Kaufmann, C., Morgado-Diaz, J.A., Bozza, P.T., and Viola, J.o.P.B. (2008). Lipid Bodies Are Reservoirs of Cyclooxygenase-2 and Sites of Prostaglandin-E2 Synthesis in Colon Cancer Cells. Cancer Research *68*, 1732-1740. 10.1158/0008-5472.CAN-07-1999.
267. Tirinato, L., Liberale, C., Di Franco, S., Candeloro, P., Benfante, A., La Rocca, R., Potze, L., Marotta, R., Ruffilli, R., Rajamanickam, V.P., et al. (2015). Lipid Droplets: A New Player in Colorectal Cancer Stem Cells Unveiled by Spectroscopic Imaging. Stem Cells *33*, 35-44. 10.1002/stem.1837.
268. Li, J., Condello, S., Thomes-Pepin, J., Ma, X., Xia, Y., Hurley, T.D., Matei, D., and Cheng, J.-X. (2017). Lipid Desaturation Is a Metabolic Marker and

Therapeutic Target of Ovarian Cancer Stem Cells. Cell Stem Cell *20*, 303-314.e305. https://doi.org/10.1016/j.stem.2016.11.004.
269. Kostecka, L.G., Mendez, S., Li, M., Khare, P., Zhang, C., Le, A., Amend, S.R., and Pienta, K.J. (2024). Cancer cells employ lipid droplets to survive toxic stress. The Prostate *n/a*. https://doi.org/10.1002/pros.24680.
270. Nardi, F., Franco, O.E., Fitchev, P., Morales, A., Vickman, R.E., Hayward, S.W., and Crawford, S.E. (2019). DGAT1 Inhibitor Suppresses Prostate Tumor Growth and Migration by Regulating Intracellular Lipids and Non-Centrosomal MTOC Protein GM130. Scientific Reports *9*, 3035. 10.1038/s41598-019-39537-z.
271. Wang, Y., Hu, Y., Xu, R., Jin, X., and Jiao, W. (2024). Plin2 inhibits autophagy via activating AKT/mTOR pathway in non-small cell lung cancer. Experimental Cell Research *435*, 113955. https://doi.org/10.1016/j.yexcr.2024.113955.
272. Roberts, M.A., Deol, K.K., Mathiowetz, A.J., Lange, M., Leto, D.E., Stevenson, J., Hashemi, S.H., Morgens, D.W., Easter, E., Heydari, K., et al. (2023). Parallel CRISPR-Cas9 screens identify mechanisms of PLIN2 and lipid droplet regulation. Developmental Cell *58*, 1782-1800.e1710. https://doi.org/10.1016/j.devcel.2023.07.001.
273. Liu, W., Liu, X., Liu, Y., Ling, T., Chen, D., Otkur, W., Zhao, H., Ma, M., Ma, K., Dong, B., et al. (2022). PLIN2 promotes HCC cells proliferation by inhibiting the degradation of HIF1α. Experimental Cell Research *418*, 113244. https://doi.org/10.1016/j.yexcr.2022.113244.
274. Carreira, S., Goodall, J., Aksan, I., La Rocca, S.A., Galibert, M.-D., Denat, L., Larue, L., and Goding, C.R. (2005). Mitf cooperates with Rb1 and activates p21Cip1 expression to regulate cell cycle progression. Nature *433*, 764-769. 10.1038/nature03269.
275. Rappsilber, J., Mann, M., and Ishihama, Y. (2007). Protocol for micro-purification, enrichment, pre-fractionation and storage of peptides for proteomics using StageTips. Nature Protocols *2*, 1896-1906. 10.1038/nprot.2007.261.
276. Olsen, J.V., de Godoy, L.M.F., Li, G., Macek, B., Mortensen, P., Pesch, R., Makarov, A., Lange, O., Horning, S., and Mann, M. (2005). Parts per Million Mass Accuracy on an Orbitrap Mass Spectrometer via Lock Mass Injection into a C-trap. Molecular & Cellular Proteomics *4*, 2010-2021. https://doi.org/10.1074/mcp.T500030-MCP200.
277. Bunkenborg, J., García, G.E., Paz, M.I.P., Andersen, J.S., and Molina, H. (2010). The minotaur proteome: Avoiding cross-species identifications deriving from bovine serum in cell culture models. PROTEOMICS *10*, 3040-3044. https://doi.org/10.1002/pmic.201000103.
278. Cox, J., and Mann, M. (2008). MaxQuant enables high peptide identification rates, individualized p.p.b.-range mass accuracies and proteome-wide protein quantification. Nature Biotechnology *26*, 1367-1372. 10.1038/nbt.1511.
279. Tyanova, S., Temu, T., and Cox, J. (2016). The MaxQuant computational platform for mass spectrometry-based shotgun proteomics. Nature Protocols *11*, 2301-2319. 10.1038/nprot.2016.136.
280. Schwanhäusser, B., Busse, D., Li, N., Dittmar, G., Schuchhardt, J., Wolf, J., Chen, W., and Selbach, M. (2011). Global quantification of mammalian gene expression control. Nature *473*, 337-342. 10.1038/nature10098.

281. Tyanova, S., Temu, T., Sinitcyn, P., Carlson, A., Hein, M.Y., Geiger, T., Mann, M., and Cox, J. (2016). The Perseus computational platform for comprehensive analysis of (prote)omics data. Nature Methods *13*, 731-740. 10.1038/nmeth.3901.
282. Kolberg, L., Raudvere, U., Kuzmin, I., Adler, P., Vilo, J., and Peterson, H. (2023). g:Profiler—interoperable web service for functional enrichment analysis and gene identifier mapping (2023 update). Nucleic Acids Research *51*, W207-W212. 10.1093/nar/gkad347.
283. Hao, Y., Stuart, T., Kowalski, M.H., Choudhary, S., Hoffman, P., Hartman, A., Srivastava, A., Molla, G., Madad, S., Fernandez-Granda, C., and Satija, R. (2024). Dictionary learning for integrative, multimodal and scalable single-cell analysis. Nature Biotechnology *42*, 293-304. 10.1038/s41587-023-01767-y.
284. Hafemeister, C., and Satija, R. (2019). Normalization and variance stabilization of single-cell RNA-seq data using regularized negative binomial regression. Genome Biology *20*, 296. 10.1186/s13059-019-1874-1.
285. Bolger, A.M., Lohse, M., and Usadel, B. (2014). Trimmomatic: a flexible trimmer for Illumina sequence data. Bioinformatics *30*, 2114-2120. 10.1093/bioinformatics/btu170.
286. Patro, R., Duggal, G., Love, M.I., Irizarry, R.A., and Kingsford, C. (2017). Salmon provides fast and bias-aware quantification of transcript expression. Nature Methods *14*, 417-419. 10.1038/nmeth.4197.
287. Love, M.I., Huber, W., and Anders, S. (2014). Moderated estimation of fold change and dispersion for RNA-seq data with DESeq2. Genome Biology *15*, 550. 10.1186/s13059-014-0550-8.
288. Subramanian, A., Tamayo, P., Mootha, V.K., Mukherjee, S., Ebert, B.L., Gillette, M.A., Paulovich, A., Pomeroy, S.L., Golub, T.R., Lander, E.S., and Mesirov, J.P. (2005). Gene set enrichment analysis: a knowledge-based approach for interpreting genome-wide expression profiles. Proc Natl Acad Sci U S A *102*, 15545-15550.
289. Gennady, K., Vladimir, S., Nikolay, B., Boris, S., Maxim, N.A., and Alexey, S. (2021). Fast gene set enrichment analysis. bioRxiv, 060012. 10.1101/060012.
290. Vlčková, K., Vachtenheim, J., Réda, J., Horák, P., and Ondrušová, L. (2018). Inducibly decreased MITF levels do not affect proliferation and phenotype switching but reduce differentiation of melanoma cells. Journal of Cellular and Molecular Medicine *22*, 2240-2251. https://doi.org/10.1111/jcmm.13506.
291. Martin, M. (2011). Cutadapt removes adapter sequences from high-throughput sequencing reads. EMBnet.journal; Vol 17, No 1: Next Generation Sequencing Data Analysis. 10.14806/ej.17.1.200.
292. Dobin, A., Davis, C.A., Schlesinger, F., Drenkow, J., Zaleski, C., Jha, S., Batut, P., Chaisson, M., and Gingeras, T.R. (2013). STAR: ultrafast universal RNA-seq aligner. Bioinformatics *29*, 15-21. 10.1093/bioinformatics/bts635.
293. Warburg , O., Wind , F., and Negelein , E. (1927). THE METABOLISM OF TUMORS IN THE BODY. Journal of General Physiology *8*, 519-530. 10.1085/jgp.8.6.519.
294. Warburg, O., Posener, K., and Negelein, E. (1924). Über den stoffwechsel der carcinomzelle. Naturwissenschaften *12*, 1131-1137.

295. Mullard, A. (2017). FDA approves first-in-class cancer metabolism drug. Nature Reviews Drug Discovery *16*, 593-593. 10.1038/nrd.2017.174.
296. Mullard, A. (2016). Cancer metabolism pipeline breaks new ground. Nature Reviews Drug Discovery *15*, 735-737. 10.1038/nrd.2016.223.
297. Stine, Z.E., Schug, Z.T., Salvino, J.M., and Dang, C.V. (2022). Targeting cancer metabolism in the era of precision oncology. Nature Reviews Drug Discovery *21*, 141-162. 10.1038/s41573-021-00339-6.
298. Cheng, X., Geng, F., Pan, M., Wu, X., Zhong, Y., Wang, C., Tian, Z., Cheng, C., Zhang, R., Puduvalli, V., et al. (2020). Targeting DGAT1 Ameliorates Glioblastoma by Increasing Fat Catabolism and Oxidative Stress. Cell Metabolism *32*, 229-242.e228. https://doi.org/10.1016/j.cmet.2020.06.002.
299. Amin, N.B., Darekar, A., Anstee, Q.M., Wong, V.W.-S., Tacke, F., Vourvahis, M., Lee, D.S., Charlton, M., Alkhouri, N., Nakajima, A., and Yunis, C. (2022). Efficacy and safety of an orally administered DGAT2 inhibitor alone or coadministered with a liver-targeted ACC inhibitor in adults with non-alcoholic steatohepatitis (NASH): rationale and design of the phase II, dose-ranging, dose-finding, randomised, placebo-controlled MIRNA (Metabolic Interventions to Resolve NASH with fibrosis) study. BMJ Open *12*, e056159. 10.1136/bmjopen-2021-056159.
300. Birch, A.M., Buckett, L.K., and Turnbull, A.V. (2010). DGAT1 inhibitors as anti-obesity and anti-diabetic agents. Curr Opin Drug Discov Devel *13*, 489-496.
301. DeVita, R.J., and Pinto, S. (2013). Current Status of the Research and Development of Diacylglycerol O-Acyltransferase 1 (DGAT1) Inhibitors. Journal of Medicinal Chemistry *56*, 9820-9825. 10.1021/jm4007033.
302. Seberg, H.E., Van Otterloo, E., Loftus, S.K., Liu, H., Bonde, G., Sompallae, R., Gildea, D.E., Santana, J.F., Manak, J.R., Pavan, W.J., Williams, T., and Cornell, R.A. (2017). TFAP2 paralogs regulate melanocyte differentiation in parallel with MITF. PLOS Genetics *13*, e1006636. 10.1371/journal.pgen.1006636.
303. Belyaeva, O.V., Adams, M.K., Popov, K.M., and Kedishvili, N.Y. (2020). Generation of Retinaldehyde for Retinoic Acid Biosynthesis. Biomolecules *10*, 5.